

## STELLINGEN

behorende bij het proefschrift

"Investigations of spatial effects in nuclear reactor kinetics"

van Jan Keijzer

April 1996

### I

Het begrip nodale reactiviteit, dat vooral in numerieke oplossingsmethodes voor de tijdsafhankelijke neutronenflux veelvuldig wordt gebruikt, is feitelijk een contradictio in terminis.

M. R. Yeung and G. B. Jiang, "Development of an efficient three-dimensional reactor core model for simulator applications", *Nucl. Techn.*, **97**, 352 (1992)

### II

Hoewel hogere orde verstoringstheorie een mathematische schoonheid in zich heeft, is haar praktische relevantie beperkt omdat ze te complex is in analytische toepassingen en achterhaald is door de rekenkracht van de huidige computers.

A. Gandini, "On the standard perturbation theory", *Nucl. Sci. & Eng.*, **79**, 426 (1981)

### III

Het scheiden van de plaatsafhankelijkheden in de "field-of-view" theorie door middel van de eigenwaarden uit de adjoint-vergelijkingen, zoals voorgesteld door Behringer *et al.* is, maakt de interpretatie van de experimentele resultaten ondoorzichtiger.

K. Behringer, G. Kosály and Lj. Kostić, "Theoretical investigation of the local and global components of the neutron-noise field in a boiling water reactor", *Nucl. Sci. & Eng.*, **306** (1977)

### IV

De toegevoegde waarde van "big sample analysis" ten opzichte van analyses met gehomogeniseerde samples is twijfelachtig als niet met tomografische technieken wordt gewerkt.

R. M. W. Overwater, *The physics of big sample instrumental neutron activation analysis*, Delft University Press, Delft, The Netherlands (1994)

## V

De vaak organisatorische scheiding van reactorfysische en thermohydraulische groepen in onderzoeksinstellingen op het gebied van kernreactoren ontkent het grote belang van de koppeling van beide vakgebieden.

## VI

De importantie van het stereoscopisch zien voor het dieptezien wordt meestal sterk overschat ten opzichte van andere cues, zoals relatieve snelheid en lineair perspectief.

J. M. Foley, "Primary distance perception", *Handbook of sensory physiology*, 8, 136, R. Held, H. W. Leibowitz and H. L. Teuber (eds.), Springer-Verlag, Berlin, Germany (1978)

## VII

Het hedendaags gebruik van de programmeertaal FORTRAN in sommige wetenschappelijke kringen is een goed voorbeeld van de wet van de remmende voorsprong.

## VIII

In een democratie zal de politiek op belangrijke, controversiële thema's over het algemeen pas achteraf wetgeving realiseren.

## IX

Het tanende respect voor de promovendus in Nederland is tekenend voor het feit dat Nederland een steeds minder vooraanstaande rol speelt in de geïndustrialiseerde wereld.

## X

Hoewel hij in de praktijk vrijwel geen invloed heeft op het volleybalspel, tast de nieuwe regel dat ook voeten mogen worden gebruikt de essentie van de sport aan en moet daarom zo snel mogelijk weer worden afgeschaft.

## XI

De slogan "We gaan ervoor" van de Nederlandse Spoorwegen kan beter gelezen worden als "We staan ervoor".

# **Investigations of spatial effects in nuclear reactor kinetics**

**J. Keijzer**

Interfaculty Reactor Institute  
Delft University of Technology  
April 1996

CIP-GEGEVENS KONINKLIJKE BIBLIOTHEEK, DEN HAAG

Keijzer, Jan

Investigations of spatial effects in nuclear reactor kinetics /

Jan Keijzer. - Delft : Interfacultair Reactor Instituut,

Technische Universiteit Delft. - I11.

Thesis Technische Universiteit Delft. - With ref.

ISBN 90-73861-30-6

NUGI 812

Subject headings: nuclear reactor kinetics / spatial effects.

Copyright © 1996 by J. Keijzer

# **Investigations of spatial effects in nuclear reactor kinetics**

## **PROEFSCHRIFT**

ter verkrijging van de graad van doctor  
aan de Technische Universiteit Delft,  
op gezag van de Rector Magnificus Prof. Ir. K. F. Wakker,  
in het openbaar te verdedigen ten overstaan van een commissie,  
door het College van Dekanen aangewezen,  
op maandag 15 april 1996 te 10.30 uur  
door

**Jan KEIJZER**



doctorandus in de wiskunde en natuurwetenschappen  
geboren te Amsterdam

Dit proefschrift is goedgekeurd door de promotor:

Prof. Dr. Ir. H. van Dam

Toegevoegd promotor:

Dr. Ir. J. E. Hoogenboom

Samenstelling promotiecommissie:

Rector Magnificus, voorzitter

Prof. Dr. Ir. H. van Dam, TU Delft, promotor

Dr. Ir. J. E. Hoogenboom, TU Delft, toegevoegd promotor

Prof. Dr. Ir. A. van den Bos, TU Delft

Prof. Dr. Ir. C. W. E. van Eijk, TU Delft

Prof. Dr. Ir. A. H. M. Verkooijen, TU Delft

Prof. I. Pázsit, Chalmers University, Sweden

Dr. J. Valkó, Nuclear consultant, Delft

Dr. J. Valkó heeft als begeleider in belangrijke mate aan het totstandkomen van het proefschrift bijgedragen

The research described in this thesis was performed at the Reactor Physics Department of the Interfaculty Reactor Institute, Delft University of Technology, Mekelweg 15, Delft, The Netherlands

This work has been accomplished in the framework of the PINK-project, program I, and has been financed by the Ministry of Economic Affairs.

Aan mijn ouders  
Aan Tjarda



# Table of contents

<b>I General introduction</b>	<b>11</b>
-------------------------------	-----------

<b>II Theory of space-time kinetics and numerical experiments for different reactor types</b>	<b>15</b>
---	-----------

Introduction	15
Theory of the time-dependent diffusion equations	16
The shape function, the dynamic reactivity and the influence of the precursors	16
The conventional point kinetic equations	21
Comments on the asymptotic shape	22
Characterization of the size of reactors in reactor physical terms	23
Space-time dependent reciprocal period	25
Description of the numerical experiments	26
Critical reactor models before the start of the transient	26
The perturbation	27
Computer code used in the experiments	29
Behaviour of the reactor model with $\Theta = 100$	30
Reactors with different sizes	35
Discussion	39
Conclusion	41

<b>III Measurements of fast transients in a nuclear research reactor</b>	<b>43</b>
--	-----------

Introduction	43
Investigation of the existence of shape changes of the flux	44
The experimental setup	45
The reactor	45

The detectors and other measuring devices .....	47
The experiments .....	49
Results of the measurements .....	50
Transient with an initial reactor power of 60 kW .....	50
Transient with an initial reactor power of 10 kW .....	52
Transient using the transfer system at G5 .....	53
Discussion and conclusion .....	54

#### **IV Theory and numerical experiments of small periodic perturbations ..... 57**

Introduction .....	57
Small changes in an initially critical system .....	59
Field-of-view theory: Determining the frequency dependent detector response using adjoint function theory .....	63
Separate treatment of global and local effects .....	65
The global effect .....	66
The local effect .....	68
Application of the theory to selected disturbers .....	69
The modulating absorber .....	69
The moving absorber .....	72
Numerical experiments .....	75
Field-of-view of a 1D-1G model of the HOR .....	76
A moving absorber in a 2D-2G model of the HOR .....	87
Discussion and conclusion .....	92

#### **V The experimental facility DISTY - Setup and methods of analysis ..... 95**

Introduction .....	95
Description of the experimental facility DISTY .....	97
General description .....	97
The disturbers .....	97
The driving mechanism .....	98
The 'disturber' part of DISTY .....	101
The detectors .....	103

The electrical equipment . . . . .	103
The reactor and the position of DISTY . . . . .	104
Testing the facility . . . . .	108
Testing the detectors . . . . .	110
The axial position and the axial flux distribution . . . . .	110
Frequency spectrum of detector signals during normal operation . . . . .	112
Methods of analysis of perturbation experiments . . . . .	114
Frequency-averaged spectra . . . . .	114
Time-averaged spectra . . . . .	116
Peak contents . . . . .	116
Factorization into a set of sine waves . . . . .	117
Discussion on the different methods . . . . .	118
Variances . . . . .	118
<b>VI Experiments with DISTY . . . . .</b>	<b>121</b>
Introduction . . . . .	121
Measurements with disturber II with DISTY at an orientation of 0° . . . . .	121
Description of the normalized time response . . . . .	121
Discussion on the probability density function . . . . .	124
Discussion on the normalized auto power spectrum . . . . .	126
Discussion on the phase . . . . .	127
Discussion on the coherence . . . . .	133
Measurements with disturber II and DISTY at an orientation of 90° . . . . .	135
Measurements with disturber II in all possible orientations . . . .	142
Experiments with disturber III and detectors at varying axial positions. . . . .	149
Experiment varying the frequency of movement of disturber II . . . . .	154
Discussion and conclusion . . . . .	156
<b>References . . . . .</b>	<b>159</b>

<b>Nomenclature</b> .....	<b>165</b>
Greek symbols .....	165
Arabic symbols .....	166
<b>Summary</b> .....	<b>169</b>
<b>Samenvatting</b> .....	<b>173</b>
<b>Curriculum Vitae</b> .....	<b>177</b>

# Chapter I

## General introduction

In the study of nuclear reactors the investigation of the dynamic processes always plays an important role. One reason is that whenever a nuclear reactor is started up or shut down, for example for refuelling or maintenance, the system is inherently non-stationary. But even under normal full-power operation dynamic processes influence the behaviour of the reactor. There are long term processes like burn-up of the fuel and build-up of neutronic poisons, which have time scales of several hours or days or even longer. Although the long term processes have a large influence, in this work focus is on another type of processes: the ones with much shorter time scales of minutes, seconds or less.

The short term processes, which play an important role in the control of reactors, can be divided into two categories: deterministic processes and stochastic ones. An example of the first is the change of position of a control rod. The influence of the boiling process on the dynamics in boiling water reactors is an example of the second category. Thorough knowledge of both is necessary for a normal safe operation of nuclear reactors.

However, the knowledge of the dynamic behaviour of reactors is not only important for the normal operation. It is even more important in order to minimize the consequences of incidents like the unanticipated withdrawal of a control rod. A careful design of the system, based on proper knowledge of the dynamics of nuclear reactors, will minimize the consequences of such incidents.

A lot of research is already done in the field. Especially the theory of the behaviour of the total power due to all kinds of disturbances either small or large can be found in many text books on the reactor physical

aspects of nuclear reactors (Bell & Glasstone, 1970; Hetrick, 1971; Henry, 1975; Duderstadt & Hamilton, 1976). The influence of spatial change of the neutron flux, however, is often neglected. In many cases the neglect of the spatial effects is a good approximation of the behaviour of the neutron flux. But in some circumstances spatial changes are important in the dynamic behaviour of nuclear reactors as shown by Yasinsky and Henry already in 1965. Since then more research is done on the implications of these spatial effects in the dynamics (see Ott & Neuhold, 1985, for a review). But still some questions are not yet investigated.

One of these questions is whether it is possible to say in advance that a certain type of reactor is more sensitive to flux shape changes during a transient than another one. If such a statement can be made a better decision on the way of analysing such a reactor becomes possible. This subject is dealt with in Chapter II. In that chapter another characterization method, which is able to show the large influence of the delayed neutron precursors on the dynamics, is also shown. In Chapter III experiments that are performed in the nuclear research reactor of the Technical University of Budapest are described. These experiments are not only used to justify the theoretical investigations as reported in Chapter II, but also to get experience with the techniques of reactor physical measurements and to test the possibility of measuring changes in the neutron flux with small self-powered neutron detectors.

In the first three chapters only relatively large transients are investigated, which are mainly of concern in situations in which the system is not working in its normal range of operation. However, during normal operation a reactor is exposed to many small disturbances. Investigations of these small disturbances are discussed in the last three chapters. The first of these (Chapter IV) is a theoretical chapter, in which two methods are described for calculating the effects of small disturbances in a nuclear reactor. A comparison of both methods is shown in numerical experiments.

Results of the theory are compared with experiments done in the research reactor of the Interfaculty Reactor Institute in Delft with a

newly built facility. The facility and the methods of analysis are described in Chapter V. Chapter VI shows the results of the measurements performed with the new experimental facility.

In the field of research of nuclear reactor dynamics a clear distinction is made between investigations in which thermal-hydraulic feedback mechanisms are taken into account and those in which they are neglected. The field in which the feedback is neglected is normally denoted by the term 'kinetics'. The reason for this clear distinction lies in the fact that the incorporation of thermal-hydraulics will usually result in complex theory, in which the neutronics is often approximated. In many cases and especially in the short term processes, in which we are interested in the thesis, however, the influence of the thermal-hydraulics is negligible and the crude approximation of the neutronics can be insufficient. Therefore in this thesis the focus lies on the kinetics.

The structure of the thesis is such that at the beginning of every chapter an introduction puts the text of that chapter in perspective. Although all chapters deal with investigations on the space-time kinetics of nuclear reactors, the individual chapters can be seen as separated aspects of it. Therefore the discussion and conclusions are put at the end of every chapter. A list of references, a list of symbols and a summary in English and Dutch are given after Chapter VI.

## Chapter II

# Theory of space-time kinetics and numerical experiments for different reactor types

### II.1 Introduction

In the designs of the new generation of nuclear reactors one can observe a tendency towards lower power densities. This is achieved either by using a number of modules with lower power for each module or by building cores with larger physical sizes. Apart from the technological difficulties of manufacturing the large cores, larger core sizes also have implications for the dynamic behaviour of these systems.

Yasinsky and Henry showed as long ago as 1965 that the global behaviour of large reactors is different from that of smaller reactor types due to the shape changes of the flux density. In order to solve the coupled space-time dependent kinetics a number of authors introduced different methods (see Hetrick (1971) and Ott & Neuhold (1985) for a review). There are methods which solve the time-dependent multi-group diffusion equations rigorously (see, for example, Chen *et al* (1992)) and several approximate methods like the multi-mode synthesis method (Kaplan *et al*, 1964), nodal methods (Wachpress *et al*, 1962), conventional point-kinetic approach (see, for example, Duderstadt & Hamilton (1976)), the adiabatic method (Henry & Curlee, 1958), the quasi-static method (Ott & Meneley, 1969; Dodds, 1975) and combinations of nodal and quasi-static methods (Beauwens *et al*, 1990).

Because of the number of different solution methods and their difference in applicability, it is difficult to select the right one for a



given problem. For this selection characterization of the system is mandatory. This characterization can be a simple one, which gives some indication beforehand as to whether the reactor can be treated with simple methods or whether one needs more complicated space-time dependent investigations. For a more detailed description of the kinetic behaviour other characterizations have to be used.

In this chapter, we present two new characterization methods, a simple one and a more complex one. We also show the development of the shape of the precursor density during a transient, since this is very important for the behaviour of the total system and is underexposed in the literature. We limit our investigation to kinetics, so no feedback is considered.

Before going into detail on the parameters that can influence the time-dependent behaviour of a reactor, the general theory of solving the time-dependent diffusion equations is discussed. Following these two theoretical sections, the third describes numerical experiments, that are performed to confirm the theory.

## II.2 Theory of the time-dependent diffusion equations

### II.2.1 The shape function, the dynamic reactivity and the influence of the precursors

We take as a basis the time- and energy-dependent diffusion equation with delayed neutrons, as described in, for example, Ott & Neuhold (1985):

$$\begin{aligned}
 \frac{1}{v} \frac{\partial \varphi(E, \mathbf{r}, t)}{\partial t} = & \nabla D(E, \mathbf{r}, t) \nabla \varphi(E, \mathbf{r}, t) - \Sigma_t(E, \mathbf{r}, t) \varphi(E, \mathbf{r}, t) + \\
 & + \int \Sigma_s(E' \rightarrow E, \mathbf{r}, t) \varphi(E', \mathbf{r}, t) dE' + \\
 & + \chi_p(E) (1 - \beta) \int v \Sigma_f(E', \mathbf{r}, t) \varphi(E', \mathbf{r}, t) dE' + \\
 & + \sum_{i=1}^m \chi_i(E) \lambda_i C_i(\mathbf{r}, t)
 \end{aligned} \tag{II.1}$$

$$\frac{\partial C_i(\mathbf{r},t)}{\partial t} = \beta_i \int v \Sigma_f(E', \mathbf{r}, t) \varphi(E', \mathbf{r}, t) dE' - \lambda_i C_i(\mathbf{r}, t) \quad i = 1 \dots m \quad (\text{II.2})$$

in which  $\varphi(E, \mathbf{r}, t)$  is the neutron flux,  $\beta$  is the fraction of delayed neutrons,  $v$  is the velocity,  $\chi_p$  is the energy spectrum of the prompt neutrons,  $C_i(\mathbf{r}, t)$  is the concentration of the neutron precursors in group  $i$ ,  $\beta_i$  is the fraction of delayed neutrons of group  $i$ ,  $\lambda_i$  is the decay constant of neutron precursor group  $i$  and  $\chi_i$  is the energy spectrum of the delayed neutrons of group  $i$ . The other symbols denote the cross sections and the diffusion coefficient in the usual way as, for example, in Duderstadt & Hamilton (1976). All equations can be seen as balance equations; the first one of the neutron flux, the others of the different groups of precursors. The first three terms at the right-hand side of Eq. II.1 denote respectively the diffusion, the absorption and the scattering of the neutrons. The fourth term expresses production of neutrons in the fission process. The last term denotes the neutrons that come from the decay of the precursors. The two terms at the right-hand side of Eqs. II.2 describe the production and the decay of the precursors respectively.

Within the diffusion approximation, this equation gives the correct flux and precursor densities as a function of time. Due to its complexity it cannot be solved analytically and even numerically it is very difficult. However, to get more insight into the behaviour of these equations it is useful to rewrite them as proposed in many textbooks (e.g. Bell & Glasstone, 1970; Henry, 1975; Ott & Neuhold, 1985).

The flux density is factorized into an amplitude part  $n(t)$  and a time-dependent shape function  $\psi(E, \mathbf{r}, t)$ :

$$\varphi(E, \mathbf{r}, t) = n(t) \psi(E, \mathbf{r}, t) \quad (\text{II.3})$$

with  $n(t)$  defined as follows:

$$n(t) \equiv \int \int \psi^\dagger(E, \mathbf{r}) \frac{1}{V} \phi(E, \mathbf{r}, t) dE dV \quad (\text{II.4})$$

In this last equation  $\psi^\dagger(E, \mathbf{r})$  is the adjoint eigenfunction for the initial steady state of the system (Ott & Neuhold, 1985), with the following constraint condition:

$$\int \int \psi^\dagger(E, \mathbf{r}) \frac{1}{V} \psi(E, \mathbf{r}, t) dE dV = 1 \quad (\text{II.5})$$

Multiplying Eq. II.1 by  $\psi^\dagger(E, \mathbf{r})$ , Eqs. II.2 by  $\chi_i(E) \psi^\dagger(E, \mathbf{r})$  and integrating subsequently over space and energy one gets the standard point kinetics equations:

$$\begin{aligned} \frac{dn(t)}{dt} &= \frac{\rho(t) - \beta^{\text{eff}}(t)}{\Lambda(t)} n(t) + \sum_{i=1}^m \lambda_i c_i(t) \\ \frac{dc_i(t)}{dt} &= \frac{\beta_i^{\text{eff}}(t)}{\Lambda(t)} n(t) - \lambda_i c_i(t) \quad i = 1 \dots m \end{aligned} \quad (\text{II.6})$$

with:

$$\begin{aligned} \rho(t) &= \frac{1}{F(t)} \int \int \psi^\dagger(E, \mathbf{r}) \{ \nabla D(E, \mathbf{r}, t) \nabla \psi(E, \mathbf{r}, t) - \Sigma_t(E, \mathbf{r}, t) \psi(E, \mathbf{r}, t) + \\ &\quad + \int \Sigma_s(E' \rightarrow E, \mathbf{r}, t) \psi(E', \mathbf{r}, t) dE' + \\ &\quad + \chi_t(E) \int v \Sigma_f(E', \mathbf{r}, t) \psi(E', \mathbf{r}, t) dE' \} dE dV \end{aligned} \quad (\text{II.7})$$

$$\Lambda(t) = \frac{1}{F(t)} \int \int \psi^\dagger(E, \mathbf{r}) \frac{1}{V} \psi(E, \mathbf{r}, t) dE dV = \frac{1}{F(t)} \quad (\text{II.8})$$

$$\beta_i^{\text{eff}}(t) = \frac{1}{F(t)} \int \int \psi^\dagger(E, \mathbf{r}) \beta_i \chi_i(E) \int v \Sigma_f(E', \mathbf{r}, t) \psi(E', \mathbf{r}, t) dE' dE dV \quad (\text{II.9})$$

$$\beta^{\text{eff}}(t) = \sum_{i=1}^m \beta_i^{\text{eff}}(t) \quad (\text{II.10})$$

$$c_i(t) = \int \int \psi^\dagger(E, \mathbf{r}) \chi_i(E) C_i(\mathbf{r}, t) dE dV \quad (\text{II.11})$$

$$F(t) = \int \int \psi^\dagger(E, \mathbf{r}) \chi_t(E) \int v \Sigma_f(E', \mathbf{r}, t) \psi(E', \mathbf{r}, t) dE' dE dV \quad (\text{II.12})$$

and:

$$\chi_t(E) = \chi_p(E)(1 - \beta) + \sum_{i=1}^m \chi_i(E) \beta_i \quad (\text{II.13})$$

The parameters  $\rho(t)$ ,  $\Lambda(t)$ ,  $\beta_i^{\text{eff}}$  and  $\beta^{\text{eff}}$  are the dynamic reactivity, generation time, the effective fraction of delayed neutrons from precursor  $i$  and the effective fraction of delayed neutrons from all precursors, respectively. Until now no approximations are made, so Eqs. II.6 with the proper definition of the variables as in Eqs. II.7 to II.13 are as general as Eqs. II.1 and II.2. The most important advantage of Eqs. II.6 is the factorization of the flux into an amplitude function and a shape function, since normally the changes of the shape are much slower than the changes in amplitude. One can use this fact to approximate the time-dependent shape function, which is often the most time-consuming part of a calculation. It can also help the interpretation of the dynamic behaviour of the system.

As can be seen the shape function appears in Eqs. II.7, II.8, II.9, II.11 and II.12. In general the generation time ( $\Lambda$ , Eq. II.8) and the effective delayed neutron fraction ( $\beta_1^{\text{eff}}$ , Eq. II.9) normally change only slightly. Moreover, in a one-energy group approximation the effective delayed neutron fraction always remains constant in time and if the fission cross section does not change either and is uniform over the reactor, the generation time also remains constant in time. The dynamic reactivity ( $\rho(t)$ , Eq. II.7), however, is a delicate balance between production terms and loss terms. Changes in the shape function can have a dramatic effect on this balance and thus on the dynamic reactivity. In fact, if all cross sections and the diffusion coefficient are unchanged from a specific moment in time, the change of the shape function is the only reason for the change in the dynamic reactivity. Moreover, in that situation a changing dynamic reactivity indicates that the flux is still changing. Therefore the dynamic reactivity can be seen as a good measure of how different reactor types react to certain disturbances.

The influence of the changing precursor densities on the reactivity is a more indirect one, via Eq. II.11 and Eqs. II.6. However, since the decay times of the precursors are orders of magnitude larger than the time scales involved in the prompt processes, the indirect influence of the precursors is very important.

As said before in a one-energy group approximation the effective delayed neutron fractions become time-independent. But in a one-group system the adjoint eigenfunction  $\psi^\dagger(\mathbf{r})$  also becomes much easier to calculate, since it is equal to the stationary neutron flux before the start of the transient. This property of the adjoint eigenfunction is especially useful if approximate analytical solutions are sought and we use it later on in this chapter and in Chapter IV.

## **II.2.2 The conventional point kinetic equations**

The most extreme approximation of the shape function is one in which it is taken time-independently. This means it is supposed that no changes in the shape of the flux take place during the transient. The advantage of this approximation is that the flux can be separated completely into a space dependent part  $\psi_0(E, \mathbf{r})$  and a time-dependent part  $n(t)$ . Consequently the parameters  $\rho$ ,  $\beta_i^{\text{eff}}$ ,  $\beta^{\text{eff}}$  and  $\Lambda$  only change due to an explicit change in the cross section. As said before the changes in  $\beta_i^{\text{eff}}$ ,  $\beta^{\text{eff}}$  and  $\Lambda$  are mild in general compared to the changes in  $\rho$  and are therefore frequently taken to be constant. Incorporating all these approximations, the set of equations II.6 reduce to the so-called conventional point kinetic equations, sometimes referred to as the point kinetic equations. This set of equations is commonly used in studies of the kinetics of nuclear reactors. Although computer codes are available to solve this set of differential equations (see, for example, Baggoura *et al* (1994)), it is still difficult to solve them in general because of, among other things, the smallness of  $\Lambda(t)$  (e.g. the 'stiffness' problem (Duderstadt & Hamilton, 1976)). Another problem is the nonlinear product of  $\rho(t)$  and  $n(t)$ , which makes it impossible to apply the well-developed methods for linear differential equations. However, in some circumstances it is possible to linearize the conventional point kinetic equations. In chapter IV, in which the theory of small disturbances is explained, we come back to this subject.

As said before, in a one-energy group approximation the adjoint eigenfunction is identical to the initial stationary flux. Together with the fact that in conventional point kinetic theory the shape function is approximated by this initial stationary flux (Ott & Neuhold, 1985), a first estimate of the reactivity effect of a change in, for example, the absorption cross section can easily be made. It is proportional to the square of the stationary flux at the position, where the absorption cross section is changed. The sign of this proportionality is negative, since if the absorption cross section is increased, the reactivity decreases.

### II.2.3 Comments on the asymptotic shape

Suppose one introduces a perturbation, which is left unchanged from a specific point in time and which leaves the reactor in a non-critical state. In that system the shape of the flux asymptotically becomes constant and the amplitude changes exponentially with a time constant  $\alpha_{as}$  (Ott & Neuhold, 1985):

$$\varphi_{as}(E, \mathbf{r}, t) = \Psi_{as}(E, \mathbf{r}) \cdot e^{\alpha_{as} t} \quad \text{and} \quad C_{i,as}(\mathbf{r}, t) = \tilde{C}_{i,as}(\mathbf{r}) \cdot e^{\alpha_{as} t} \quad (\text{II.14})$$

Substituting these expressions into Eqs. II.1 and II.2 and eliminating  $\tilde{C}_{i,as}(\mathbf{r})$ , leads to the following equation for the asymptotic shape function, the so-called delayed  $\alpha$ -mode:

$$\begin{aligned} \frac{\alpha_{as}}{v} \Psi_{as}(E, \mathbf{r}) = & \nabla D(E, \mathbf{r}) \nabla \Psi_{as}(E, \mathbf{r}) - \Sigma_t(E, \mathbf{r}) \Psi_{as}(E, \mathbf{r}) + \\ & + \int \Sigma_s(E' \rightarrow E, \mathbf{r}) \Psi_{as}(E', \mathbf{r}) dE' + \\ & + [\chi_p(E)(1 - \beta) + \sum_{i=1}^m \frac{\lambda_i \beta_i \chi_i(E)}{\alpha_{as} + \lambda_i}] \int v \Sigma_f(E', \mathbf{r}) \Psi_{as}(E', \mathbf{r}) dE' \end{aligned} \quad (\text{II.15})$$

where the cross sections are taken from the asymptotic situation. For a mono-energetic approach this equation can be rewritten as:

$$[-\nabla D(\mathbf{r}) \nabla + \Sigma_a(\mathbf{r})] \Psi_{as}(\mathbf{r}) = [1 - \sum_{i=1}^m \frac{\alpha_{as} \beta_i}{\alpha_{as} + \lambda_i} - \frac{\alpha_{as}}{v \Sigma_f(\mathbf{r})}] v \Sigma_f(\mathbf{r}) \Psi_{as}(\mathbf{r}) \quad (\text{II.16})$$

In case of a homogeneous fission cross section  $\Sigma_f$  this equation can be solved as a static eigenvalue problem with the eigenvalue  $1 - \rho_{as}$ , where:

$$\rho_{as} = \sum_{i=1}^m \frac{\alpha_{as} \beta_i}{\alpha_{as} + \lambda_i} + \alpha_{as} \Lambda \quad \text{and} \quad \Lambda = \frac{1}{v \Sigma_f} \quad (\text{II.17})$$

and  $\rho_{as}$  is called the asymptotic reactivity. Eq. II.17 is generally known as the inhour equation, from which the algebraically largest solution for  $\alpha_{as}$  must be taken. So, in the particular case of a one-energy group reactor model with homogeneous fission cross section, the asymptotic shape can exactly be calculated. In that case the strength of the perturbation can be measured in terms of the asymptotic reactivity. In more general cases with heterogeneous cores or more energy groups it is more complicated to solve Eq. II.15 directly.

#### **II.2.4 Characterization of the size of reactors in reactor physical terms**

Intuitively one would say that changes of the shape of the flux density are likely to be larger in a physically large reactor than in small ones. However, this statement is not very specific. In fact in an actual situation with a real reactor, it is still not possible to predict whether the flux shape changes are important in that reactor or not. A more precise and more quantitative characterization is needed for that. This can be done by relating the physical size of the reactor to the neutron migration length  $M$  as follows.

The migration area  $M^2$  can be interpreted to be  $1/6$  times the mean square distance a neutron travels 'as the crow flies' from its appearance as a fast neutron to its capture as a thermal neutron in an infinite medium (Duderstadt & Hamilton, 1976). In a multiplying system one newly born neutron from a source of neutrons can start a fission chain of prompt neutrons. In a subprompt critical reactor the chains die away. The total number of fission neutrons participating in such a chain is  $1/(\beta - \rho)$  on average. The mean square length 'as the crow flies' of this chain of neutrons  $\langle l^2 \rangle$  can be estimated by multiplying the mean square distance that one single neutron travels, being  $6M^2$ , by the average number of fissions in a chain. Therefore the root mean square length of the prompt fission chain is:

$$\langle l^2 \rangle^{1/2} = Q \cdot M \quad (\text{II.18})$$



where

$$Q = \sqrt{\frac{6}{\beta - \rho}} \quad (\text{II.19})$$

This only holds in 3-dimensional models. In one dimension the value for  $Q$  is  $\sqrt{2/(\beta - \rho)}$ , since in that case the migration area has to be interpreted as half the mean square distance travelled by a neutron. Note that in writing the root mean square length of the prompt fission chain as in Eq. II.18, we have split it into a part that is mainly dependent on the reactor type ( $M$ ) and a part that is mainly dependent on the strength of the perturbation ( $Q$ ).

The source mentioned above can, for example, be the neutrons from the decay of the precursors. In fact, in a nuclear reactor these neutrons start the fission chain. So the kinetic behaviour of the system is heavily dependent on the behaviour of the precursor density. Since the decay times of the precursors are orders of magnitude longer than the time scales involved in the prompt processes, the precursors have a retardation effect. In particular, if the core is large with respect to the root mean square length of the chain of prompt neutrons, the influence of precursors is relatively important for parts of the reactor far away from the disturbance. In other words, if the size of the reactor is much larger than this root mean square length of the prompt chain then the different parts of the reactor are loosely coupled and large changes in shape in the neutron flux density and the precursor densities can occur.

So with the ratio of the mean square length of the prompt fission chain to the size of the reactor a quantitative measure of the importance of shape changes as mentioned above is obtained. However, defining  $\Theta$  to be the ratio of the characteristic size of a reactor to the migration length  $M$ , a quantitative comparison between the strength of the perturbation and the reactor type can be made as follows: If  $\Theta$ , which defines the reactor type, is large compared to  $Q$ , which defines the strength of the perturbation, the reactor is loosely coupled and the

shape changes are large. If it is small there is a strong coupling and only there are minor changes in flux shape.

## **II.2.5 Space-time dependent reciprocal period**

As stated before, the dynamic reactivity is a good measure to indicate the dynamic behaviour of reactors. To describe the time processes involved in more detail, however, we define another parameter, the space-time dependent reciprocal period, as follows:

$$\omega_0(E, \mathbf{r}, t) = \frac{1}{\varphi(E, \mathbf{r}, t)} \cdot \frac{\partial \varphi(E, \mathbf{r}, t)}{\partial t} \quad (\text{II.20})$$

and

$$\omega_i(\mathbf{r}, t) = \frac{1}{C_i(E, \mathbf{r}, t)} \cdot \frac{\partial C_i(\mathbf{r}, t)}{\partial t} \quad i = 1 \dots m \quad (\text{II.21})$$

If a parametric change, which is finite in time, is introduced to the system, all these space-time dependent reciprocal periods asymptotically have the same value  $\alpha_{as}$  as defined in section II.2.3. During the transient, however, they can be much smaller or larger, depending on the rate of change of the flux density or the precursor density at a particular position. With the space-time dependent reciprocal period it is, for example, possible to indicate at which positions either the prompt changes or changes in one of the precursor groups contribute most to the kinetic behaviour of the reactor at a certain point in time.

## II.3 Description of the numerical experiments

### II.3.1 Critical reactor models before the start of the transient

In the following results of numerical experiments with one-energy group, one-dimensional models of reactor cores with variable size are shown. In the numerical experiments we use a slab geometry with zero-flux boundary condition at  $x = 0$  and  $x = a$ , with  $a$  the size of the reactor model, and with zero buckling in the other two directions. For an initially homogeneous system the effective multiplication factor is:

$$k_{\text{eff}} = \frac{v\Sigma_f}{\Sigma_a \left( 1 + \left( \frac{\pi}{\Theta} \right)^2 \right)}, \quad \text{where } \Theta = \frac{a}{M} \quad (\text{II.22})$$

Since we are interested in the effect of different values of  $\Theta$  and start with an initially critical reactor, either  $v\Sigma_f$  or  $\Sigma_a$  or both have to be adjusted for the different reactor models. We choose to take  $v\Sigma_f$  to be constant, since this means that the generation time  $\Lambda = 1/(v\Sigma_f)$  is constant. The generation time plays a part in the kinetic behaviour, so changing this parameter surely obscures the results of the comparison for different  $\Theta$ .

As a starting-point homogenized one-energy group cross sections of a typical light water reactor from Fisher *et al* (1989) are taken. These values are modified to get a somewhat larger value of  $\Theta$  without having too large a core size (Table II.1). To generate reactor types with different  $\Theta$ , we change the size of the reactor model, keeping  $M$  constant. To get a critical reactor  $\Sigma_a$  is adjusted using Eq. II.22 with  $k_{\text{eff}} = 1$  and taking  $v\Sigma_f$  the same as in Table II.1. Since we use values for  $\Theta$  ranging from 10 to 300,  $k_{\infty}$  lies in between 1.0987 and 1.0001.

Six groups of precursors are used in the calculations. The values for the fractions  $\beta$  and the decay constants  $\lambda$  are given in Table II.2. The

Table II.1: Cross sections and other parameters used for a reactor model with  $\Theta = 100$ . Cross sections are modified values of Fisher *et al* (1989).

M	4.0 cm	a	400 cm
$\Theta$	100	$\Sigma_a$	$2.498 \cdot 10^{-2} \text{ cm}^{-1}$
$\nu \Sigma_f$	$2.5 \cdot 10^{-2} \text{ cm}^{-1}$	$\Lambda$	$1.818 \cdot 10^{-5} \text{ s}$
$\nu$	$2.2 \cdot 10^6 \text{ cm s}^{-1}$	$k_\infty$	1.001

data for these precursor groups are for Uranium-235 and taken from the JEF 2.2-library (OECD/NEA Data Bank, 1995).

### II.3.2 The perturbation

A small region of approximately 7% of the size of the reactor, that is called the rod region, is used to initiate the transient. In this region the absorption cross section  $\Sigma_a$  is suddenly reduced at  $t = 0 \text{ s}$ , introducing a positive reactivity. This may be interpreted as withdrawing a control rod. After this change in absorption cross section in the rod region, the configuration is no longer homogeneous. The position of the rod region can be anywhere in the reactor. To indicate the rod position we use the position of the middle of the rod region  $x_R$ . Since the reactor model without a rod region is symmetrical around  $x = a/2$ , only values of the rod position smaller than or equal to  $x_R/a = 1/2$  are used. The amount of reduction of  $\Sigma_a$  in the rod region is adjusted in such a way that the

Table II.2: Properties of the precursor groups. The values are the values for  $^{235}\text{U}$ , taken from the JEF2-2 Nuclear Data Library (OECD/NEA Data Bank, 1995)

group	$\lambda \text{ [ s}^{-1} \text{ ]}$	T [s]	$\beta \cdot 10^{-3}$	$\beta/\lambda \cdot 10^{-3}$	$(\beta/\lambda)/(\beta/\lambda)_6$
1	$1.27 \cdot 10^{-2}$	54.49	0.2345	18.45	160.5
2	$3.17 \cdot 10^{-2}$	21.84	1.2108	38.20	332.0
3	0.116	5.975	1.1560	9.966	86.6
4	0.311	2.229	2.5916	8.333	72.4
5	1.4	0.495	1.0624	0.759	6.6
6	3.87	0.179	0.4452	0.115	1
$\beta_{\text{total}} = 6.7006 \cdot 10^{-3}$					

asymptotic reactivity has a specific value. This is done by solving Eq. II.16 for the non-homogeneous configuration iteratively, adjusting the absorption cross section of the rod region until the eigenvalue, corresponding to the desired asymptotic reactivity, is reached.

It is already stated in section II.2.3 that this asymptotic reactivity can be seen as a measure of the strength of the perturbation. Therefore adjusting the absorption cross section and holding  $\rho_{\text{as}}$  constant for different reactor sizes, the effect of parameters like  $\Theta$  or the rod position on the space-time behaviour of different reactor models can be analysed.

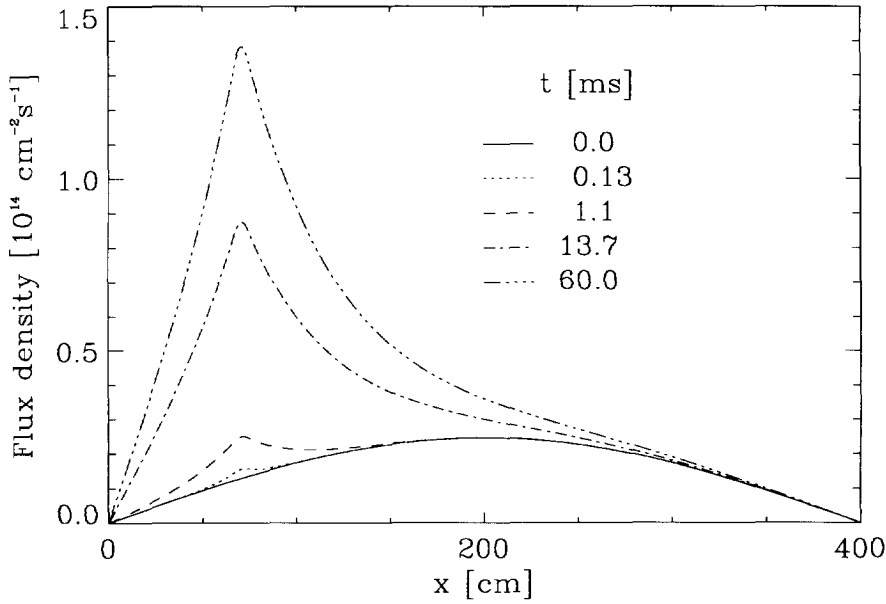


Figure II.1: Flux density for reactor with  $\Theta = 100$  in critical state at  $t = 0.00$  s and at  $t = 0.06$  s after the introduction of the perturbation.

### II.3.3 Computer code used in the experiments

In all calculations described below the space-time dependent diffusion code FX2-TH is used (Shober *et al*, 1978). This code solves the exact point-kinetic equation II.6 by the quasi-static algorithm. The algorithm uses the separation method explained in section II.2.1 by defining two different time scales. One is used to calculate the dynamic reactivity, whereas at a larger time scale the change in the time-dependent shape function is calculated. With a proper choice of the two time scales the method can obtain practically the same solution as by rigorous numerical calculations within smaller CPU-times (Ott & Meneley, 1969). The original version of FX2-TH is adapted in order to get not only the flux density but also the precursor density as a function of

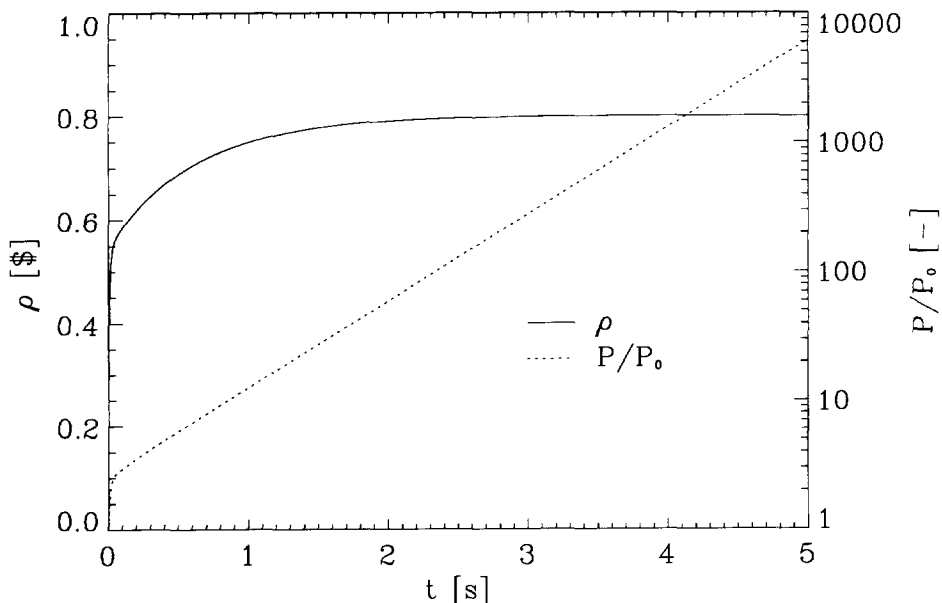


Figure II.2: Normalized power  $P/P_0$  and dynamic reactivity  $\rho$  versus time;  $\Theta = 100$

time in the output stream. With this modification it is possible to investigate the development of the precursor density in time after introduction of the perturbation.

### II.3.4 Behaviour of the reactor model with $\Theta = 100$

In this section we describe the space-time dependent effects in a reactor with parameters as defined in Table II.1 and Table II.2 and a change in absorption cross section in the rod region. The rod region lies between  $x = 67$  cm and  $x = 74$  cm. This rod position is chosen to give an asymmetrical asymptotic flux shape, without being too close to the boundary of the reactor. The asymptotic reactivity is  $0.8\text{\$}$ . For this reactor and with this perturbation  $Q = 38.6$  and according to Eq. II.18 the rms length of the chain of prompt neutrons is 155 cm.

In Figure II.1 the flux density at  $t = 0$  s and at some points in time after the introduction of the disturbance are plotted. At 13.7 ms the

flux density already changes considerably. This can be explained if we consider the time the chain of prompt neutrons needs to die away (Ott & Neuhold, 1985), which is  $\Lambda/(\beta-\rho)$  (13.6 ms in this case). Since the rms length of the chain is 155 cm, we expect that the major changes take place within a region around the rod position with a size of about 155 cm. Since the rod region lies only 67 cm from the left boundary the whole region between this boundary and the rod position is strongly influenced. At the right side of the rod region the major change is between the rod and about  $x = 225$  cm. Figure II.1 confirms this expectation.

The changes of the flux density are reflected in the dynamic reactivity and the power. In Figure II.2 both are drawn. As we reduce the absorption cross section in the rod region, the reactor is supercritical. This means that the average power increases exponentially at long times, which can be seen in the figure. In a short time interval after  $t = 0$  s, the dynamic reactivity rapidly increases to a certain level, which is smaller than its asymptotic value. Later on, the value of the dynamic reactivity slowly increases approaching the asymptote from below. To explain this behaviour we need to consider the behaviour of the delayed neutron precursors.

Therefore in Figure II.3 the flux density and the precursor density are plotted normalized to the integral over space for these functions. Because of this normalization only shape changes in time are seen. The average flux density and thus the power increase as shown in Figure II.2. The first plot of Figure II.3 is at 0.06 s, well after the die-away time of the prompt neutrons. We can see that at that time the shape of the flux density is already relatively close to its asymptotic shape. The shape of the density of the six precursor groups, however, changes so far very little. Especially the precursors with the smallest decay constant, indicated by  $C_1$ , keep the initial shape very long. After the decay of the chain of prompt neutrons the change of the shape of the precursors density is the only important source of changes in the reactor. This means that the change of the precursor densities is the only reason for the flux density to change its shape. This can be seen in Eq. II.1, where the balance of the first three terms at the right-hand side



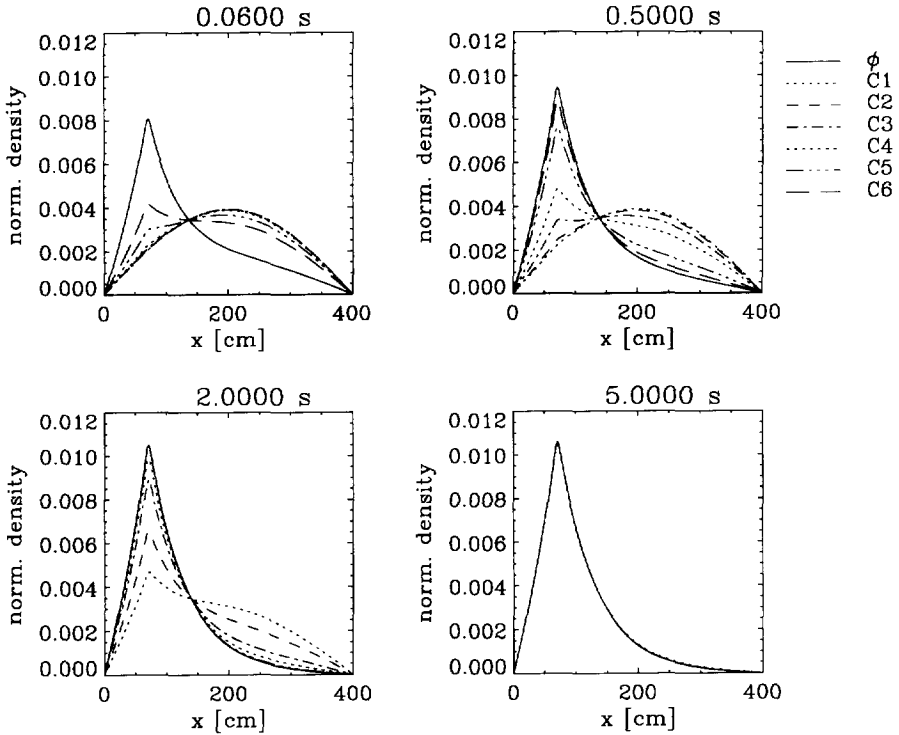


Figure II.3: Normalized flux and precursor densities versus position for different times;  $\Theta = 100$

of the upper equation is established quickly and the major change at longer times is in the summation over  $C_i$ .

To address these delicate processes in time in more detail, the space-time dependent reciprocal periods versus time for different positions and versus position for different times are plotted in Figure II.4 and Figure II.5. From these figures, the general tendency for  $\omega_0$  can be described as follows. First the values are quite large, especially for positions close to the rod region. Then, after a transition period, the values approach an asymptotic value. The maximum value in the rod region is reached within  $100 \mu\text{s}$ , so within approximately  $5 \Lambda$ . The way the curves approach that value in the transition period

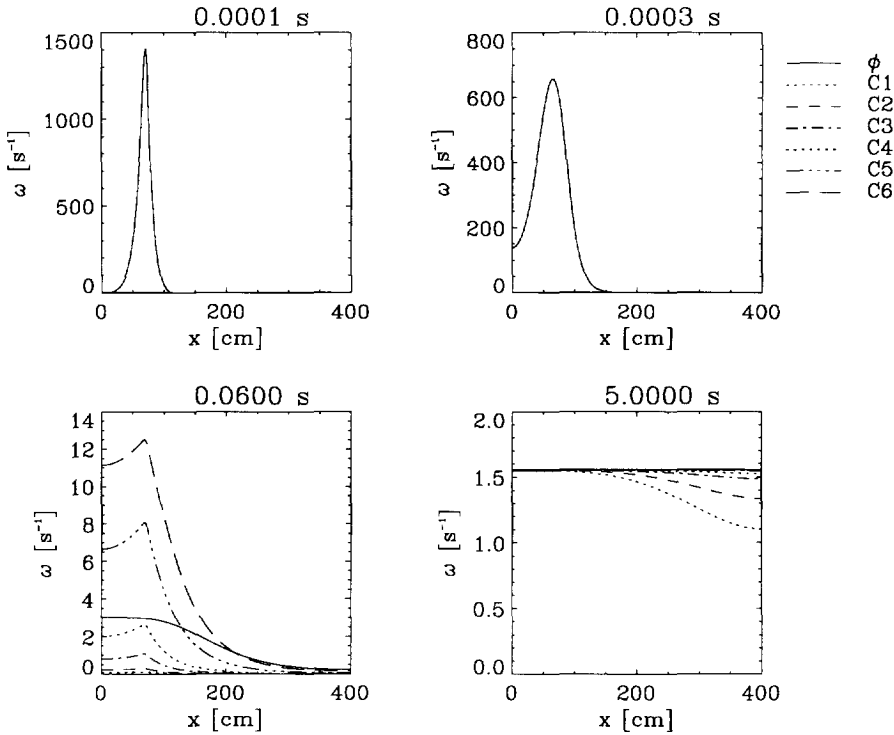


Figure II.4: Space-time dependent reciprocal periods versus position for different points in time

depends heavily on the position with respect to the rod region. For positions close to the rod region, the curves decrease monotonically after their initial increase, so approaching the asymptotic value from above. For remote regions the values for  $\omega_0$  of the neutron flux distribution can be lower than the asymptotic value in the transition period. For these regions the asymptotic value is approached from below. For the space-time dependent reciprocal periods corresponding to the six different precursor groups a similar behaviour can be seen for the last three groups, with the largest decay constants, in the vicinity of the rod region. The maximum, though, is reached much later in time. For the reciprocal periods of the groups with the smallest

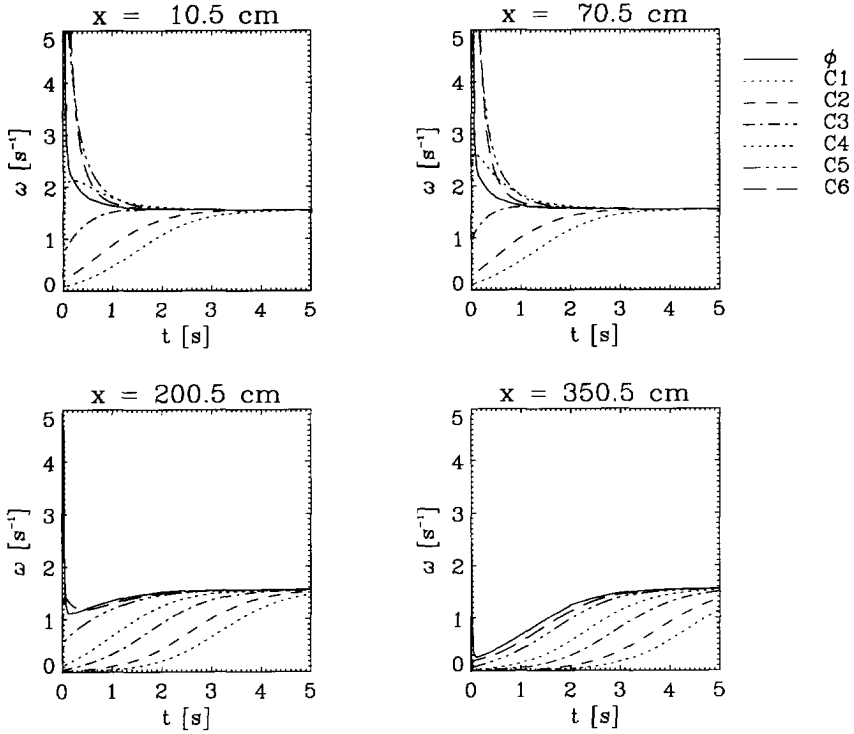


Figure II.5: Space-time dependent reciprocal periods versus time for different positions. Position  $x = 70.5$  cm is the middle of the rod region.

decay constants and for the ones for positions far away from the rod region, the values are always smaller than the asymptotic value.

The asymptotic value of the reciprocal period  $\alpha_{as}$  can be calculated also by solving Eq. II.17. The asymptotic reactivity  $\rho_{as}$ , which is needed to solve the inhour equation is obtained by solving Eq. II.16 for the non-homogeneous reactor with the disturbance. Doing so the value for  $\alpha_{as}$  appears to be  $1.54 \text{ s}^{-1}$ . The value of  $\omega_0$  averaged over space at  $t = 5.0 \text{ s}$ , obtained from the numerical experiments is  $1.55 \text{ s}^{-1}$ . The difference is about 1%, which can be explained by numerical rounding errors.

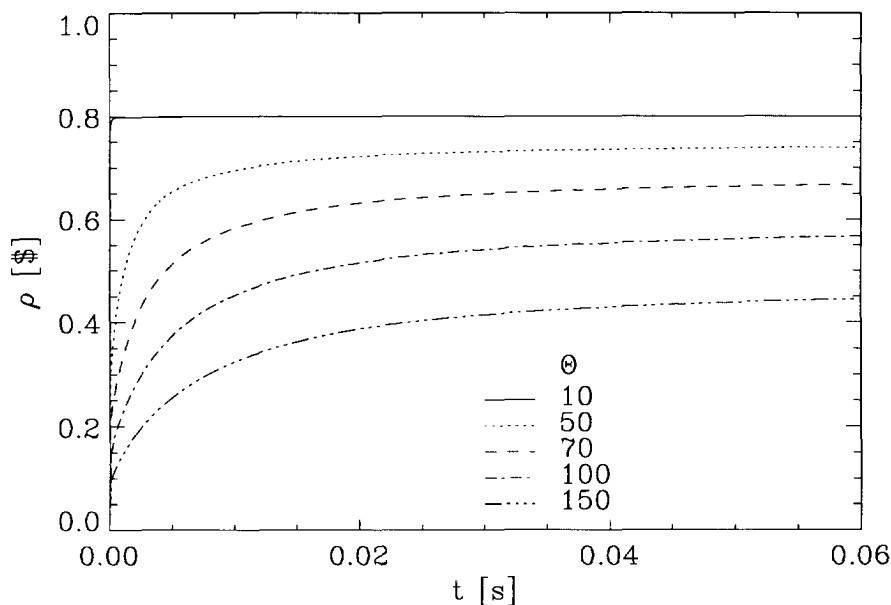


Figure II.6: Dynamic reactivity versus time for different values of the ratio  $\Theta$  of the size of the reactor to the migration length.

The way the reciprocal periods for the different precursor groups relate, needs some comments. Precursor groups with the largest decay constants have the strongest effect on the first few seconds of the development of the dynamic reactivity, because the relative changes in precursor densities are the highest for these groups. The longest living precursors have a higher equilibrium density, so their relative change is rather small in the initial stage of the transient.

### II.3.5 Reactors with different sizes

So far the behaviour of only one reactor has been described. Varying the size of the reactor will have an important effect as can be seen in Figure II.6. In this figure the dynamic reactivity as a function of time is plotted for several values of  $\Theta$  after introduction of a perturbation similar to the previous example. The absorption cross section in the rod

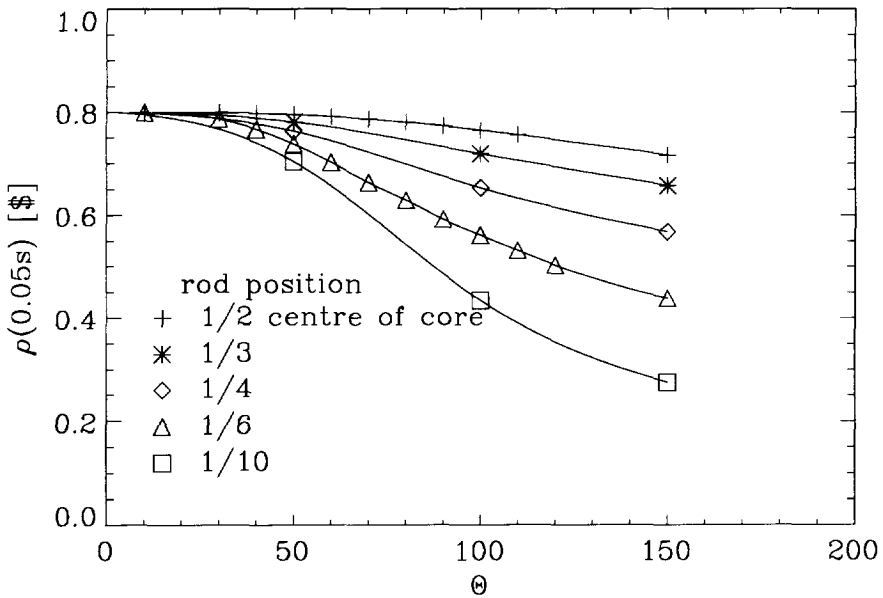


Figure II.7: Dynamic reactivity at  $t = 0.05$  s versus  $\Theta$  for different rod positions. Symbols indicate the difference in rod position.

region is decreased in such a way, that the asymptotic reactivity  $\rho_{as}$  is 0.8\$ in all reactor models. The rod position is  $x_R/a = 1/6$  in all cases. The value for  $Q$  is again 39. This means that for reactor cores with  $\Theta$  much larger than 39, the changes in shape are significant and the development of the dynamic reactivity to its asymptotic value is much slower.

It can be seen in the figure that at every point in time the reactivity of the reactor core with the largest value of  $\Theta$  is smaller than that of smaller cores. To investigate these differences in more detail, we compare the values of the dynamic reactivity at  $t = 0.05$  s (Figure II.7). As we can see, the dynamic reactivity at  $t = 0.05$  s depends on the ratio of the size of the reactor to the migration length. For all rod positions, the tendency is the same. For small values of  $\Theta$ , the dynamic reactivity is very close to its asymptotic value already at this point in time. Going

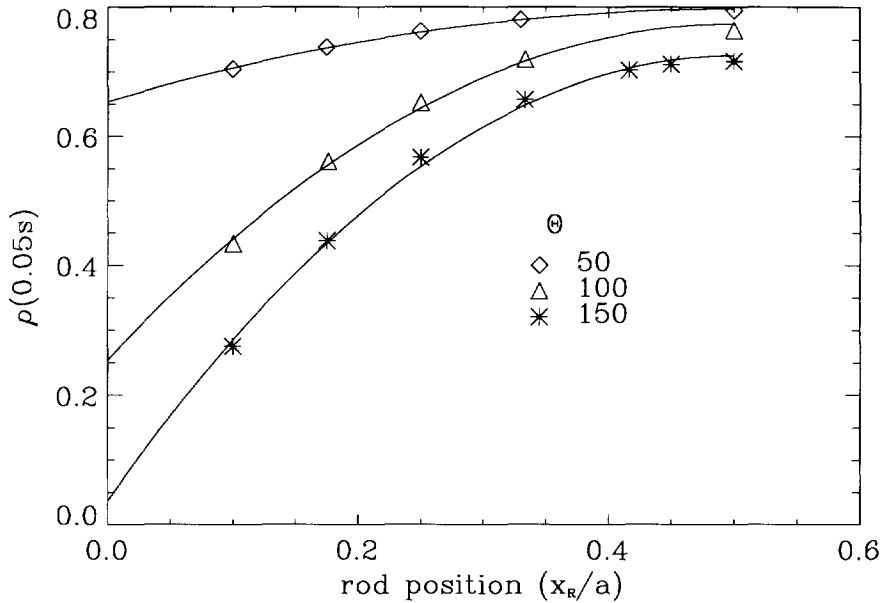


Figure II.8: Dynamic reactivity versus rod position for three different values of  $\Theta$ : 50, 100 and 150. The solid lines are second-order polynomial fits.

to reactor types with larger  $\Theta$ , the deviation increases. The dynamic reactivity does not only depend heavily on the size of the reactor, but also on the position of the rod region.

In Figure II.8 the dependency on the position of the rod region is shown for three values of  $\Theta$ . The solid lines are second-order polynomial fits to the points. The fact that a second-order polynomial fits well can be explained heuristically as follows. Going from the middle of the core to the boundary, the distance to the opposite boundary becomes larger, linearly with the rod position. Therefore it becomes increasingly difficult for the chain of prompt neutrons to spread out over the whole reactor. On the other hand moving the rod position to the boundary will make the asymptotic flux shape more asymmetrical. The asymmetry will be roughly linear with the rod position. Since the shape of the precursor density has to change more in a more asymmetrical case, the change of the dynamic reactivity will

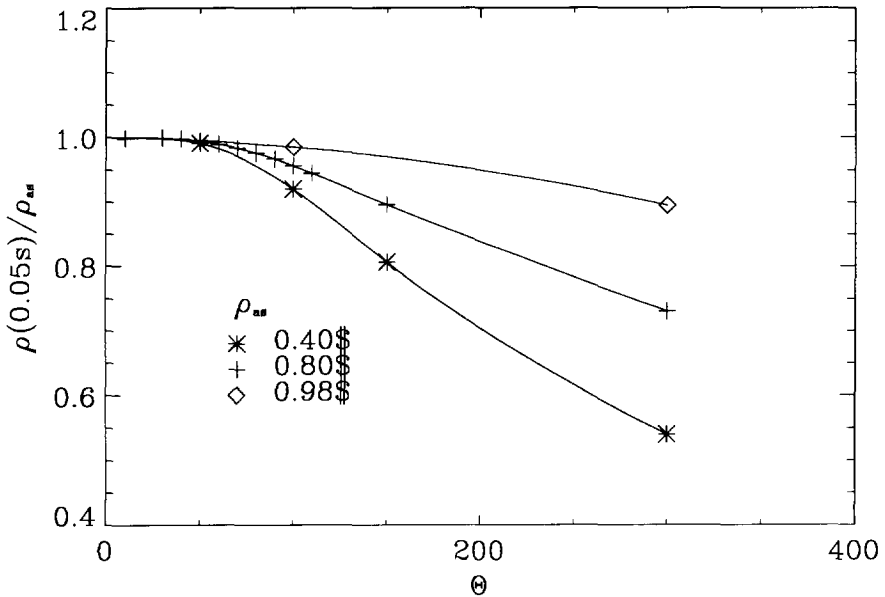


Figure II.9: The dynamic reactivity at  $t = 0.05$  s relative to the asymptotic reactivity versus  $\Theta$ , for different asymptotic reactivities. The relative rod position is  $1/2$ .

take a longer time. Both effects, the distance to the opposite boundary and the asymmetry, act in the same direction, which explains the parabolic shape of the dynamic reactivity versus the rod position curve.

Up to now the asymptotic reactivity is  $0.8\$$  in all cases. However, the strength of the perturbation will also have an effect on the behaviour of the reactor. Therefore in Figure II.9 the dynamic reactivity at  $t = 0.05$  s relative to the asymptotic reactivity is plotted as a function of  $\Theta$  for different asymptotic reactivities. The position of the rod region is always  $x_R/a = 1/2$ . From Figure II.9 it is clear that for systems with equal  $\Theta$ , the smaller the asymptotic reactivity, the lower the relative reactivity at  $0.05$  s. In other words a stronger perturbation will cause the same reactor to be more strongly coupled than a weak perturbation.

To compare the influence of the strength of the perturbation better, in Figure II.10 the relative reactivity at  $0.05$  s is plotted versus  $\Theta/Q$ . As

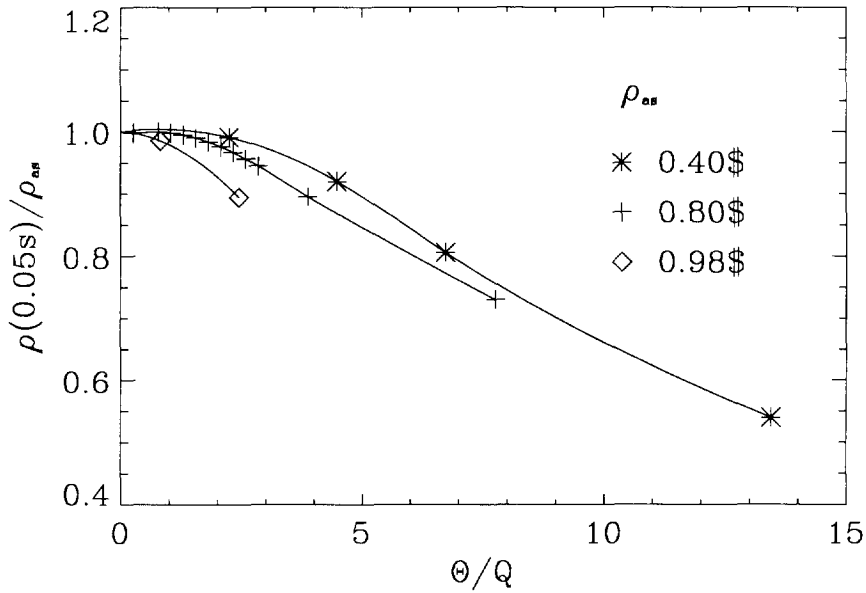


Figure II.10: The normalized dynamic reactivity at  $t = 0.05$  s versus  $\Theta/Q$  for different asymptotic reactivities. The rod position is  $1/2$ .

we can see the larger the ratio of  $\Theta/Q$  the smaller the relative reactivity at  $0.05$  s. This confirms the theory that the larger the value of  $\Theta$  compared to  $Q$ , the more loosely coupled the system.

## II.4 Discussion

First we give some comments on the calculation of the rms length of the chain of prompt neutrons. The interpretation of the migration length as "1/6th of the root mean square distance a neutron travels from its appearance as a fast neutron to its capture as a thermal neutron" is only valid in an infinite three-dimensional homogeneous medium. Therefore strictly speaking the actual root mean square value of the distance in our cases differs. However, it is impossible to calculate this distance in general analytically and the migration length can really be seen as a first approximation to this distance. Using  $M$  makes it possible to get an indication of the reactor physical dimension



of a reactor core. For the estimation of the number of fissions in the prompt fission chain the restriction of a finite homogeneous medium also holds. Again using this value in our calculation is not fully correct, but it gives a fair indication. Therefore the value  $Q$  in Eq. II.19 can be seen as a measure to indicate whether a given reactor can be interpreted as a small reactor, for which simple codes are good enough, or it is more like a large reactor, for which complicated codes have to be used.

Although in the numerical experiments only asymptotic reactivities between 0 and  $1\beta$  are shown, for negative reactivities no fundamental differences appear; the larger the subcriticality the larger the influence of shape changes in the reactor. However, the way the dynamic reactivity reacts to a sudden decrease of the reactivity is quite different. First the dynamic reactivity jumps to a large negative value, but later on it becomes less negative, due to the flux shape change.

For asymptotic reactivities above  $1\beta$  the prompt fission chain does not die away anymore, but will either remain forever in the case of a reactivity of  $1\beta$  or even increase when the reactivity is larger than  $1\beta$ . This means that in that case shape changes of the precursor densities are no longer important and the reactor is strongly coupled anyway.

All reactor cores are one-dimensional, one-energy group, initially homogeneous models, in which only the absorption cross section is changed. On one hand this is to avoid time consuming calculations. On the other hand simple analytical expressions can be given for the flux density, the density of the precursors in the initial stable situations, the migration length and the chain of prompt neutrons. An advantage of keeping the fission cross section constant is that the effective parameters  $\Lambda$  and  $\beta$  remain constant during the transient. If calculations had been performed using either more energy groups or changing the fission cross section, then comparison between different models would be obscured by the change in these parameters.

As a rough estimation whether a certain type of reactor needs the inclusion of advanced computer codes to get reliable results for the space-time behaviour, the concept of relating the size of that reactor in units of the migration length  $\Theta$  to the  $Q$  value as in Eq. II.19 can be

used effectively. As shown in the one dimensional one-energy group calculations, for values of  $\Theta$  smaller than  $Q$ , the reactor can be treated with simple algorithms like the conventional point-kinetics approach. In cases with values of  $\Theta$  larger than  $Q$  space-time dependent processes can be seen, which require the use of more complicated methods. On the basis of the previous analyses one can expect that the adiabatic method, for example, can be used for reactors with intermediate values of  $\Theta$  relative to  $Q$ . In the adiabatic method, namely, the retardation effect in the change of the shape of the precursors is neglected by taking the precursor density proportional to the flux density at every moment in time. In that case the shape changes are overestimated, but the calculated dynamic reactivity will only differ from the actual dynamic reactivity during a relatively short time. Of course, if the perturbation changes faster and in cases where  $\Theta$  is much larger than  $Q$ , algorithms like the quasi-static method or methods that solve the space-time dependent diffusion equations rigorously are inevitable.

As said in the introduction no thermo-hydraulics is taken into account. This, though, will influence the space-time behaviour of a reactor considerably, so the theory presented above only is approximately valid. Depending on the kind of thermo-hydraulic feedback the spatial changes of the neutronics can be enhanced as, for example, in boiling water reactors (March-Leuba & Blakeman, 1991). However, it is still worthwhile to look at the value of  $\Theta$  in relation to  $Q$ , because in case of large  $\Theta$  the reactor is loosely coupled and therefore more sensitive to spatial changes. These changes can be initiated by thermal-hydraulic events.

## **II.5 Conclusion**

We showed the importance of the behaviour of the precursor groups on the behaviour of the reactor. We also focused on how the densities of these precursor groups develop in a model of a large light water reactor. Introducing the space-time dependent reciprocal period, a good distinction in time and space could be made as to which part of the reactor at a certain point in time contributed most to the kinetic

behaviour of the reactor. It could also be used to distinguish between the behaviour of the flux density and the density of the different precursor groups. A remarkable effect was the difference in behaviour of these reciprocal periods for regions in the vicinity of the perturbation and for areas farther away.

As far as the comparison of the behaviour of different reactors is concerned, the concept of relating the ratio of the size of the reactor and the migration length to the  $Q$  value of Eq. II.19 was useful. Although it could be used only as a rough estimate, it could be valuable in deciding which code one had to use in the calculation of the space-time kinetic behaviour of a specific reactor.

# **Chapter III**

## **Measurements of fast transients in a nuclear research reactor**

### **III.1 Introduction**

In safety analyses for nuclear reactors, the unanticipated ejection of a control rod is a major concern. Much effort is done to calculate the consequences of such an incident. In addition to such calculations well-controlled experiments of such fast transients are still valuable. They can give more insight into the physics of the dynamics of a reactor. Especially the changes of the flux shape during the transients are not fully understood. Therefore we performed some experiments, in which one of our objective was to measure the changes of the flux shape during fast transients. The experiments were also used to investigate whether small self-powered neutron detectors could measure the flux in such low power reactors. A third reason for the experiments was to get experience with experimental techniques in nuclear reactor and to measure the influence of the thermal-hydraulics on the spatial behaviour of the neutron flux. In this chapter we describe the experiments, which were done in March 1994 in the reactor of the Technical University of Budapest, and show the results.

### III.2 Investigation of the existence of shape changes of the flux

As said before our main objective for the experiments is to investigate the changes in the shape of the flux during a transient. In chapter II it is already shown that the neutron flux can be factorized into an amplitude part  $n(t)$  and a time-dependent shape function  $\psi(E, \mathbf{r}, t)$ :

$$\varphi(E, \mathbf{r}, t) = n(t) \psi(E, \mathbf{r}, t) \quad (\text{III.1})$$

If no changes occur in the flux shape, the shape function will no longer be time-dependent:  $\psi(E, \mathbf{r}, t) = \psi(E, \mathbf{r}, t=0) = \psi_0(E, \mathbf{r})$ . This means that the flux can be separated into a time-dependent part  $\tilde{n}(t)$  and a space-dependent part  $\psi_0(E, \mathbf{r})$ :

$$\varphi(E, \mathbf{r}, t) \approx n(t) \psi_0(E, \mathbf{r}) \quad (\text{III.2})$$

This method of factorization is usually called the conventional point kinetic approach.

With the definition shown above a more specific question can be posed in our experiments: is it possible to measure deviations from the point kinetic behavior in the small research reactor of Budapest? If so this shows the existence of shape changes during the transient, if not the much more easy way of point kinetic modelling can be used to calculate the dynamic behavior of this small research reactor.

Suppose the signal of the detectors is proportional to the flux at the position of the detector as follows:

$$h_i(t) = \int_{V_i} \int_E s_i(E) \varphi(E, \mathbf{r}, t) dE dV \quad (\text{III.3})$$

where  $h_i(t)$  is the response of detector  $i$ ,  $V_i$  is the effective volume of detector  $i$  and  $s_i(E)$  is the sensitivity of the detector. If point kinetics is applicable, one could rewrite the above equation as follows:

$$h_i(t) = n(t) \int_{V_i} \int_E s_i(E) \psi_0(E, \mathbf{r}) dE dV \equiv n(t) h_{i,0} \quad (\text{III.4})$$

Defining the normalized detector response  $h_i^N(t)$  as the ratio of the detector response and the response at  $t = 0$  s this normalized response becomes independent of the position of the detector, if point kinetics holds:

$$h_i^N(t) \equiv \frac{h_i(t)}{h_i(0)} \approx \frac{n(t) h_{i,0}}{n(0) h_{i,0}} = \frac{1}{n(0)} n(t) \quad (\text{III.5})$$

This means that differences in the time response of the normalized detector signals show that changes of the flux shape occur. Taking one detector as a reference, the ratio of the normalized signals of the other detectors to this reference provides an easy way of testing whether point kinetics holds. If this ratio differs significantly from 1, this is an indication that shape changes of the flux during the transient occur and that point-kinetics fails.

### III.3 The experimental setup

#### III.3.1 The reactor

The nuclear research reactor of the Technical University of Budapest is located in the courtyard of the university near the Danube (Csom & Lévai, 1983). The reactor is a tank-type swimming pool with water used as coolant and moderator. Since the reactor is designed for education and scientific research in the field of nuclear engineering and nuclear energy, it is only operational during experiments, irradiations

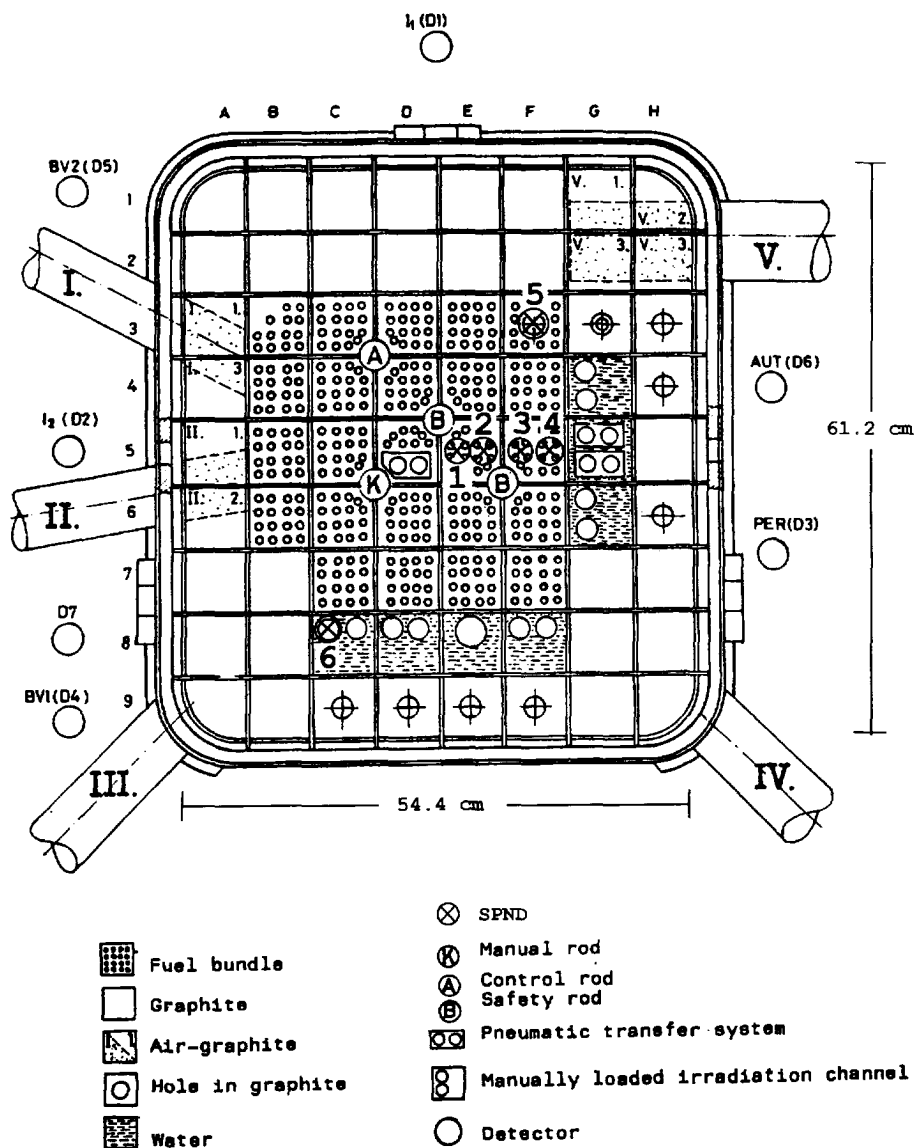


Figure III.1: Horizontal cross section of the reactor of the Technical University of Budapest (Csom & Lévai, 1983). The numbers 1 to 6 indicate the positions of the different self-powered neutron detectors used in the experiment. The transfer systems at D5 and G5 are used to shoot the cadmium into and out of the core

and training and is shut down in between. The maximum allowable power during operation is 100 kW. During operation at high power, which is about 10 kW or higher for this reactor, the core must be cooled by forced circulation cooling. The flow rate of the coolant is then  $6 \text{ m}^3/\text{h}$ .

In Figure III.1 a horizontal cross section of the reactor is drawn. The control rod, which is shown by A in the figure, is an automatic one. This rod normally controls the reactor. The manual control rod (K) is mainly used to compensate the burn-up of the fuel, whereas the two safety rods (B) are used to shut down the reactor in case of an emergency or at the end of normal operation. The graphite around the fuel bundles and the water gaps serve as a reflector. In the middle of the core at position D5 and in the reflector at position G5 pneumatic transfer systems are available, which are normally used for irradiation experiments.

The core itself consists of 24 fuel bundles of  $6.8 \text{ cm} \times 6.8 \text{ cm}$ , with 16 rod-shaped fuel elements each and a active height of 50 cm. The fuel type is  $\text{UO}_2$ , which is enriched to 10% in  $^{235}\text{U}$ . For the cold reactor the critical mass is 2740 g of  $^{235}\text{U}$ . At the first startup in 1971 the total mass of  $^{235}\text{U}$  in the core was 2952 g. In March 1994, when our experiments take place, the fuel elements of 1971 are still being used and due to the burn-up only just enough excess reactivity is left to operate the reactor and to do our measurements.

### III.3.2 The detectors and other measuring devices

As said before our main objective is to measure shape changes of the flux during the transients. Care is taken to put the detectors as close to the transfer system as possible. To achieve this objective self-powered neutron detectors are used, small enough to fit between the fuel elements in a fuel bundle. The emitter material of the detectors is Hafnium. As indicated in Figure III.1 four detectors are put in the middle of the reactor at positions E5 and F5. The distance of the detector closest to the transfer system at D5, indicated by 1, is approximately 4 cm. The distances of the other three detectors,



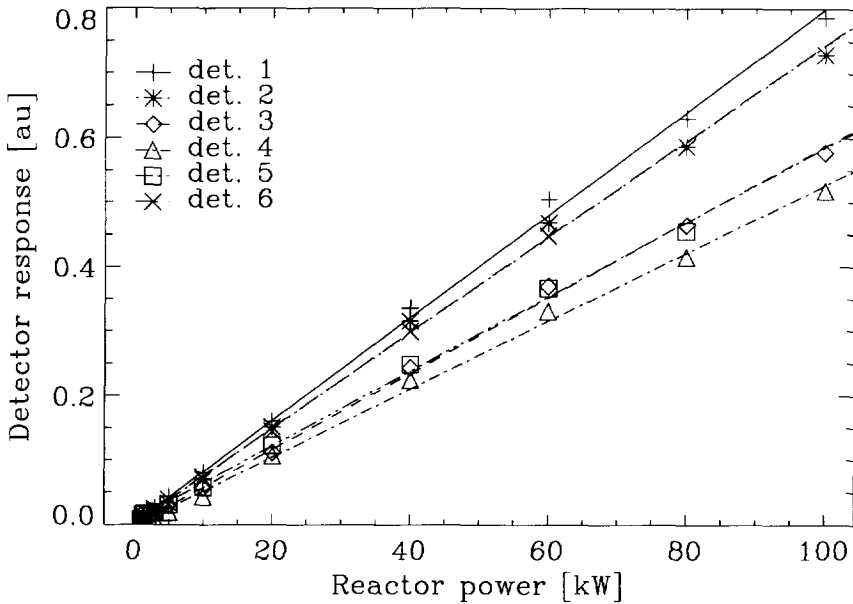


Figure III.2: The calibration of the detectors. The straight lines are linear fits to the curves.

indicated by 2, 3 and 4, are 7, 11 and 14 cm, respectively. Besides these four detectors, two detectors are put at a larger distance from the transfer system; one at F3 and one at C8, indicated by 5 and 6, respectively.

The signals of the detectors are amplified and sampled directly with a sample frequency of 60 Hz. The data is put on diskettes and analysed off-line at our institute in Delft. Information about the core temperature, the temperatures before and after the heat exchanger, the water level, the pressure and the flow rate and the reactor power, as indicated by the reactor instrumentation, is logged manually every minute.

### III.3.3 The experiments

To simulate the withdrawal of control rods in our experiments, we use the pneumatic transfer systems to shoot a small piece of cadmium into and out of the reactor. The reactivity value of the cadmium is measured by the control rod compensation method, for which the automatic control rod is used. The reactivity value of the piece of cadmium at position D5, so in the middle of the core, and at a power of 10 W is 17¢. In the reflector the reactivity value of that piece of cadmium is 2.5¢. Several

Table III.1: Relative standard deviation of the first 100 seconds at a stationary power of 60 kW and 10 kW.

Detector	std./mean at 60 kW [%]	std./mean at 10 kW [%]
1	1.5	10
2	1.7	11
3	2.0	13
4	2.3	17
5	0.4	2.0
6	0.2	1.6

transient experiments are done. The difference between the experiments is either the starting power, ranging from 5 to 100 kW, or the way the cadmium piece move, i.e., into or out of the core.

Before the actual transient measurements, we do several stationary experiments at different power levels. This is done in order to calibrate our detectors. Since we operate the self-powered neutron detectors in a power range which is lower than the normal range of the detectors, we want to be sure that the response of the detectors is linear with respect to the reactor power.

Figure III.2 gives an overview of results of the calibration. The symbols show the measured responses of the detectors. The lines are linear fits to the points. As can be seen between about 5 and 100 kW, which is the range used in the experiments, the responses of the detector are linear.

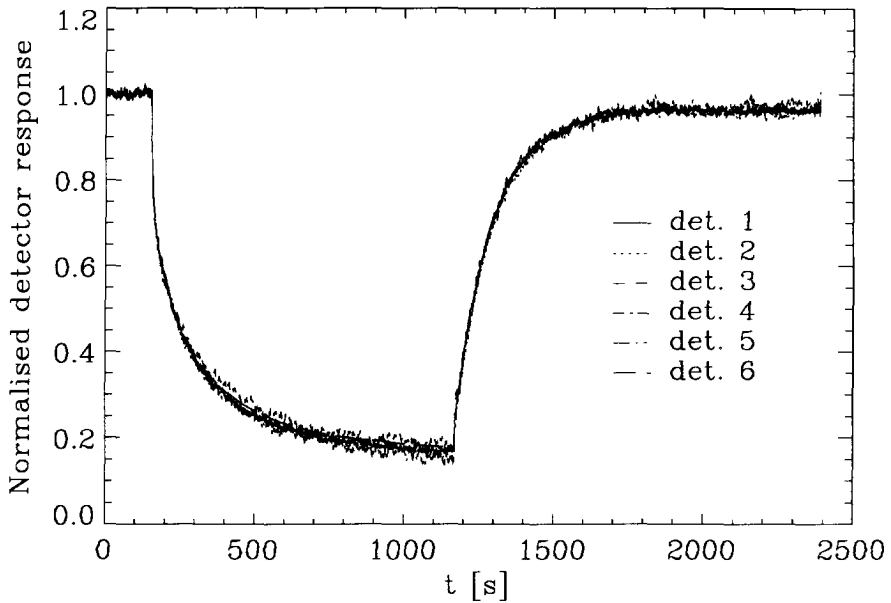


Figure III.3: Transient measurement using the transfer system at D5. At about 180 s the cadmium piece is shot into the reactor. At about 1200 s it is shot out of the reactor again. Initial power is 60 kW.

### III.4 Results of the measurements

#### III.4.1 Transient with an initial reactor power of 60 kW

The first experiment that will be shown here is a transient experiment, in which the transfer system at D5 in the middle of the core is used. The reactor is made critical at a power of 60 kW and before the measurement is started we wait for about 15 minutes to have a power level as stable as possible. After about 180 s from the start of the measurement the piece of cadmium is shot into the reactor and the reactor power drops to about 10 kW. After about 1180 seconds the piece of cadmium is shot out of the core and the reactor power increases again to about 57 kW.

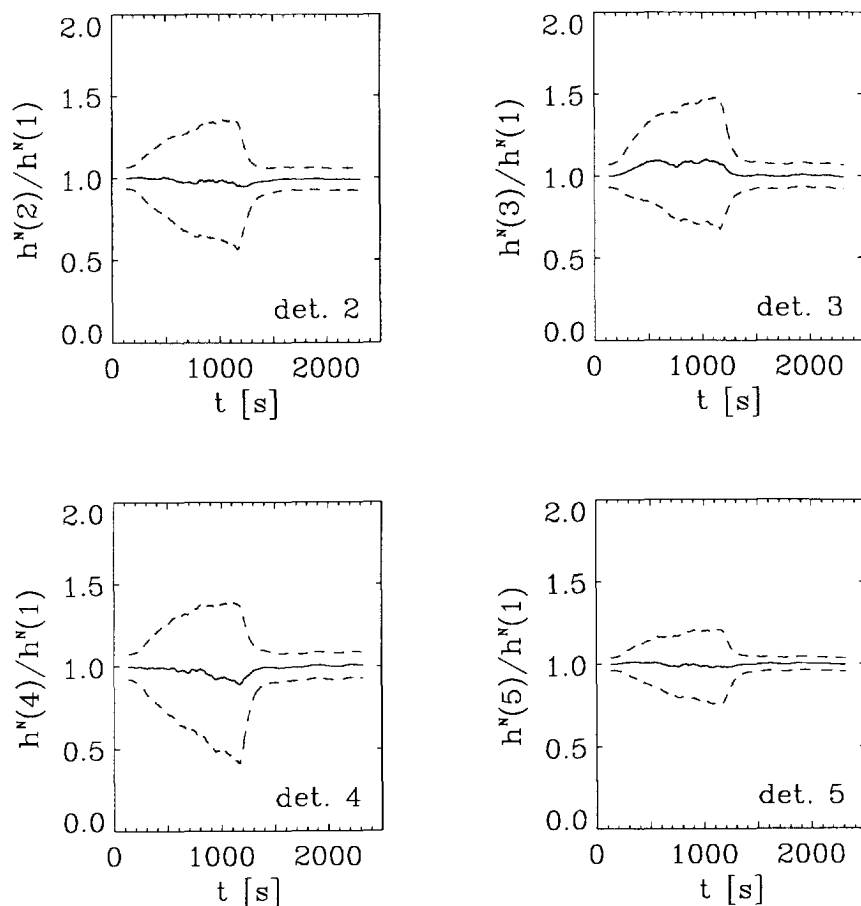


Figure III.4: Normalized detector responses of detectors 2, 3, 4 and 5 relative to the normalized response of detector 1 during the transient of the first experiment. The dashed lines indicate the  $2\sigma$  error bands.

In Figure III.3 the normalized responses of all self-powered neutron detectors, smoothed digitally by a rectangular moving average filter of 9 points, are shown. The mean of the first 100 seconds of the measurement is taken as the normalization value. The relative standard deviation of these values for this experiment is shown in the second column of Table III.1. As can be seen, the values for detectors 5 and 6

are an order of magnitude smaller than the other values. This is because the two detectors are more sensitive since they are longer than the other ones.

From the figure one can observe that all curves approximately fall together. Especially immediately after the movement of the cadmium piece, no distinction can be made between the response of the detectors. As explained before this would show that point-kinetics is valid in this reactor. This conclusion is confirmed in the next figure (Figure III.4), where we plot the ratio of the normalized responses of detectors 2, 3, 4 and 5 to the response of reference detector 1, which is closest to the transfer system. Before taking the ratio of the curves the signals are smoothed digitally with a rectangular moving average filter of 1023 points. To show the influence of the statistical error in the normalization value the curves of twice the standard deviation are also drawn. From the figure it can be concluded that no evidence for flux shape changes during the transient can be found and point kinetic theory can be applied to model the dynamics of this small reactor.

#### **III.4.2 Transient with an initial reactor power of 10 kW**

To see the influence of another initial power level in Figure III.5, results of a similar experiment at an initial reactor power of 10 kW are shown. In this experiment, however, the piece of cadmium is shot into the reactor before making the reactor critical at 10 kW. After that the measurement is started and about 150 seconds later the piece of cadmium is shot out of the reactor. The reactor power increases to about 60 kW and after approximately 1100 seconds the cadmium piece is shot into the reactor again. The power decreases to about 10 kW. Now it seems that we can observe a large difference in the way of curves behave during the transient. However, as indicated in Table III.1 the relative error in the normalization values is much larger, since we start at a much lower power. Therefore the statistical error during the transient is also larger.

The importance of normalization can be seen in Figure III.6. In this figure the normalization of the detector responses is done with values

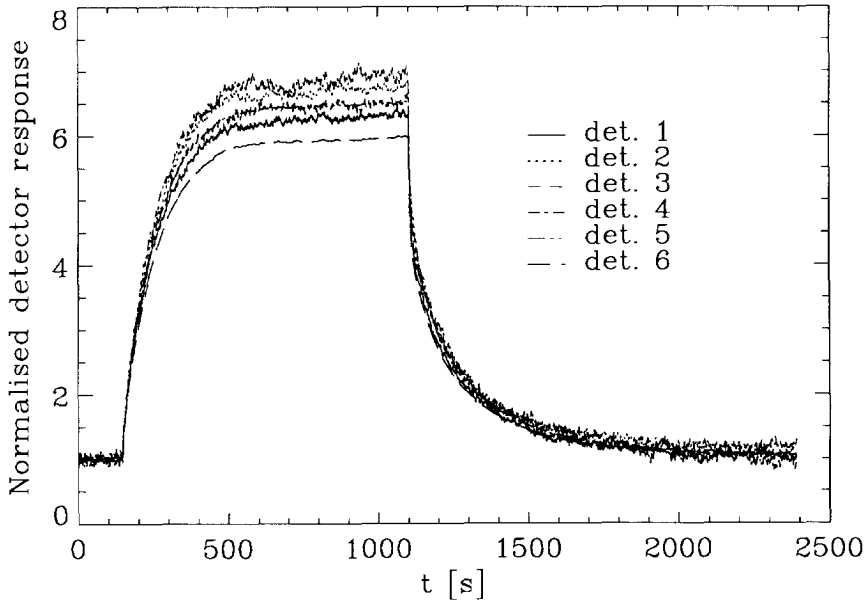


Figure III.5: Transient measurement using the transfer system at D5. At about 180 s the cadmium piece is shot out of the reactor. At about 1100 s it is shot into the reactor again. Initial power is 10 kW. Normalization values are taken from the first 100 seconds of the measurement.

from the calibration curves as in Figure III.2. The coefficients of the different calibration curves are used to calculate the value at 10 kW. As can be seen in Figure III.6 the curves are much more similar. Again no evidence of shape changes can be found.

#### III.4.3 Transient using the transfer system at G5

The last example of the series of experiments is an experiment in which the transfer system at G5 is used to shoot the piece of cadmium. As previously mentioned the change in reactivity is now much smaller: about 2.5 $\delta$ . The initial reactor power is stabilized at 60 kW. First the piece of cadmium is shot into the reactor at  $t = 160$  s. After about 620 s the piece is shot out of the reactor again. As we can see in Figure III.7,

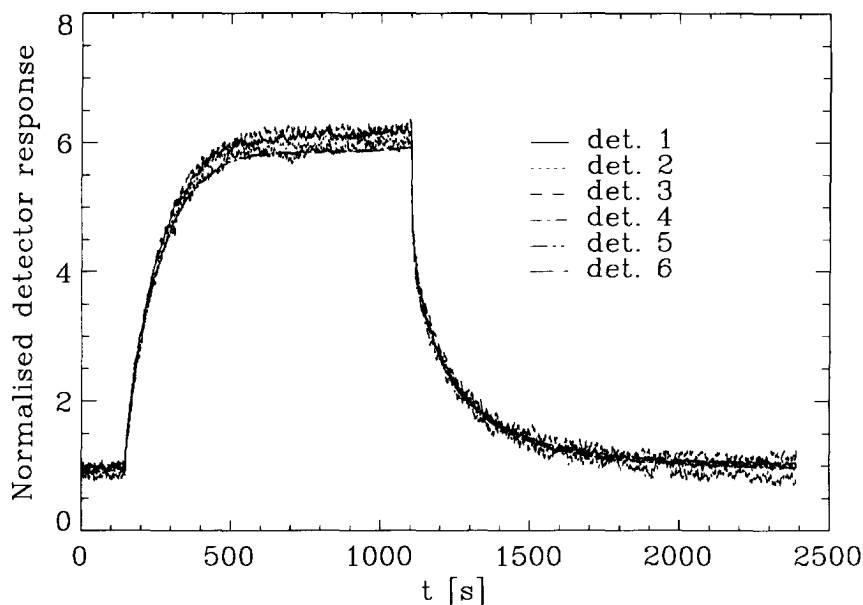


Figure III.6: Transient measurement using the transfer system at D5. At about 180 s the cadmium piece is shot out of the reactor. At about 1100 s it is shot into the reactor again. Initial power is 10 kW. Normalization values are taken from the calibration of Figure III.2

the same conclusion holds as before. The normalized responses of the detectors do not show significant differences.

### III.5 Discussion and conclusion

Although only the results of three experiments are shown above, we have analysed the experiments at other initial power levels as well. In none of the experiments we can find evidence of a change of the flux shape during the transient.

An important reason for the lack of evidence for shape changes is that the space-dependent effect for small reactors like the one used in these experiments will be very small, as shown in chapter II. With a

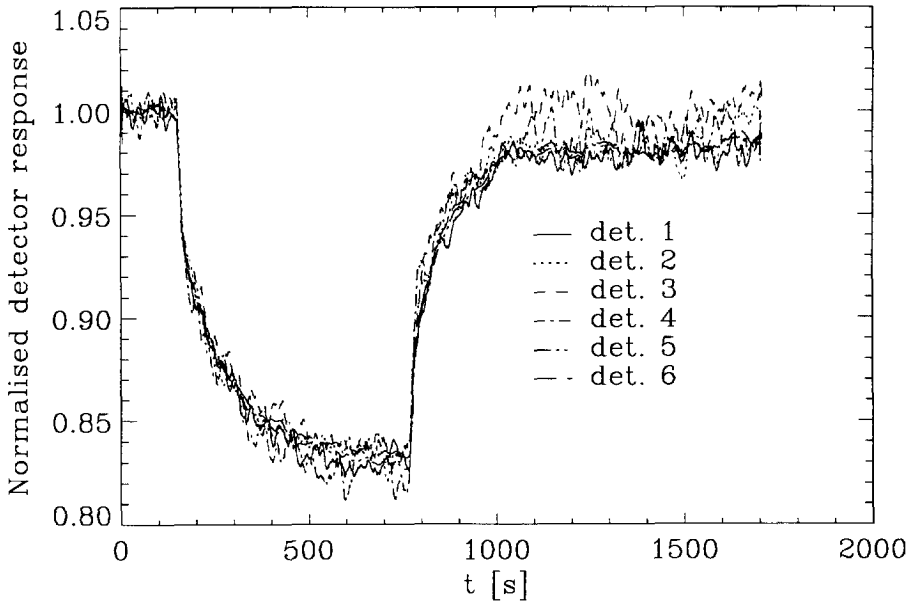


Figure III.7: Transient measurement using the transfer system at G5. At about 160 s the cadmium piece is shot into the reactor. At about 790 s it is shot out of the reactor again. Initial power is 60 kW. Normalization values are taken from the first 100 seconds of the measurement.

migration length in this reactor of about 7 cm, a delayed neutron fraction  $\beta$  of about 0.007 and an inserted reactivity of 0.17\$ in case of using the transfer system at D5 we can learn from chapter II that  $Q$  is 19 and the length of the fission chain is about 130 cm. Since this length is much larger than the characteristic size of 60 cm for this reactor, only minor changes are expected. If we use the transfer system at G5, which causes a reactivity change of 0.025\$, the value for  $Q$  is 17 and the length of the fission chain is 120 cm, which is also much larger than the size of the reactor.

A second reason for the lack of evidence for shape changes in our measurements is that the detectors are not sufficiently sensitive. Although the self-powered neutron detectors responded surprisingly



well, to measure the tiny change in the flux shape they are still not sensitive enough due to too much background noise. Consequently one needs to have detectors that have larger effective volumes. However, only limited space for the detectors is available since the detectors have to fit between the fuel elements. If they are put outside the core, the distance between the disturber and the detectors becomes too large.

Another possibility of increasing the signal-to-noise ratio in the measurements is to repeat the experiment in a sort of boxcar manner. In such experiments the piece of cadmium is shot into and out of the reactor several times. Using the start of the movement of the cadmium as a trigger for the measurement and averaging the result, a better signal-to-noise ratio can be achieved. However, doing such an automated experiment is not possible with the equipment of the reactor in Budapest.

The possibility of measuring shape changes during transients is larger in large reactors. However, research reactors, in which transient experiments can be done safely, are small in general. Larger reactors are normally used to generate electricity and are not meant to do experiments like the ones described in this chapter. Nevertheless it would be worthwhile to perform similar experiments in such large reactors in order to provide further confirmation of the theory in chapter II.

As a general conclusion we can say that the experiments show that point kinetic approach of modelling the dynamics in the reactor in Budapest is a valid one. This is according to the prediction as formulated in chapter II. Besides that no evidence can be found that thermal-hydraulic feedback mechanisms change that conclusion. Further more the experiments show that it is possible to measure the neutron flux with small self-powered neutron detectors in this low power reactor.

# **Chapter IV**

## **Theory and numerical experiments of small periodic perturbations**

### **IV.1 Introduction**

In chapter II general theory on the time-dependent diffusion equations was formulated. It was shown that in large reactors shape changes of the flux during a transient are likely to occur. It was also shown that in small reactors shape changes are very small especially in cases with perturbations that have a relatively large positive asymptotic reactivity. For smaller positive reactivities, however, it was expected that changes in the flux shape could be seen. But the experiments of chapter III with the disturber at the reflector position, in which the asymptotic reactivity was very small, could not confirm that idea. However, it was already mentioned in that chapter that the signal-to-noise ratio was low especially in that last experiment. To increase the accuracy of the measurement it was suggested to repeat the experiment in a boxcar manner. In fact this means one performs an experiment with a small periodic perturbation.

The periodicity together with the smallness of the perturbation gives the opportunity to use other methods of investigation than the ones shown in chapter II and III. In the existing literature a large amount of publications can be found on that subject. A classical paper is one by Hansson and Foulke (1963), who investigated spatial effects due to a modulating absorber in a zero power reactor both experimentally and numerically. In 1977 Kosály *et al* used the adiabatic-approximation to explain the spatial effect of a modulating absorber theoretically. Investigations of spatial effects due to vibrating absorbers are reported

in several other articles (Weinberg & Schweinler, 1948; Williams, 1970; Pázsit, 1977, 1978). More general investigations of space-dependent effects in neutron noise can be found in papers by Kosály *et al* (1975), Pohlus & Scholz (1981) and a review article by Kosály (1980). However, especially concerning experimental investigations on the responses of detectors due to small periodic perturbations more detailed research is desirable. Therefore this is the subject of the next two chapters (V and VI). In this chapter a firm theoretical basis is laid for the experiments in chapter V and VI. However, we also add new aspects to the existing theory, which simplify the interpretation and the numerical calculation of detector signals.

First an equation is derived which can be used to calculate the variations in the flux due to perturbations in the cross sections. In this so-called forward calculation, the flux variations in the whole system can be found as a response to a single perturbation. But in some cases one does not need to know the changes in the flux for every point in the reactor. For example, if the response of a single detector is needed only the flux at the detector position is used. This means that the flux values at any other positions are not used, which usually means a waste of calculation time.

It was shown by Van Dam (1976, 1977) that it is possible to obtain the response of one detector due to different disturbers without repeating the time consuming calculations for every disturber. The basics of this so-called frequency dependent detector response theory are described in this chapter. Since the development of the detector response theory was mainly inspired by the experimental and theoretical investigation of neutron noise in boiling water reactors (Seifritz & Cioli, 1973; Wach & Kosály, 1974), most applications of the theory lay in this field. Behringer *et al* (1977, 1979), for example, showed that the detector response theory could be used to explain the measured phenomenon of local and global effects in boiling water reactor noise. The existence of local and global effects in boiling water reactor neutron noise was later supported by other investigations (Fuge *et al*, 1977; Kleiss & Van Dam, 1979).

Although this theory was developed for and applied to neutron noise in boiling water reactors, there is no fundamental reason why the frequency dependent detector response theory cannot be applied to other fields of reactor physical research. To demonstrate that, we show results of numerical experiments in which the perturbation is a periodic change in the absorption cross section at a certain position in a light water reactor in this chapter. The choice of this kind of perturbation is mainly inspired by the experiments performed by Van der Hagen (1993). In these experiments a piece of cadmium was rotated in a flux gradient to prove the principle of a new type turbine flow meter.

A different approach to calculating the effect of a perturbation is to take advantage of the knowledge that the effect can be separated into a global and a local effect. In this approach the global effect is taken into account using first-order perturbation theory and the local effect is modelled by approximate neutron wave theory as described by Beckurts and Wirtz (1964). This approach is very useful to explain the main features in experiments as shown by Van der Hagen (1993). The basics of this approach are explained at the end of this chapter.

## IV.2 Small changes in an initially critical system

In an initially critical system the time-dependent diffusion equations II.1 and II.2 will reduce to the following two equations, in which  $\varphi_0(E, \mathbf{r})$  and  $C_{i,0}(\mathbf{r})$  are the stationary flux and the precursor densities respectively and  $D_0(E, \mathbf{r})$ ,  $\Sigma_{t,0}(E, \mathbf{r})$ ,  $\Sigma_{s,0}(E' \rightarrow E, \mathbf{r})$  and  $\Sigma_{f,0}(E, \mathbf{r})$  denote the diffusion coefficient, the removal cross section, the differential scattering cross section and the fission cross section in the stationary system.

$$\begin{aligned}
0 = & \nabla D_0(\mathbf{E}, \mathbf{r}) \nabla \varphi_0(\mathbf{E}, \mathbf{r}) - \Sigma_{t,0}(\mathbf{E}, \mathbf{r}) \varphi_0(\mathbf{E}, \mathbf{r}) + \\
& + \int \Sigma_{s,0}(\mathbf{E}' \rightarrow \mathbf{E}, \mathbf{r}) \varphi_0(\mathbf{E}', \mathbf{r}) d\mathbf{E}' + \\
& + \chi_p(\mathbf{E}) (1 - \beta) \int v \Sigma_{f,0}(\mathbf{E}', \mathbf{r}) \varphi_0(\mathbf{E}', \mathbf{r}) d\mathbf{E}' + \\
& + \sum_{i=1}^m \chi_i(\mathbf{E}) \lambda_i C_{i,0}(\mathbf{r})
\end{aligned} \tag{IV.1}$$

$$0 = \beta_i \int v \Sigma_{f,0}(\mathbf{E}', \mathbf{r}) \varphi_0(\mathbf{E}', \mathbf{r}) d\mathbf{E}' - \lambda_i C_{i,0}(\mathbf{r}) \quad i = 1 \dots m \tag{IV.2}$$

Suppose one disturbs the diffusion coefficient and the cross sections by a small amount:

$$\begin{aligned}
D(\mathbf{E}, \mathbf{r}, t) &= D_0(\mathbf{E}, \mathbf{r}) + \delta D(\mathbf{E}, \mathbf{r}, t), \\
\Sigma_t(\mathbf{E}, \mathbf{r}, t) &= \Sigma_{t,0}(\mathbf{E}, \mathbf{r}) + \delta \Sigma_t(\mathbf{E}, \mathbf{r}, t), \\
\Sigma_s(\mathbf{E}' \rightarrow \mathbf{E}, \mathbf{r}, t) &= \Sigma_{s,0}(\mathbf{E}' \rightarrow \mathbf{E}, \mathbf{r}) + \delta \Sigma_s(\mathbf{E}' \rightarrow \mathbf{E}, \mathbf{r}, t) \text{ and} \\
\Sigma_f(\mathbf{E}, \mathbf{r}, t) &= \Sigma_{f,0}(\mathbf{E}, \mathbf{r}) + \delta \Sigma_f(\mathbf{E}, \mathbf{r}, t)
\end{aligned}$$

If we assume that the resulting changes in the flux and the precursor densities are also small the flux and the precursor densities can be written as

$$\begin{aligned}
\varphi(\mathbf{E}, \mathbf{r}, t) &= \varphi_0(\mathbf{E}, \mathbf{r}) + \delta \varphi(\mathbf{E}, \mathbf{r}, t) \quad \text{and} \\
C_i(\mathbf{E}, \mathbf{r}, t) &= C_{i,0}(\mathbf{E}, \mathbf{r}) + \delta C_i(\mathbf{E}, \mathbf{r}, t).
\end{aligned}$$

Substituting all the disturbed variables into the time-dependent diffusion equations II.1 and II.2, using the stationary solutions IV.1 and IV.2 and neglecting the products of small quantities like  $\delta D(\mathbf{E}, \mathbf{r}, t) \nabla \delta \varphi(\mathbf{E}, \mathbf{r}, t)$  the following linearized equations appear:

$$\begin{aligned}
\frac{1}{v} \frac{\partial \delta \varphi(E, \mathbf{r}, t)}{\partial t} = & \nabla \delta D(E, \mathbf{r}, t) \nabla \varphi_0(E, \mathbf{r}) - \delta \Sigma_t(E, \mathbf{r}, t) \varphi_0(E, \mathbf{r}) + \\
& + \int \delta \Sigma_s(E' \rightarrow E, \mathbf{r}, t) \varphi_0(E', \mathbf{r}) dE' + \\
& + \chi_p(E) (1 - \beta) \int v \delta \Sigma_f(E', \mathbf{r}, t) \varphi_0(E', \mathbf{r}) dE' + \\
& + \nabla D_0(E, \mathbf{r}) \nabla \delta \varphi(E, \mathbf{r}, t) - \Sigma_{t,0}(E, \mathbf{r}) \delta \varphi(E, \mathbf{r}, t) + \quad (IV.3) \\
& + \int \Sigma_{s,0}(E' \rightarrow E, \mathbf{r}) \delta \varphi(E', \mathbf{r}, t) dE' + \\
& + \chi_p(E) (1 - \beta) \int v \Sigma_{f,0}(E', \mathbf{r}) \delta \varphi(E', \mathbf{r}, t) dE' + \\
& + \sum_{i=1}^m \chi_i(E) \lambda_i \delta C_i(E, \mathbf{r}, t)
\end{aligned}$$

$$\begin{aligned}
\frac{\partial \delta C_i(\mathbf{r}, t)}{\partial t} = & -\lambda_i \delta C_i(\mathbf{r}, t) + \beta_i \int v \Sigma_{f,0}(E', \mathbf{r}) \delta \varphi(E', \mathbf{r}, t) dE' + \\
& + \beta_i \int v \delta \Sigma_f(E', \mathbf{r}, t) \varphi_0(E', \mathbf{r}) dE' \quad i = 1 \dots m \quad (IV.4)
\end{aligned}$$

The assumption that due to a small change in the cross sections the flux and the precursor densities change only a small amount is not true in general. This we have already seen in chapter II, where the asymptotic shape of the flux and the precursor densities were discussed. There it was stated that in any reactor that was left in a non-critical state, even if the changes in the cross section are small, the amplitude of the flux and the precursor densities change exponentially without bounds. It is clear that in that case the assumption of small changes of the flux and the precursor densities is not valid. However, in case of sufficiently fast periodic variations around the critical state the change of the amplitude is small.

If periodic variations are concerned a representation of the equations in the frequency domain can be helpful. This is easily achieved by Laplace transformation of the set of linear equations IV.3 and IV.4:

$$\begin{aligned}
\frac{s}{v} \delta \tilde{\varphi}(E, \mathbf{r}, s) = & \nabla \delta \tilde{D}(E, \mathbf{r}, s) \nabla \varphi_0(E, \mathbf{r}) - \delta \tilde{\Sigma}_t(E, \mathbf{r}, s) \varphi_0(E, \mathbf{r}) + \\
& + \int \delta \tilde{\Sigma}_s(E' \rightarrow E, \mathbf{r}, s) \varphi_0(E', \mathbf{r}) dE' + \\
& + \chi_p(E) (1 - \beta) \int v \delta \tilde{\Sigma}_f(E', \mathbf{r}, s) \varphi_0(E', \mathbf{r}) dE' + \\
& + \nabla D_0(E, \mathbf{r}) \nabla \delta \tilde{\varphi}(E, \mathbf{r}, s) - \Sigma_{t,0}(E, \mathbf{r}) \delta \tilde{\varphi}(E, \mathbf{r}, s) + \quad (IV.5) \\
& + \int \Sigma_{s,0}(E' \rightarrow E, \mathbf{r}) \delta \tilde{\varphi}(E', \mathbf{r}, s) dE' + \\
& + \chi_p(E) (1 - \beta) \int v \Sigma_{f,0}(E', \mathbf{r}) \delta \tilde{\varphi}(E', \mathbf{r}, s) dE' + \\
& + \sum_{i=1}^m \chi_i(E) \lambda_i \delta \tilde{C}_i(\mathbf{r}, s)
\end{aligned}$$

$$\begin{aligned}
s \delta \tilde{C}_i(\mathbf{r}, s) = & -\lambda_i \delta \tilde{C}_i(\mathbf{r}, s) + \beta_i \int v \Sigma_{f,0}(E', \mathbf{r}) \delta \tilde{\varphi}(E', \mathbf{r}, s) dE' + \\
& + \beta_i \int v \delta \tilde{\Sigma}_f(E', \mathbf{r}, s) \varphi_0(E', \mathbf{r}) dE' \quad i = 1 \dots m \quad (IV.6)
\end{aligned}$$

where  $s$  is the Laplace variable and the tilde denotes a Laplace transform. Substituting Eqs. IV.6 into Eq. IV.5 and taking  $s$  to be  $j\omega$  gives one equation for the variation of the flux:

$$\begin{aligned}
& \left[ \frac{j\omega}{v} - \nabla D_0(E, \mathbf{r}) \nabla + \Sigma_{t,0}(E, \mathbf{r}) \right] \delta \tilde{\varphi}(E, \mathbf{r}, \omega) + \\
& - \int \Sigma_{s,0}(E' \rightarrow E, \mathbf{r}) \delta \tilde{\varphi}(E', \mathbf{r}, \omega) dE' + \\
& - \int \left[ \chi_p(E) (1 - \beta) + \sum_{i=1}^m \frac{\chi_i(E) \beta_i \lambda_i}{j\omega + \lambda_i} \right] v \Sigma_{f,0}(E', \mathbf{r}) \delta \tilde{\varphi}(E', \mathbf{r}, \omega) dE' = \quad (IV.7) \\
& = [\nabla \delta \tilde{D}(E, \mathbf{r}, \omega) \nabla - \delta \tilde{\Sigma}_t(E, \mathbf{r}, \omega)] \varphi_0(E, \mathbf{r}) + \\
& + \int \delta \tilde{\Sigma}_s(E' \rightarrow E, \mathbf{r}, \omega) \varphi_0(E', \mathbf{r}) dE' + \\
& + \int \left[ \chi_p(E) (1 - \beta) + \sum_{i=1}^m \frac{\chi_i(E) \beta_i \lambda_i}{j\omega + \lambda_i} \right] v \delta \tilde{\Sigma}_f(E', \mathbf{r}, \omega) \varphi_0(E', \mathbf{r}) dE'
\end{aligned}$$

In principle all variables in the equation are known except for the flux variation  $\delta\tilde{\varphi}(E, \mathbf{r}, \omega)$ . Moreover, for a given value of  $\omega$  the equation can be seen as a stationary diffusion equation with a source term on the right-hand side and therefore can be solved likewise. A large number of methods is available to solve such problems, as, for example, reviewed in Duderstadt and Hamilton (1976). Using properly modified cross section data in these methods, one obtains the Laplace transform of the flux variations, instead of the stationary flux. In this way a coupled space and frequency dependent solution of the flux due to one disturber can be obtained for all space coordinates in one calculation (Van der Hagen *et al.*, 1992).

### IV.3 Field-of-view theory: Determining the frequency dependent detector response using adjoint function theory

The usefulness of adjoint function theory in reactor physical calculation was already shown by Lewins (1965). Greenspan in 1976 focused on the applicability of the theory in various fields, for example in determining the detector response. This concept was extended to the frequency domain by Van Dam (1976; 1977). In this way it is possible to calculate the response of a detector to oscillating sources and parametric fluctuations in the cross sections of the system. In this section the frequency dependent detector response theory is outlined.

As stated in the previous section, to calculate the response of a detector only the flux of the small region of the detector is of importance. Mathematically the change in the detector response can be expressed as

$$R(t) = \int \int_{V_{\text{det}}} \Sigma_d(E, \mathbf{r}) \delta\varphi(E, \mathbf{r}, t) d\mathbf{r} dE \quad (\text{IV.8})$$

in time domain and



$$\tilde{R}(\omega) = \int \int_{V_{\text{det}}} \Sigma_d(E, \mathbf{r}) \delta \tilde{\phi}(E, \mathbf{r}, \omega) d\mathbf{r} dE \quad (\text{IV.9})$$

in frequency domain, where  $\Sigma_d(E, \mathbf{r})$  is the macroscopic detector cross section, which expresses the space and energy dependent sensitivity of the detector to the flux, and  $V_{\text{det}}$  is the volume of the detector.

To be able to calculate the detector responses to fluctuations in the parameters, an equation that is adjoint to Eq. IV.7 must be defined:

$$\begin{aligned} & \left[ \frac{j\omega}{v} - \nabla D_0(E, \mathbf{r}) \nabla + \Sigma_{t,0}(E, \mathbf{r}) \right] g(E, \mathbf{r}, \omega) + \\ & - \int \Sigma_{s,0}(E \rightarrow E', \mathbf{r}) g(E', \mathbf{r}, \omega) dE' + \\ & - \int [\chi_p(E')(1-\beta) + \sum_{i=1}^m \frac{\chi_i(E')\beta_i\lambda_i}{j\omega + \lambda_i}] v \Sigma_{f,0}(E, \mathbf{r}) g(E', \mathbf{r}, \omega) dE' = \quad (\text{IV.10}) \\ & = \Sigma_d(E, \mathbf{r}) \end{aligned}$$

with  $g(E, \mathbf{r}, \omega)$  being the solution of the adjoint equation. The function  $g(E, \mathbf{r}, \omega)$  is usually called the frequency dependent field-of-view of the detector in focus. As can be seen the left-hand side of Eq. IV.10 is similar to the left-hand side of Eq. IV.7 except for the interchange of the variables  $E$  and  $E'$  in the integrals. In fact Eq. IV.10 can be seen as a stationary diffusion equation with modified cross sections. The right-hand side acts as a source term for this equation. A detailed description of how to modify the cross sections to obtain the field-of-view using a multi-group diffusion model can be found in Van der Hagen *et al* (1992). An important fact to note is that Eq. IV.10 consists of a real and an imaginary part. As a consequence the adjoint equation of a reactor model with  $n$  energy groups has to be modeled with  $2n$  modified neutron diffusion equations and the field-of-view consists of a real and an imaginary part.

Multiplying Eq. IV.7 by  $g(E, \mathbf{r}, \omega)$  and Eq. IV.10 by  $\delta\tilde{\phi}(E, \mathbf{r}, \omega)$  and subtracting both equations gives one new equation. If this new equation is integrated over energy and the total system volume and if conventional diffusion boundary conditions are used together with the vector identity  $\mathbf{a} \cdot \nabla \mathbf{b} = \nabla \cdot \mathbf{a} \mathbf{b} - \mathbf{b} \cdot \nabla \mathbf{a}$ , the expression for the frequency-dependent detector response  $\tilde{R}(\omega)$  appears:

$$\begin{aligned} \tilde{R}(\omega) = & \int_V \int \{ -\delta\tilde{D}(E, \mathbf{r}, \omega) \nabla g(E, \mathbf{r}, \omega) \cdot \nabla \phi_0(E, \mathbf{r}) + \\ & -\delta\tilde{\Sigma}_t(E, \mathbf{r}, \omega) g(E, \mathbf{r}, \omega) \phi_0(E, \mathbf{r}) + \\ & + g(E, \mathbf{r}, \omega) \int \delta\tilde{\Sigma}_s(E' \rightarrow E, \mathbf{r}, \omega) \phi_0(E', \mathbf{r}) dE' + \\ & + g(E, \mathbf{r}, \omega) \chi_p(E)(1-\beta) \int v \delta\tilde{\Sigma}_f(E', \mathbf{r}, \omega) \phi_0(E', \mathbf{r}) dE' + \\ & + g(E, \mathbf{r}, \omega) \sum_{i=1}^m \frac{\chi_i(E) \beta_i \lambda_i}{j\omega + \lambda_i} \int v \delta\tilde{\Sigma}_f(E', \mathbf{r}, \omega) \phi_0(E', \mathbf{r}) dE' \} dV dE \end{aligned} \quad (IV.11)$$

Once  $g(E, \mathbf{r}, \omega)$  is calculated by Eq. IV.10 it is possible to calculate the frequency-dependent detector response  $\tilde{R}(\omega)$  by the integration of Eq. IV.11. Since solving a diffusion equation is usually more time-consuming than solving integrals, this means that once the field-of-view  $g(E, \mathbf{r}, \omega)$  is known for one detector, the response of that detector to various fluctuations in the parameters is relatively simple to calculate. If one were to use Eq. IV.7 for the problem, then one would have to solve that diffusion equation every time one of the parameters changes. Note that since the field-of-view is a complex function, the resulting detector response contains both amplitude and phase information.

#### IV.4 Separate treatment of global and local effects

A different approach to estimating the effect of small disturbances is one in which the knowledge that local and global effects exist is taken as a starting point. In that approach the global effect is taken into account by using linearized conventional point kinetic theory and the

local effect by approximate neutron wave theory. In this section both approximations are explained.

#### IV.4.1 The global effect

As said already in chapter II the conventional point kinetic equations are a set of non-linear differential equations. The non-linearity lies in the product of the reactivity  $\rho(t)$  and the amplitude  $n(t)$  and makes it impossible to use the elaborated techniques of linear differential equations. However, in situations of small disturbances of the reactivity, the conventional point kinetic equations can be linearized as follows. Suppose the reactivity  $\rho(t)$  can be written as  $\rho_0 + \delta\rho(t)$ , where  $\rho_0$  is the reactivity of the initial system and  $\delta\rho(t)$  is a small change in the reactivity. This small change in reactivity leads to a small change in the flux amplitude  $n(t) = n_0 + \delta n(t)$  and the precursor concentration  $c_i(t) = c_{i,0} + \delta c_i(t)$ . Substituting these expressions into Eqs. II.6, neglecting the product of the two small quantities  $\delta\rho(t)$  and  $\delta n(t)$  and remembering that in the conventional point kinetic approach  $\beta_i^{\text{eff}}$ ,  $\beta^{\text{eff}}$ ,  $\Lambda$  are taken constant in time, one ends up with a set of first-order differential equations with constant coefficients:

$$\begin{aligned} \frac{d\delta n(t)}{dt} &= \frac{\rho_0 - \beta}{\Lambda} \delta n(t) + \frac{n_0}{\Lambda} \delta\rho(t) + \sum_{i=1}^m \lambda_i \delta c_i(t) \\ \frac{d\delta c_i(t)}{dt} &= \frac{\beta_i}{\Lambda} \delta n(t) - \lambda_i \delta c_i(t) \quad i = 1 \dots m \end{aligned} \quad (\text{IV.12})$$

in which  $\beta_i^{\text{eff}}$  and  $\beta^{\text{eff}}$  are written as  $\beta_i$  and  $\beta$  for convenience. In this form the point kinetic equation can be Laplace transformed. Doing this and taking  $s = j\omega$  gives the following expression:

$$\delta \tilde{n}(\omega) = \frac{n_0}{j\omega\Lambda - \rho_0 + \sum_{i=1}^m \frac{j\omega\beta_i}{j\omega + \lambda_i}} \delta \tilde{\rho}(\omega) \equiv n_0 G(\omega) \delta \tilde{\rho}(\omega) \quad (\text{IV.13})$$

where the tildes denote the Laplace transforms of  $\delta n(t)$  and  $\delta \rho(t)$  and  $G(\omega)$  is the sub-critical zero-power reactivity transfer function. The properties of this reactivity transfer function are described in many textbooks treating the fundamentals of nuclear reactor dynamics (see, for example, Lewins (1977)). The most important property is that for a large range of frequencies  $\lambda < \omega < \beta/\Lambda$ , the "plateau region", the amplitude of this function is approximately constant and equal to  $1/\beta$  and the phase is approximately zero. This means that the change in the flux amplitude can be estimated by dividing the change in reactivity by the delayed neutron fraction  $\beta$ . The change in reactivity has to be calculated using Eq. II.7.

Using this theory, the response of a detector  $R$  which only senses the global effect of a disturbance relative to the response  $R_0$  of that detector without the disturber can now be approximated as follows:

$$\frac{\tilde{R}(\omega)}{R_0} = G(\omega) \delta \tilde{\rho}(\omega) \quad (\text{IV.14})$$

or, if the disturbance acts in the plateau region:

$$\frac{R(t)}{R_0} = \frac{\delta \rho(t)}{\beta} \quad (\text{IV.15})$$

The change in the reactivity in all the expressions has to be calculated using Eq. II.7. Since conventional point kinetics is taken as a starting point in this section it means that for the shape function in Eq. II.7 the initial stationary flux is taken. This approximation of calculating the value of the reactivity is often called the first-order perturbation approximation.

#### IV.4.2 The local effect

To derive an analytical expression for the local effect of the disturber we use diffusion theory of monoenergetic neutrons in an infinite non-multiplying medium as described by Beckurts and Wirtz (1964). In this monoenergetic and non-multiplying medium Eqs. II.1 and II.2 for a harmonically modulated point source reduce to:

$$\frac{1}{v} \frac{\partial \varphi(\mathbf{r}, t)}{\partial t} - \nabla D(\mathbf{r}) \nabla \varphi(\mathbf{r}, t) + \Sigma_a(\mathbf{r}) \varphi(\mathbf{r}, t) = \frac{Q_0 + \delta Q e^{j\omega t}}{4\pi r^2} \delta(\mathbf{r}) \quad (\text{IV.16})$$

The solution of this equation in an infinite medium is:

$$\varphi(\mathbf{r}, t) = \varphi_0(r) + \delta\varphi(r, t) \quad (\text{IV.17})$$

with

$$\varphi_0(r) = \frac{Q_0}{4\pi D} \frac{e^{-r/L}}{r} \quad \text{with } L = \sqrt{\frac{D}{\Sigma_a}} \quad (\text{IV.18})$$

and

$$\delta\varphi(r, t) = \frac{\delta Q}{4\pi D} \frac{e^{-r/L_\omega}}{r} e^{j\omega t} \quad \text{with } \frac{1}{L_\omega} = \sqrt{\frac{1}{L^2} + \frac{j\omega}{vD}} \quad (\text{IV.19})$$

The “complex” diffusion length  $L_\omega$  can be approximated for low frequencies ( $\omega \ll v\Sigma_a$ ), which yields the following expression for the flux variations:

$$\delta \varphi(r,t) = \frac{\delta Q}{4\pi D} \frac{e^{-r\kappa}}{r} e^{j(\omega t - rk)} \quad (\text{IV.20})$$

$$\text{with } \kappa \approx \frac{1}{L} \quad \text{and} \quad k \approx \frac{\omega}{2vL\Sigma_a}$$

Suppose a detector is placed at a position  $\mathbf{r}_{\text{det}}$  and the position of the point source can be written as  $\mathbf{r}$ , then the response  $R$  relative to its stationary response  $R_0$  is:

$$\frac{R(t)}{R_0} = \frac{\delta Q}{\varphi_0(\mathbf{r}_{\text{det}})} \frac{1}{4\pi D} \frac{e^{-|\mathbf{r}_{\text{det}} - \mathbf{r}|/L}}{|\mathbf{r}_{\text{det}} - \mathbf{r}|} e^{j(\omega t - |\mathbf{r}_{\text{det}} - \mathbf{r}|k)} \quad (\text{IV.21})$$

where  $\varphi_0(\mathbf{r}_{\text{det}})$  is the initial stationary flux at the detector position. For small distances between the detector and the disturber ( $|\mathbf{r}_{\text{det}} - \mathbf{r}| \ll 1/k$ ) the phase change can be neglected, yielding the following equation:

$$\frac{R(t)}{R_0} = \frac{\delta Q}{\varphi_0(\mathbf{r}_{\text{det}})} \frac{1}{4\pi D} \frac{e^{-|\mathbf{r}_{\text{det}} - \mathbf{r}|/L}}{|\mathbf{r}_{\text{det}} - \mathbf{r}|} e^{j\omega t} \quad (\text{IV.22})$$

## IV.5 Application of the theory to selected disturbers

### IV.5.1 The modulating absorber

As an example the response is shown of a global detector to a modulating absorber with a strength equal to the thermal absorption cross section of cadmium ( $\Sigma_a^{\text{Cd}}$ ) and a volume of  $V^{\text{Cd}}$ . Using a factor  $\alpha^{\text{Cd}}$  as a self-shielding factor (Beckurts & Wirtz, 1964), the change in

the absorption cross section due to this piece of cadmium can be written as:

$$\delta \Sigma_a(E, \mathbf{r}, t) = \sum_a^{Cd} \alpha^{Cd} V^{Cd} \delta(E_{th} - E) \delta(\mathbf{r}_{Cd} - \mathbf{r}) \sin(\omega_0 t) \quad (IV.23)$$

in time domain, or

$$\delta \tilde{\Sigma}_a(E, \mathbf{r}, \omega) = \sum_a^{Cd} \alpha^{Cd} V^{Cd} \delta(E_{th} - E) \delta(\mathbf{r}_{Cd} - \mathbf{r}) \delta(\omega_0 - \omega) \quad (IV.24)$$

in frequency domain, where  $E_{th}$  denotes the thermal energy group,  $\mathbf{r}_{Cd}$  is the position of the cadmium,  $\omega_0$  is the frequency of the modulation and only positive frequencies are regarded. Substituting Eq. IV.24 into Eq. IV.11 gives the detector response as predicted from the field-of-view theory:

$$R(\omega) = -\sum_a^{Cd} V^{Cd} \alpha^{Cd} \varphi_0(E_{th}, \mathbf{r}_{Cd}) g(E_{th}, \mathbf{r}_{Cd}, \omega) \delta(\omega - \omega_0) \quad (IV.25)$$

As we can see, the response of the detector is proportional to the flux at the position of the cadmium and the field-of-view at that position. The negative sign reminds us of the fact that if the absorption increases the response of the detector decreases, since the flux density also decreases. The expression also gives a good insight into the interpretation of the field-of-view function. In a system with a flat flux the field-of-view can be seen as the sensitivity of the detector to a sinusoidal modulating absorber. If the function is large, the influence of such an absorber is large, if it is small the detector hardly senses the disturber.

In the separate global theory approach the response of a global detector to the same modulating absorber can also be calculated, provided the distance between the detector and the disturber is larger than a few times the migration length. The change in reactivity to a

changing absorber in first-order perturbation can be calculated from Eq. II.7 resulting in the following:

$$\delta \rho(t) = \frac{-\int \int \delta \Sigma_a(E, \mathbf{r}, t) \psi^\dagger(E, \mathbf{r}) \phi_0(E, \mathbf{r}) dE dV}{\int \int \psi^\dagger(E, \mathbf{r}) \chi_t(E) \int v \Sigma_f(E', \mathbf{r}) \phi_0(E', \mathbf{r}) dE' dV} \quad (\text{IV.26})$$

In a two-energy group approximation, in which all neutrons are born in the fast group ( $E_{\text{fast}}$ ) and the fission cross section is zero in the fast group, substitution of Eq. IV.23 gives the following expression for the detector response in global theory approach:

$$\frac{\tilde{R}(\omega)}{R_0} = -G(\omega_0) \frac{\Sigma_a^{\text{Cd}} V^{\text{Cd}} \alpha^{\text{Cd}} \phi_0(E_{\text{th}}, \mathbf{r}_{\text{Cd}}) \psi^\dagger(E_{\text{th}}, \mathbf{r}_{\text{Cd}})}{\int v \Sigma_f(E_{\text{th}}, \mathbf{r}) \phi_0(E_{\text{th}}, \mathbf{r}) \psi^\dagger(E_{\text{fast}}, \mathbf{r}) dV} \delta(\omega - \omega_0) \quad (\text{IV.27})$$

in the frequency domain and

$$\frac{R(t)}{R_0} = -\frac{1}{\beta} \frac{\Sigma_a^{\text{Cd}} V^{\text{Cd}} \alpha^{\text{Cd}} \phi_0(E_{\text{th}}, \mathbf{r}_{\text{Cd}}) \psi^\dagger(E_{\text{th}}, \mathbf{r}_{\text{Cd}})}{\int v \Sigma_f(E_{\text{th}}, \mathbf{r}) \phi_0(E_{\text{th}}, \mathbf{r}) \psi^\dagger(E_{\text{fast}}, \mathbf{r}) dV} \sin(\omega_0 t) \quad (\text{IV.28})$$

in the time domain, if the angular frequency of the disturber  $\omega_0$  lies in the plateau region.

The local effect of a modulated point source can be calculated by taking the reaction rate of the absorber,  $\Sigma_a^{\text{Cd}} V^{\text{Cd}} \alpha^{\text{Cd}} \phi_0(\mathbf{r}_{\text{Cd}})$  to be the negative source term  $\delta Q$  in Eq. IV.21:

$$\frac{R(t)}{R_0} = -\frac{\Sigma_a^{\text{Cd}} V^{\text{Cd}} \alpha^{\text{Cd}}}{4\pi D} \frac{\phi_0(\mathbf{r}_{\text{Cd}})}{\phi_0(\mathbf{r}_{\text{det}})} \frac{e^{-|\mathbf{r}_{\text{Cd}} - \mathbf{r}_{\text{det}}|/L}}{|\mathbf{r}_{\text{Cd}} - \mathbf{r}_{\text{det}}|} \sin(\omega_0 t - |\mathbf{r}_{\text{det}} - \mathbf{r}|k) \quad (\text{IV.29})$$



in the time domain and

$$\frac{\tilde{R}(\omega)}{R_0} = -\frac{\sum_a^{Cd} V^{Cd} \alpha^{Cd}}{4\pi D} \frac{\varphi_0(\mathbf{r}_{Cd})}{\varphi_0(\mathbf{r}_{det})} \frac{e^{-|\mathbf{r}_{Cd}-\mathbf{r}_{det}|/L}}{|\mathbf{r}_{Cd}-\mathbf{r}_{det}|} e^{-j|\mathbf{r}_{Cd}-\mathbf{r}_{det}|k} \delta(\omega-\omega_0) \quad (IV.30)$$

in the frequency domain.

The modulating source provides a good opportunity to compare the field-of-view theory with both the global and local theory in the frequency domain as follows:

$$g(E_{th}, \mathbf{r}_{Cd}, \omega_0) = G(\omega_0) \frac{\psi^\dagger(E_{th}, \mathbf{r}_{Cd}) R_0}{\int v \Sigma_f(E_{th}, \mathbf{r}) \varphi_0(E_{th}, \mathbf{r}) \psi^\dagger(E_{fast}, \mathbf{r}) dV} \quad (IV.31)$$

for the global effect (Eq. IV.25 and Eq. IV.27) and

$$g(E_{th}, \mathbf{r}_{Cd}, \omega_0) = \frac{R_0 e^{-|\mathbf{r}_{Cd}-\mathbf{r}_{det}|/L}}{4\pi D \varphi_0(\mathbf{r}_{det}) |\mathbf{r}_{Cd}-\mathbf{r}_{det}|} \quad (IV.32)$$

for the local effect (Eq. IV.25 and Eq. IV.30).

#### IV.5.2 The moving absorber

If the absorber is moving then the removal cross section can be written as:

$$\delta \Sigma_a(E, \mathbf{r}, t) = \sum_a^{Cd} \alpha^{Cd} V^{Cd} \delta(E_{th}-E) \delta(\mathbf{r}_{Cd}(t) - \mathbf{r}) \quad (IV.33)$$

with  $\mathbf{r}_{Cd}(t)$  a time-dependent function denoting the position of the absorber. This expression can be substituted into Eqs. IV.15 and IV.21

in the same manner as shown above for the modulating absorber to get the detector response in the global approach

$$\frac{R(t)}{R_0} = -\frac{1}{\beta} \frac{\sum_a^{Cd} V^{Cd} \alpha^{Cd} \varphi_0(E_{th}, \mathbf{r}_{Cd}(t)) \psi^\dagger(E_{th}, \mathbf{r}_{Cd}(t))}{\int v \Sigma_f(E_{th}, \mathbf{r}) \varphi_0(E_{th}, \mathbf{r}) \psi^\dagger(E_{fast}, \mathbf{r}) dV} \quad (IV.34)$$

and the local approach

$$\frac{R(t)}{R_0} = -\frac{\sum_a^{Cd} V^{Cd} \alpha^{Cd}}{4\pi D} \frac{\varphi_0(\mathbf{r}_{Cd}(t))}{\varphi_0(\mathbf{r}_{det})} \frac{e^{-|\mathbf{r}_{Cd}(t) - \mathbf{r}_{det}|/L}}{|\mathbf{r}_{Cd}(t) - \mathbf{r}_{det}|} \quad (IV.35)$$

Due to the implicit time dependency in the function, however, it is impossible to Laplace transform Eq. IV.33 directly. Therefore it is not straightforward to obtain the detector response in the frequency domain. To get around this problem one has to know more about the exact movement of the piece of cadmium. Let the disturber be an absorber that oscillates between two positions  $\mathbf{r}_1$  and  $\mathbf{r}_2$  with an angular frequency of  $\omega_0$ . To model this disturber in frequency domain we assume that it can be seen as two modulating absorbers both having an angular frequency  $\omega_0$  but with opposite phase:

$$\begin{aligned} \delta \tilde{\Sigma}_a(E, \mathbf{r}, \omega) = & \frac{\sum_a^{Cd} \alpha^{Cd} V^{Cd}}{2} \delta(E_{th} - E) \times \\ & \times \left[ \delta(\mathbf{r}_1 - \mathbf{r}) + \delta(\mathbf{r}_2 - \mathbf{r}) e^{j\pi} \right] \delta(\omega - \omega_0) \end{aligned} \quad (IV.36)$$

This expression can now be substituted into the frequency dependent forms of the detector responses in exactly the same manner as for the single modulating absorber but with two terms. This yields the following expressions for the detector response in the field-of-view theory, using Eq. IV.11:

$$\begin{aligned} \tilde{R}(\omega) = & -\frac{\sum_a^{Cd} V^{Cd} \alpha^{Cd}}{2} \left[ \varphi_0(E_{th}, \mathbf{r}_1) g(E_{th}, \mathbf{r}_1, \omega) + \right. \\ & \left. + \varphi_0(E_{th}, \mathbf{r}_2) g(E_{th}, \mathbf{r}_2, \omega) e^{j\pi} \right] \delta(\omega - \omega_0) \end{aligned} \quad (IV.37)$$

in the global approach, using Eq. IV.14 and Eq. IV.26 in a two-energy group approximation in the same way as in the previous section:

$$\begin{aligned} \frac{\tilde{R}(\omega)}{R_0} = & -\frac{G(\omega_0) \sum_a^{Cd} V^{Cd} \alpha^{Cd}}{2 \int v \Sigma_f(E_{th}, \mathbf{r}) \varphi_0(E_{th}, \mathbf{r}) \psi^\dagger(E_{fast}, \mathbf{r}) d\mathbf{r}} \times \\ & \times \left[ \varphi_0(E_{th}, \mathbf{r}_1) \psi^\dagger(E_{th}, \mathbf{r}_1) + \varphi_0(E_{th}, \mathbf{r}_2) \psi^\dagger(E_{th}, \mathbf{r}_2) e^{j\pi} \right] \delta(\omega - \omega_0) \end{aligned} \quad (IV.38)$$

and in the local approach, using Eq. IV.22:

$$\begin{aligned} \frac{\tilde{R}(\omega)}{R_0} = & -\frac{\sum_a^{Cd} V^{Cd} \alpha^{Cd}}{2 \cdot 4\pi D \varphi_0(\mathbf{r}_{det})} \left[ \frac{\varphi_0(\mathbf{r}_1) e^{-|\mathbf{r}_1 - \mathbf{r}_{det}|/L}}{|\mathbf{r}_1 - \mathbf{r}_{det}|} + \right. \\ & \left. + \frac{\varphi_0(\mathbf{r}_2) e^{-|\mathbf{r}_2 - \mathbf{r}_{det}|/L}}{|\mathbf{r}_2 - \mathbf{r}_{det}|} e^{j\pi} \right] \delta(\omega - \omega_0) \end{aligned} \quad (IV.39)$$

Notice that if the product of  $\varphi_0(E_{th}, \mathbf{r})$  and  $\psi^\dagger(E_{th}, \mathbf{r})$  is equal for both positions  $\mathbf{r}_1$  and  $\mathbf{r}_2$ , the response of a detector in the global approach is zero, independent of the strength of the moving absorber.

This concept of modelling a moving absorber by a set of absorbers with different phases is not restricted to an oscillator. If, for example, one wants to calculate the response to an absorber that rotates, one can use four modulating absorbers, which have  $90^\circ$  phase shifts. The expressions of the detector response for such a rotator are similar to the

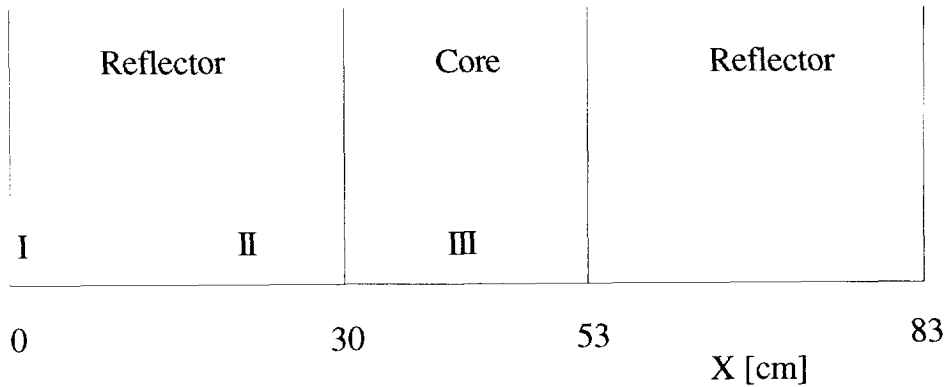


Figure IV.1: Geometry of the 1D-1G model of the HOR. The roman numbers indicate the detector position: I at 1.75 cm, II at 21.75 cm and III at 41.25 cm.

one shown above. They have four terms between the right brackets with exponents of  $j0$ ,  $j\pi/2$ ,  $j\pi$ , and  $3j\pi/2$ . The amplitude has to be divided by 4 instead of 2 (Keijzer, 1992).

## IV.6 Numerical experiments

In this section some numerical experiments are described in which the theory presented above is used. First we focus on the possibilities of the field-of-view theory. We show the field-of-view of detectors in two systems and the detector response, using these fields-of-view, to some disturbances, such as moving absorbers.

Most of the results of the field-of-view calculations are compared with calculations in which the separate global theory is used to obtain the response of a specific detector. As expected the global theory fails in situations where changes occur in the flux shape. However, as explained above, the modelling of moving absorbers in field-of-view theory is not straightforward and can only be done in such a way that the main features are incorporated. Some aspects of the response of moving absorbers cannot be modelled the way we proposed in the

Table IV.1: Data of the one-dimensional, one-energy group model of the 'Hoger Onderwijs Reactor'. The values are based on the two energy group values of De Vries (1974), with  $\Sigma_a$  in the core modified to obtain a slightly subcritical system.

	Core	Reflector	General	
D [cm]	1.1093	0.0966	$\beta$	0.0062
$\Sigma_a$ [cm <sup>-1</sup> ]	$5.99 \cdot 10^{-3}$	0.0220	$\lambda$ [s <sup>-1</sup> ]	0.0767
$v\Sigma_f$ [cm <sup>-1</sup> ]	$9.4108 \cdot 10^{-3}$	0.0	$\Lambda$ [s]	$6.64 \cdot 10^{-5}$
L [cm]	13.6	2.10	$k_{\text{eff}}$	0.9997486
1/L [cm <sup>-1</sup> ]	0.0735	0.477	$\rho$ [pcm]	-25.14
$k'$ [°/(cm s <sup>-1</sup> )]	$1.38 \cdot 10^{-3}$	$2.44 \cdot 10^{-3}$	$\beta/(2\pi\Lambda)$ [Hz]	14.9
$v$ [cm s <sup>-1</sup> ]	$1.60 \cdot 10^6$	$1.60 \cdot 10^6$	$\lambda/(2\pi)$ [Hz]	0.0122

field-of-view theory and can only be seen in the global and local theory in time domain.

#### IV.6.1 Field-of-view of a 1D-1G model of the HOR

The first example is based on a one-dimensional and one-energy group slab reactor model of the 'Hoger Onderwijs Reactor' in Delft. It consists of a homogenized core of 23 cm surrounded by a water reflector with a thickness of 30 cm at each side of the core (Figure IV.1). The values of the diffusion coefficient, the absorption cross section, the fission cross section and the velocity are based on the two-group parameters of De Vries (1974). They are condensed to one-energy group values (Table IV.1). To obtain a slightly subcritical system, the absorption cross section of the core is adjusted. The subcriticality of the system is essential, since otherwise it is impossible

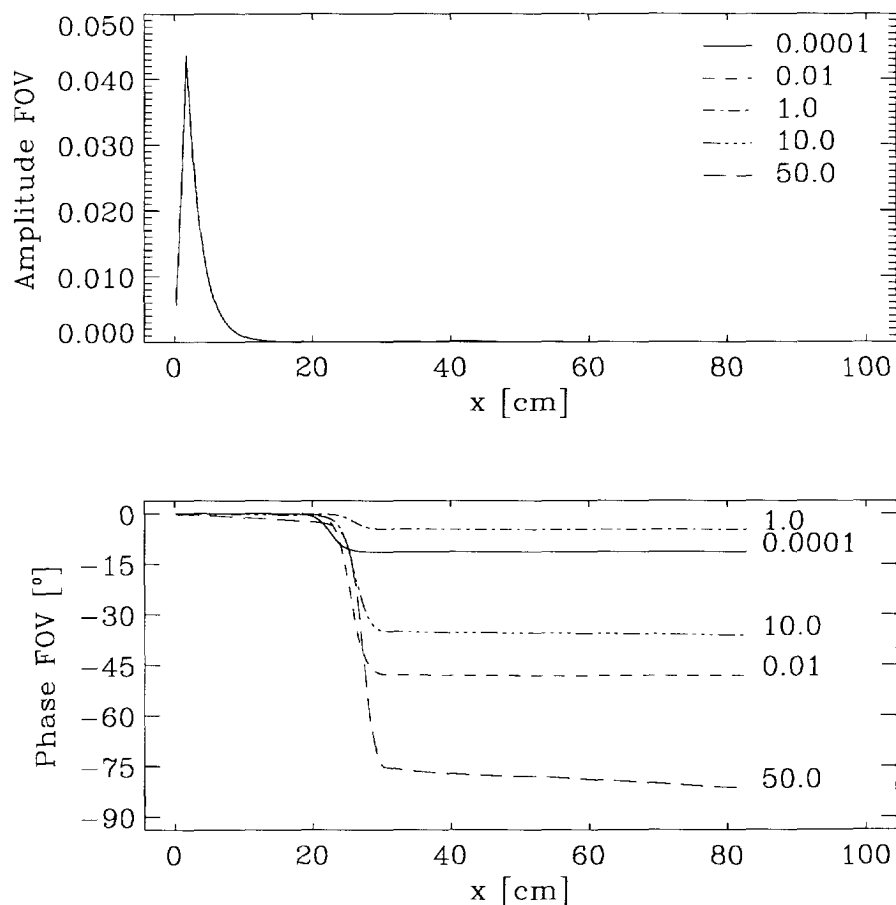


Figure IV.2: Amplitude and phase of the field-of-view for detector I ( $x_{\text{det}} = 1.75$  cm) for five frequencies. The system is a 1D-1G model of the HOR, with a homogenized core surrounded by water. The core boundaries are at  $x = 30$  cm and  $x = 53$  cm.

to calculate the field-of-view because of the source term in the calculation.

The actual calculation of the field-of-view of the detectors is done with the static diffusion code CITATION (Fowler *et al*, 1971). Therefore we need to transform the physical cross sections into pseudo cross sections as shown by Van der Hagen *et al* (1992), resulting in a

two-energy group static diffusion calculation. In this section we show the results of three detectors which are situated, respectively, in the reflector far from the core (I,  $x_{\text{det}} = 1.75$  cm), in the reflector but close to the core boundary (II,  $x_{\text{det}} = 21.75$  cm) and in the core (III,  $x_{\text{det}} = 41.25$  cm).

The amplitude and phase of the fields-of-view of detector I for five frequencies ( $f = 0.1$  mHz, 10 mHz, 1 Hz, 10 Hz and 50 Hz) are shown in Figure IV.2. A distinct peak around the detector can be seen, whereas for remote positions the amplitude is negligible. The height of the peak is independent of frequency. A remarkable feature of the phase the large change around  $x = 30$  cm. This is the transition from the reflector to the core. The magnitude of the jump in phase depends on the frequency. The meaning of the jump in the phase is explained on page 83.

First we go into detail on the behavior in the vicinity of the detector. We have therefore plotted the amplitude and the phase in Figure IV.3 for values of the position in the range of 0 to 16 cm. The amplitude plotted on a logarithmic scale shows a linear behavior with a slope of  $-0.476 \text{ cm}^{-1}$ . The phase also shows a linear behavior, plotted on a linear scale and dependent on frequency. The slope for  $f = 10$  Hz, for example, is  $-0.0243^\circ/\text{cm}$ . This behavior in the vicinity of the detector can be seen in the light of the theory of the local effect, which has been presented in section IV.4.2. But we have to be careful, since the formulas cannot be used directly. In this 1-D slab model the point source changes into a plate source. This means that Eq. IV.29 for this case must be written as follows:

$$\frac{R(t)}{R_0} = - \frac{\Sigma_a^{\text{Cd}} V^{\text{Cd}} \alpha^{\text{Cd}} \varphi_0(x_{\text{Cd}})}{\varphi_0(x_{\text{det}})} \frac{L}{2D} e^{-x/L} \sin(\omega_0 t - x k) \quad (\text{IV.40})$$

$$\text{with } x = |x_{\text{Cd}} - x_{\text{det}}| \text{ and } k = \frac{\omega_0}{2vL\Sigma_a}$$

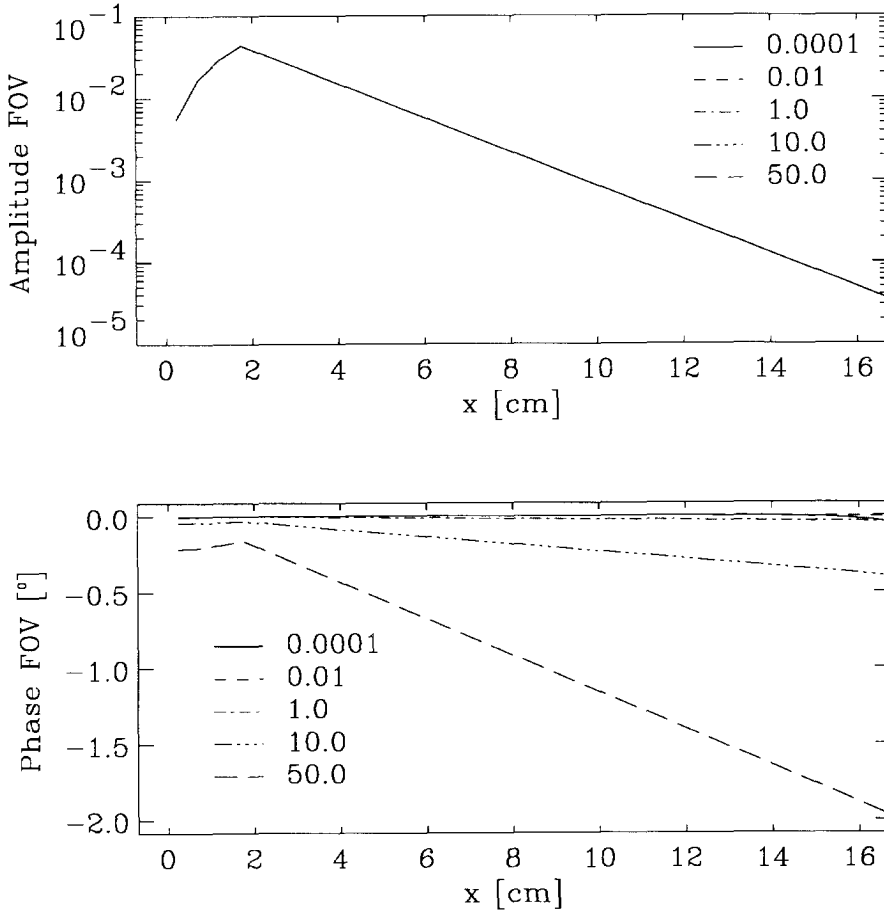


Figure IV.3: Amplitude and phase of the field-of-view for detector I ( $x_{\text{det}} = 1.75$  cm) for five frequencies in the reflector. The system is a 1D-1G model of the HOR, with a homogenized core surrounded by water. The core boundaries are at  $x = 30$  cm and  $x = 53$  cm.

From Table IV.1 we can learn that the decay in amplitude must be  $-0.477 \text{ cm}^{-1}$  and the change in phase along the distance must be  $-0.0244^\circ/\text{cm}$  for  $f = 10$  Hz. This comes very close to the values from the figures.



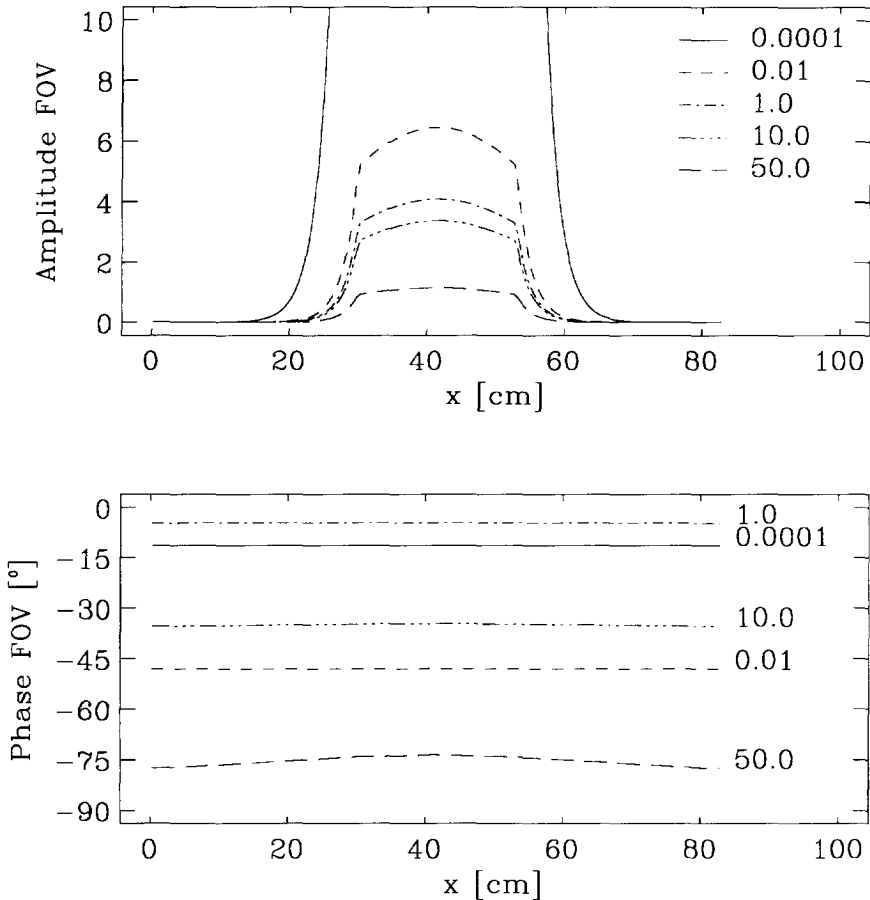


Figure IV.4: Amplitude and phase of the field-of-view for detector III ( $x_{\text{det}} = 41.25$  cm) for five frequencies. The system is a 1D-1G model of the HOR, with a homogenized core surrounded by water. The core boundaries are at  $x = 30$  cm and  $x = 53$  cm.

The response of detector III, however, is completely different as shown in Figure IV.4. Instead of a peak in the amplitude in the vicinity of the detector, independent of frequency, in this case the amplitude is high along the total core length and is strongly dependent on frequency. The phase does not show the sudden jump at the core boundary, but we can still observe the gradual increase of the phase in the reflector.

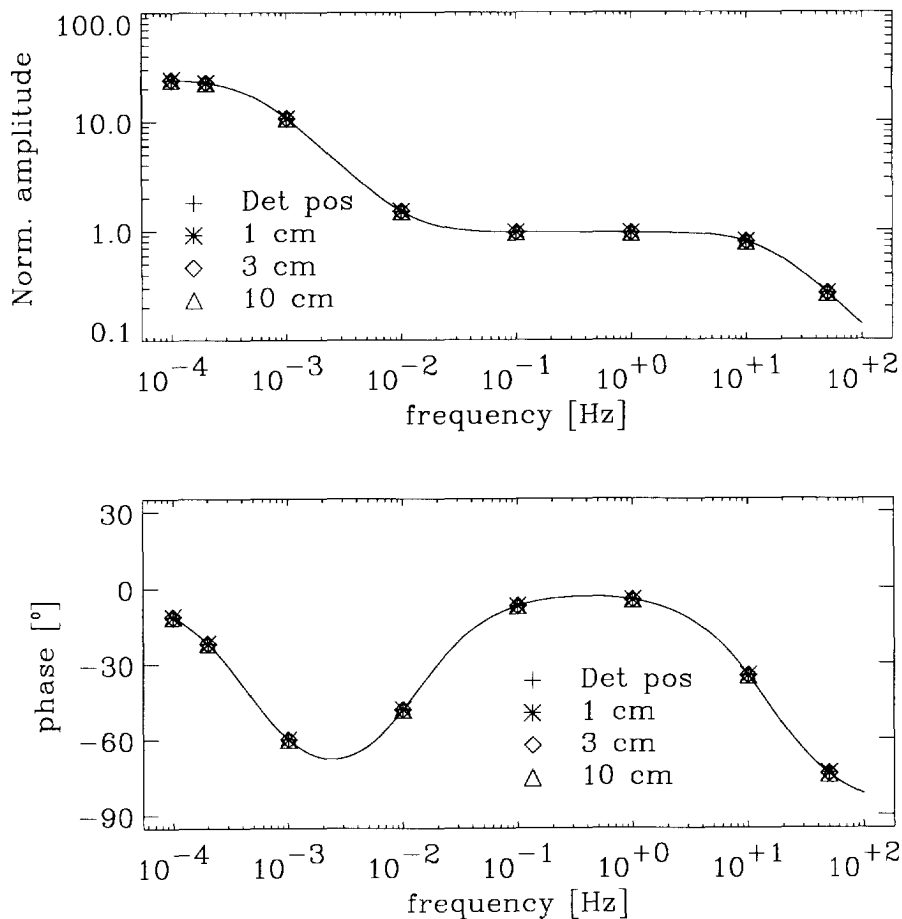


Figure IV.5: Amplitude and phase of the field-of-view for detector III ( $x_{\text{det}} = 41.25$  cm) versus frequency for three different positions: at the detector position, and at 1, 3 and 10 cm from the detector in the core. The solid line indicates the result of the reactivity transfer function multiplied by  $\beta$ . The system is the 1D-1G model of the HOR.

To understand this, Figure IV.5 shows the detector responses at four positions in the core versus the frequency together with the result of the reactivity transfer function for this reactor. The values from the field-of-view calculations are normalized with the second part on the right-hand side of Eq. IV.31. Both this normalized field-of-view

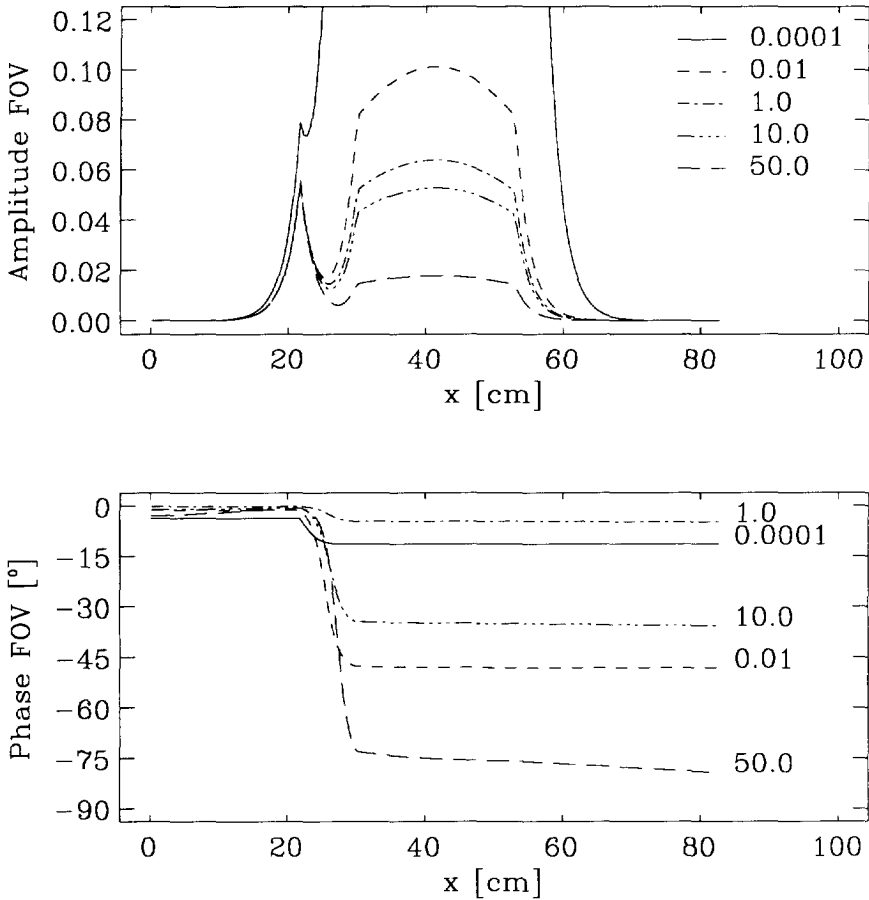


Figure IV.6: Amplitude and phase of the field-of-view for detector II ( $x_{\text{det}} = 21.75$  cm) for five frequencies. The system is a 1D-1G model of the HOR, with a homogenized core surrounded by water. The core boundaries are at  $x = 30$  cm and  $x = 53$  cm.

function and the reactivity transfer function are multiplied by  $\beta$ . From the figure we can see that there is an excellent correlation between the results of the field-of-view theory and the global theory. This means that the neutrons detected by detector III are mainly the ones from the fission chain, with their corresponding characteristics.

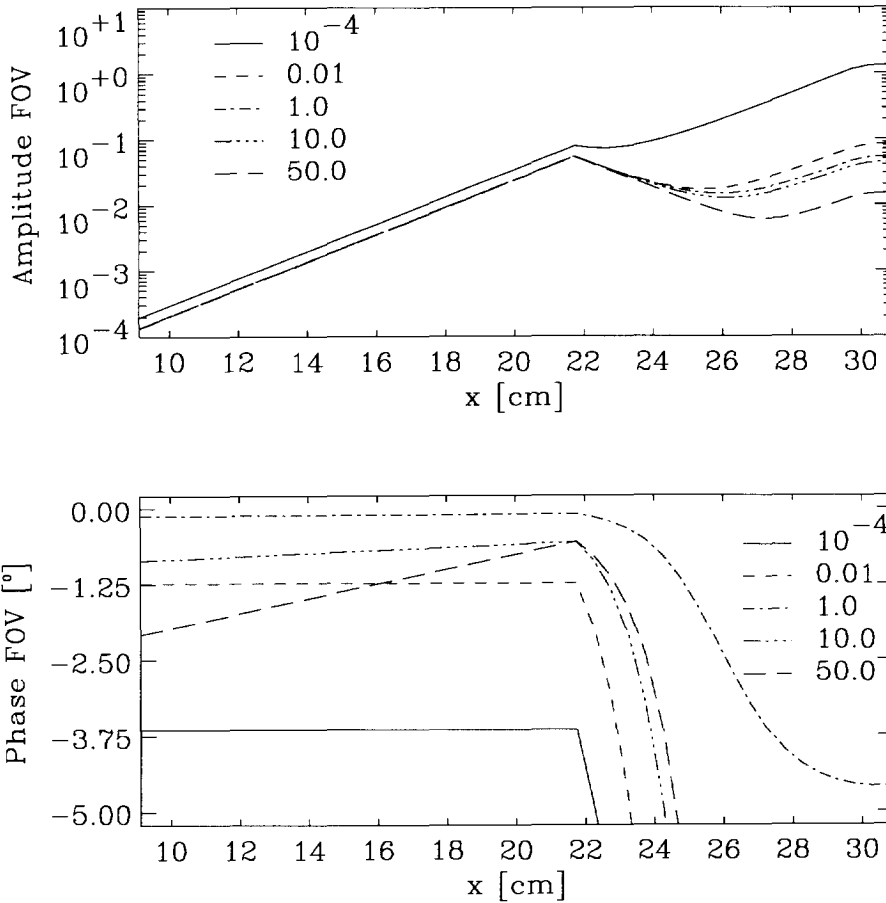


Figure IV.7: Amplitude and phase of the field-of-view for detector II ( $x_{\text{det}} = 21.75$  cm) for five frequencies in the reflector. The system is a 1D-1G model of the HOR, with a homogenized core surrounded by water. The core boundary is at  $x = 30$  cm.

This also gives insight into the reason for the sudden jump in the phase of Figure IV.2. Although the chance that the detector far in the reflector responds to a neutron coming from the core is very small, if it does sense one it is most probably one coming from the fission chain. Therefore the detector response function of detector I for the core

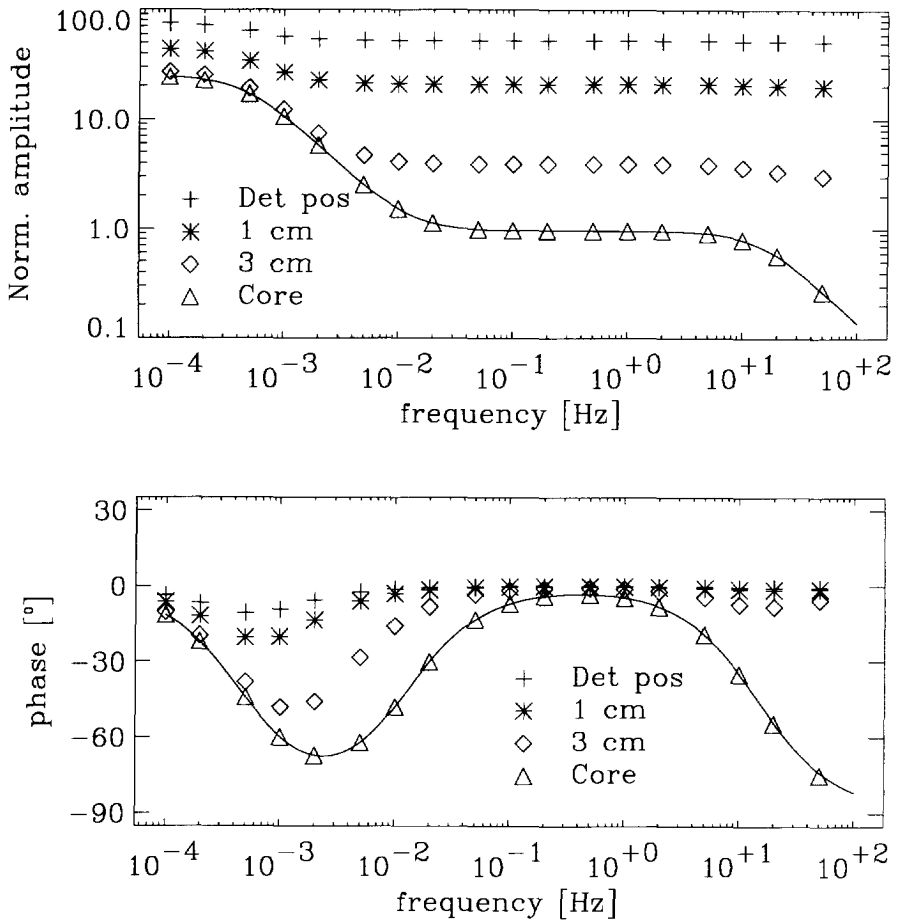


Figure IV.8: Amplitude and phase of the field-of-view for detector II ( $x_{\text{det}} = 21.75$  cm) versus the frequency for three different positions: at the detector position, at 1 and 3 cm from the detector towards the core boundary and in the middle of the core. The system is a 1D-1G model of the HOR, with a homogenized core surrounded by water. The core boundaries are at  $x = 30$  cm and  $x = 53$  cm.

region has the characteristics corresponding to the characteristics of the fission chain and thus has a frequency dependent phase change.

Up to now we have shown the responses of two detectors which can be seen as a practically pure local detector (detector I) or as a

practically pure global detector (detector III) due to their position far from the core or in the core respectively. But the position of detector II is neither far from the core nor in the core. This of course influences the behavior of the detector response as we can observe in Figure IV.6. Both the amplitude and the phase have features of the detectors I and III. For example, there is a clear peak in the amplitude for almost all frequencies, but we can also see the large increase in amplitude going to very low frequencies, which must be ascribed to a global effect. The peak is no longer independent of the frequency. Besides, the sudden jump in the phase at the core boundary is present, which is an indication of the local component of the detector response.

To emphasize the local component, in Figure IV.7 the amplitude and the phase of the detector response are drawn for positions closely around the detector. We can see the linear behaviour again for both the amplitude on a logarithmic scale and the phase on a linear scale for positions that are located to the left of the detector. The slopes are again in close agreement with the ones predicted by local theory.

However, at the right-hand side the local theory fails completely. But for these positions the global theory is the better approach as can be seen in Figure IV.8. The response of the detector as calculated by field-of-view theory matches almost exactly the solid curve of the reactivity transfer function for positions in the core. But for the positions in the reflector close to the detector the global theory fails.

The effect of adding the global effect and the local effect is shown in Figure IV.9. The upper part shows the different components in relation to the results of the field-of-view calculation. The difference between the summation of the global and local effect and the field-of-view calculation is hardly noticeable. Therefore in the lower part the ratio between the amplitude of the field-of-view and the summation of the global and the local component is shown. We can see that for practically every position in the system the difference is less than 1%. Only for positions very close to the boundary of the system, where the values are small in absolute sense, this does not hold. From this comparison we can conclude that the combination of the global and the

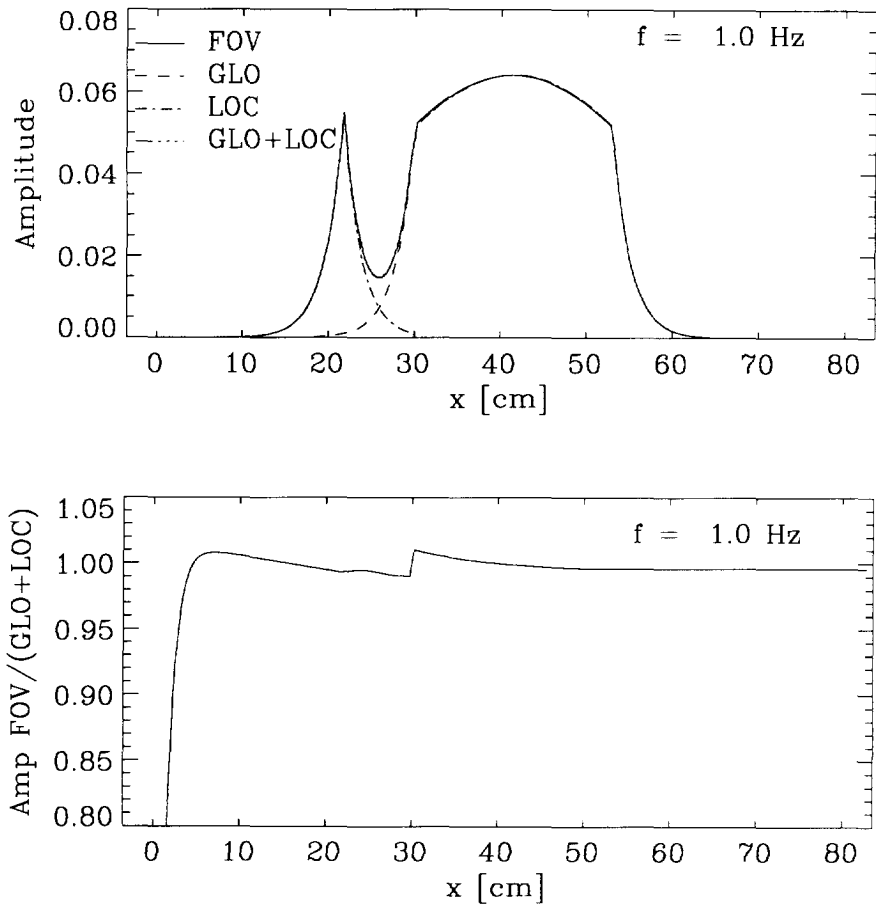


Figure IV.9: Comparison of the detector response of detector II ( $x_{\text{det}} = 21.75$  cm) calculated by the field-of-view theory (FOV), the global theory (GLO), the local theory (LOC) and the summation of the global and the local theory (GLO+LOC) for a frequency of 1 Hz. In the lower plot the ratio in amplitude of the field-of-view theory and the combination of the global and local theory is plotted. The system is a 1D-1G model of the HOR, with a homogenized core surrounded by water. Core boundaries are at  $x = 30$  cm and  $x = 53$  cm.

Table IV.2: Data of the two-dimensional, two-energy group model of the 'Hoger Onderwijs Reactor'. The values are based on the two-energy group values of De Vries (1974).

	Core		Reflector	
	group 1	group 2	group 1	group 2
D [cm]	1.43	0.207	1.05	0.146
$\Sigma_a$ [cm <sup>-1</sup> ]	$2.84 \cdot 10^{-3}$	$7.06 \cdot 10^{-2}$	$4.00 \cdot 10^{-4}$	$1.97 \cdot 10^{-2}$
$\Sigma_{s,1i}$ [cm <sup>-1</sup> ]	-	$2.13 \cdot 10^{-2}$	-	$3.4 \cdot 10^{-2}$
$\Sigma_{s,2i}$ [cm <sup>-1</sup> ]	0.0	-	0.0	-
$v\Sigma_f$ [cm <sup>-1</sup> ]	$4.25 \cdot 10^{-3}$	0.107	0.0	0.0
$\chi_p = \chi_i$	1.0	0.0	1.0	0.0
$v$ [cm·s <sup>-1</sup> ]	$2.5 \cdot 10^8$	$2.2 \cdot 10^5$	$2.5 \cdot 10^8$	$2.2 \cdot 10^5$

local theory is a very good approximation for the total detector response in a one energy group model.

#### IV.6.2 A moving absorber in a 2D-2G model of the HOR

A more realistic picture can be given in a multi-dimensional model with more energy groups. Therefore we model the same reactor as in the previous section in a two energy group way in two dimensions. Table IV.2 shows the cross section. They are taken from De Vries (1974). The kinetic parameters are:  $\beta = 0.62\%$ ,  $\lambda = 0.0767 \text{ s}^{-1}$  and  $\Lambda = 6.63 \cdot 10^{-5} \text{ s}$ . The reactor geometry is shown in Figure IV.10. The core is again taken as being homogenized. It is surrounded by water. The position of the detector used in this section is indicated by a cross. The reactor is slightly subcritical:  $\rho_0 = -5.0 \text{ pcm}$ .



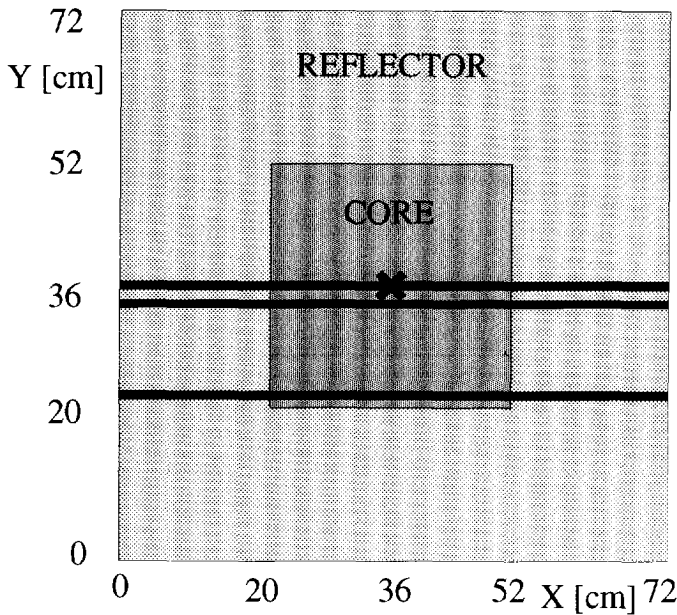


Figure IV.10: Geometry of the 2D-2G model of the HOR. The cross indicates the detector position. The solid lines show the x-positions of the oscillator (see Figure IV.11 and Figure IV.12).

The numerical experiments in this 2G-2D model with an oscillating absorber can be seen as a qualitative simulation of the experiments to be described in Chapters V and VI. The movement of the absorber is modelled with two modulating absorbers which differ by  $180^\circ$  in phase. In our case the  $0^\circ$  phase point is always put at the left-hand side of the oscillator, i.e. for smaller values of  $x$ , whereas the  $180^\circ$  phase point is always at the right-hand side of the oscillator. All phases shown in the figure are relative to the  $0^\circ$  phase of the left-hand side point. In the numerical experiments described below the oscillator is modelled with two adjacent mesh points. The distance between the mesh points is always 1 cm. In the following 'moving the oscillator to another position' means that both points of the oscillator are displaced and the new position is the middle of both oscillator points.

In Figure IV.11 and Figure IV.12 the results of calculations are shown for a cadmium oscillator placed at various positions in the

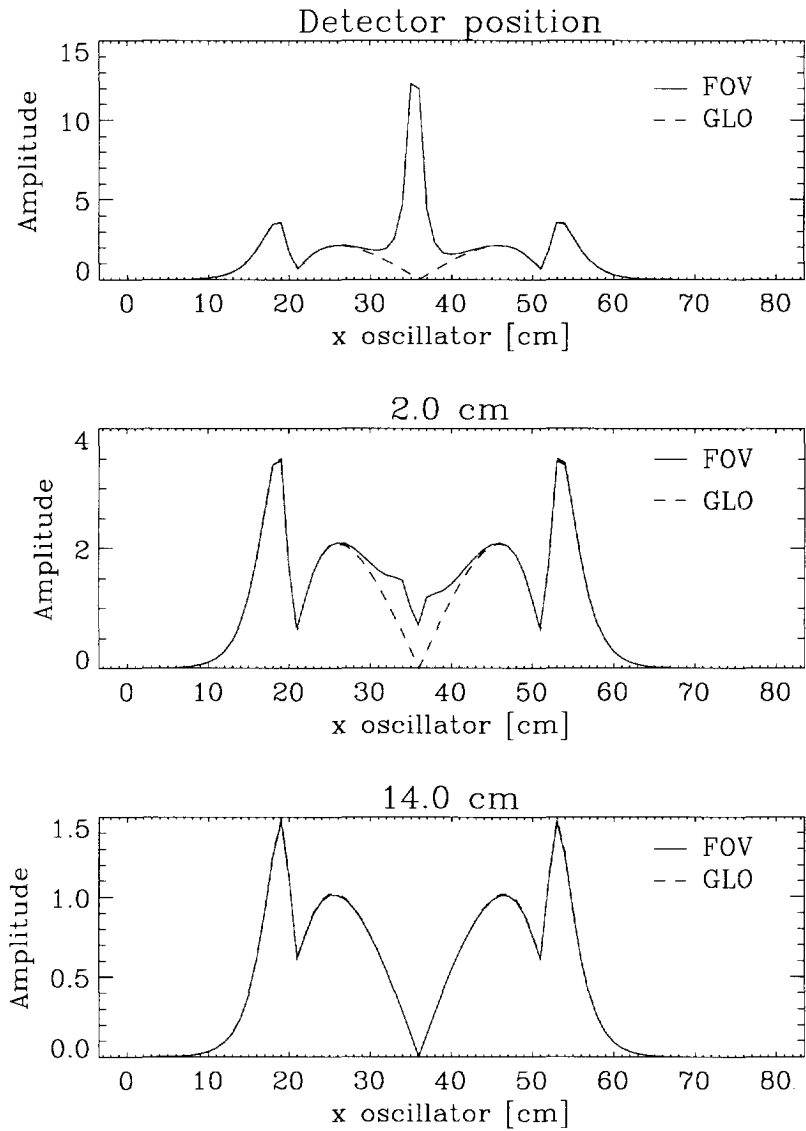


Figure IV.11: The amplitude of the detector response calculated by the field-of-view theory (FOV) and the global theory (GLO) to an oscillating absorber versus the x-position of the absorber for three different positions of the absorber in y-direction (see Figure IV.10 for a description of the geometry and the positions of the detector).

system. In the upper plots the oscillator is placed at the same y-position as the detector. The oscillator is then moved from one side of the reactor to the other side along the x-direction. In Figure IV.10 this has been indicated by the upper solid line. Both amplitude and phase of the field-of-view calculation are compared with the results as predicted from global theory. As we can see, for parts of the system far away from the detector position the amplitude of both theories only differ slightly. But if the absorber comes close to the middle of the core, the reactivity effect of the oscillator decreases, due to the flatter flux. The result is a decreasing response of the global effect. If the oscillator position is exactly at the middle of the x-axis the reactivity effect is even zero due to the symmetry of the reactor model. This zero amplitude at 36 cm, which is the middle of the reactor in x-direction, is confirmed in the figure. The field-of-view calculation, however, shows a sharp increase at that point, since then the oscillator has strong local effect on the detector response.

As far as the phase is concerned in the upper left part of Figure IV.12 we can see that at the left side and in the vicinity of the detector the response gradually increases from the  $-5^\circ$  of the reactivity transfer function to approximately  $0^\circ$  at the detector position. The upper right plot shows the phase of the detector response if the oscillator is put at the right-hand side of the detector position. Here we can see that for positions of the oscillator close to the detector position the phase is about  $180^\circ$  and that it decreases to about  $175^\circ$  for larger distances.

This phase behavior can be understood realizing that the oscillator has been modelled to have a  $0^\circ$  phase at the left-hand side and a  $180^\circ$  phase at the right-hand side. For all positions at the left-hand side of the detector the  $180^\circ$  point of the oscillator is closest to the detector and has the major influence on the detector response. Since the oscillator is an absorber a higher influence results in a smaller detector signal. This gives another  $180^\circ$  phase shift and thus a  $0^\circ$  phase in total. The  $-5^\circ$  comes from the phase of the reactivity transfer function. If the oscillator is moved to the right-hand side of the detector the  $0^\circ$

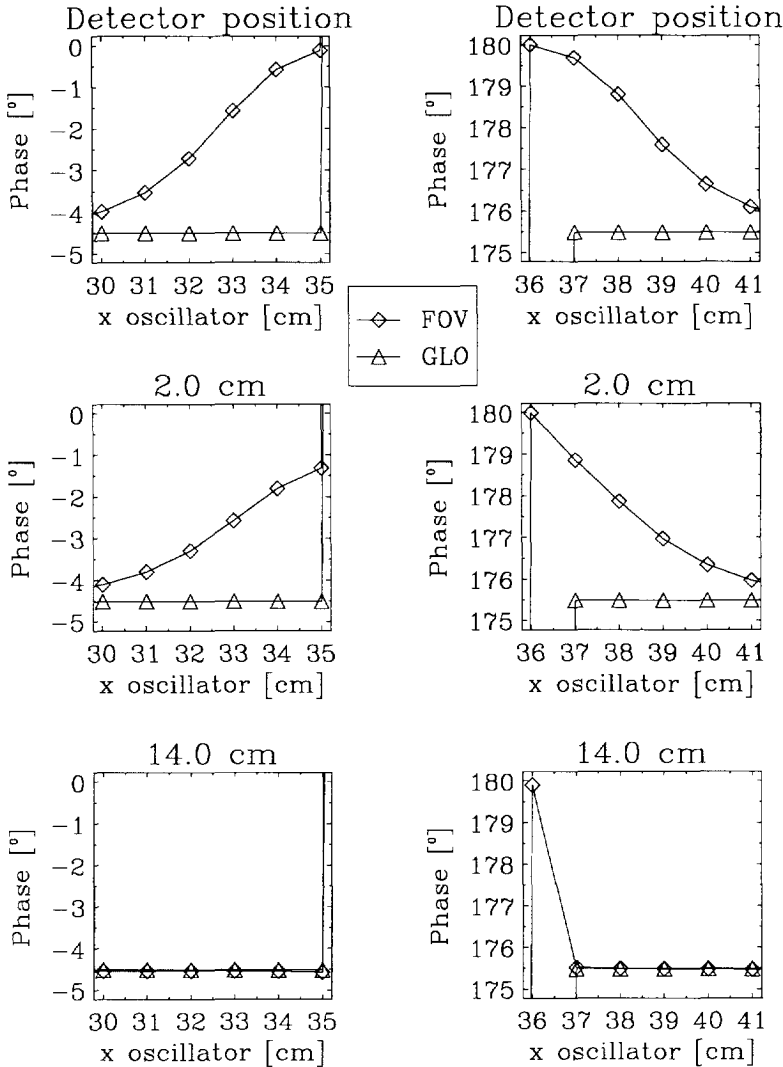


Figure IV.12: The phase of the detector response calculated by the field-of-view theory (FOV) and the global theory (GLO) to an oscillating absorber versus the x-position of the absorber for three different positions of the absorber in y-direction: at the same y-position as the detector, and at 2 and 14 cm from the y-position of the detector. The position of the detector is (36 cm, 36 cm). The system is a 2D-2G model of the HOR, with a homogenized core surrounded by water. Core boundaries in both x and y direction are at 20 cm and 52 cm.

point of the oscillator has a larger influence resulting in the  $180^\circ$  phase in the detector response due to the negative influence of the absorber.

In the figures we can also see the response of the detector calculated by field-of-view theory and the global theory for y-positions farther away from the position of the detector. It is clear that both theories become gradually more similar.

## **IV.7 Discussion and conclusion**

Both theoretical concepts, the field-of-view theory and the combination of the global and local theory, show a large degree of similarity in the results. But if one had to choose between both methods, from a theoretical point of view the field-of-view theory is preferable, since no assumptions on the existence of global and local components have to be made. However, there are some problems with the applicability of the theory.

The first one is that the field-of-view calculation must be done in the frequency domain. One has to perform a new calculation for every single frequency that is in the source. This is no problem, if the source is a truly sinusoidal modulated perturbation as shown in section IV.5.1. But in other cases like the one in which an absorber is moving (section IV.5.2) approximations as to the movement have to be made. It is possible to approximate the field-of-view function to a frequency independent function shown, for example, by Kleiss & Van Dam (1979) However, in that case the theory loses an important feature. Of course one can try to solve the field-of-view problem in the time domain, but in that case the inverse Laplace transform of the field-of-view function has to be found. In some very special cases this is possible, but in the majority of practical problems it is not.

In the global theory no such fundamental problem arises. Although we have given the frequency independent form in our equations of the global theory in the time domain above, in principle one can perform a convolution with the inverse Laplace transform of the reactivity transfer function (see, for example, Duderstadt & Hamilton, 1976).

Another consideration in the comparison between the field-of-view theory and the combination of the global and local theory can be that the combination explains the different phenomena in the detector response very intuitively. Besides that, in many cases it is easier to calculate the detector response if we use the separate global and local theories than to calculate the detector response with the field-of-view theory.

However, to be able to verify the seriousness of the approximations in the theory it is important to perform experiments in a real reactor. In the last two chapters we show results of experiments in which we test the theory of small variations.



# **Chapter V**

## **The experimental facility DISTY - Setup and methods of analysis**

### **V.1 Introduction**

In the late sixties and early seventies some publications of, among others, Seifritz and Cioli (1973) and Wach and Kosály (1974) drew attention to the space-dependent effects of small disturbances in nuclear reactors. They measured and interpreted the cross spectra of in-core neutron detectors in boiling water reactors and suggested the existence of local and global driving sources. It was already known that the global noise could give important information of the state of the reactor, but the existence of a local component could add some interesting aspects. The fact that this phenomenon of local and global neutron reactor noise was investigated first in boiling water reactor was because of the boiling process in the reactor vessel. The boiling namely evoked a strong local noise. This local noise, for example, could be used to measure the flow rate in a boiling water reactor. Especially in reactors with a natural circulation of the cooling water, this method of measuring the flow velocity was applicable, since in this type of reactors the flow rate is inherently unknown beforehand (Stekelenburg, 1993).

A lot of experimental research has also been performed on this local/global neutron noise. For example Fuge *et al* (1977) and Kleiss & Van Dam (1979) performed experiments in which detectors were placed somewhere in a core. Close to the detectors bubbles of air were released which disturbed the flux and so the response of the detectors. Although care was taken to control the release of the bubbles



as carefully as possible, information of the exact position was hard to get in such a set-up. Not knowing the exact position of the disturber was a drawback in the interpretation of the responses of the different detectors. Therefore new experiments, in which the position of the disturber was available were mandatory.

The apparent and inherent existence of local and global noise sources in boiling water reactors was the main reason why the early investigations were related to the boiling processes in the reactors. But other neutron noise sources can also play an important role. An example is the vibration of control rods. An enormous amount of experimental and theoretical data is available of spectra of vibrating rods (Laggiard *et al*, 1993). Usually the spectra come from real power plant data and are used to determine the possible failure of structures around the control rods. The drawback of the experiments is once again the lack of knowledge of the exact position of the disturber.

In view of the aforementioned lack of experimental data with well-defined disturbers we performed more suitable experiments. A first attempt has been made with the so-called TURBO facility. This facility was mainly designed to investigate the principle of a special turbine flow meter to be used in natural circulation boiling water reactors. This investigation has been described by Van der Hagen (1993). In that experiment a piece of cadmium was rotated in a flux gradient. Due to this movement fluctuations in the neutron flux occur, which can be measured by neutron detectors. The smallest distance between the detectors and the disturber in this experiment was about 6 cm. Although this was close enough to prove the principle of the turbine flow meter, for more detailed investigations it would be better to put the detector closer to the disturber. Besides this, the TURBO facility was not very flexible in use. It was, for example, very difficult to change the position of the disturber. Although we performed some preliminary experiments with the TURBO facility, we decided to build a new facility.

In this chapter the experimental facility, which we named 'DISTY', are described. The reactor in Delft, the 'Hoger Onderwijs Reactor', will also be described, since the facility was designed to be used in this

reactor. After this the methods of analysis of the experimental data are explained.

## **V.2 Description of the experimental facility DISTY**

### **V.2.1 General description**

The main features of the new facility are the following. The detectors can be placed at different distances from the disturber. Besides the facility has different kinds of disturbances and is driven in such a way that the movement of the disturber is well determined. The disturbers and the detectors can also be put at different positions with respect to the reactor core. Finally, the direction of movement of the disturber can be changed. This means that the disturber can move either to and from the core or along the core side.

To achieve a well-defined movement of the disturbers a stepping motor is used to drive the disturbers mechanically. A problem we are faced with is the fact that the electric components can not be put close to the reactor core because of the intense radiation and because of the water which is used for moderation and cooling. Therefore we put the stepping motor above the water level of the basin of the reactor. The disturber is put near the core in the lower part of the basin. The distance between the motor and the disturbers, which is about 7 metres, is bridged over by long shafts. Therefore the facility effectively consists of three parts: the 'driver' part with the motor and some transmission mechanism, the 'disturber' part with the disturbers and a middle part, which connects the other two parts.

### **V.2.2 The disturbers**

The facility contains three disturbers. Two of them have cadmium as perturber material, the other one is a vacuum box. The difference between the two pieces of cadmium is the way they move: one moves horizontally and the other one vertically. The exact movement of all disturbers will be explained later. The pieces of cadmium have the

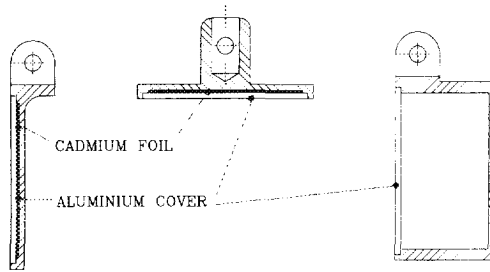


Figure V.1: Sketch of the disturbers. The left one is cadmium disturber that moves horizontally, the middle one is cadmium disturber that moves vertically and the right one the vacuum box.

following dimensions: 9 mm x 30 mm x 0.5 mm (height x width x thickness). These small pieces of cadmium are put in a small, closed box (see Figure V.1). The vacuum box is 9 mm x 30 mm x 12 mm. Both containers are made from aluminium, because this material is almost transparent for neutrons. Cadmium is used due to its strong absorbing

effect, simulating the absorbing property of control rods. The vacuum box simulates a well-described movement of a void.

### V.2.3 The driving mechanism

Figure V.2 shows a schematic view of the 'driver' part. The axis of the motor is connected to an excenter. The other end of the excenter is connected to the so called guide block by the transmission shaft. Since both sides of this transmission shaft are turning-points and the guide block is guided in guiding tubes, the guide block moves up and down. The construction leads to an approximately sinusoidal movement of the guide block. The amplitude of the oscillation can be varied from 0 mm to 1 mm by sliding the transmission shaft more or less excentrically. The oscillation of the guide block is transmitted to the three disturbers by three long shafts. The length of the shafts is approximately 9 metres. Only one shaft and thus only one disturber can be connected to the guide block at a time.

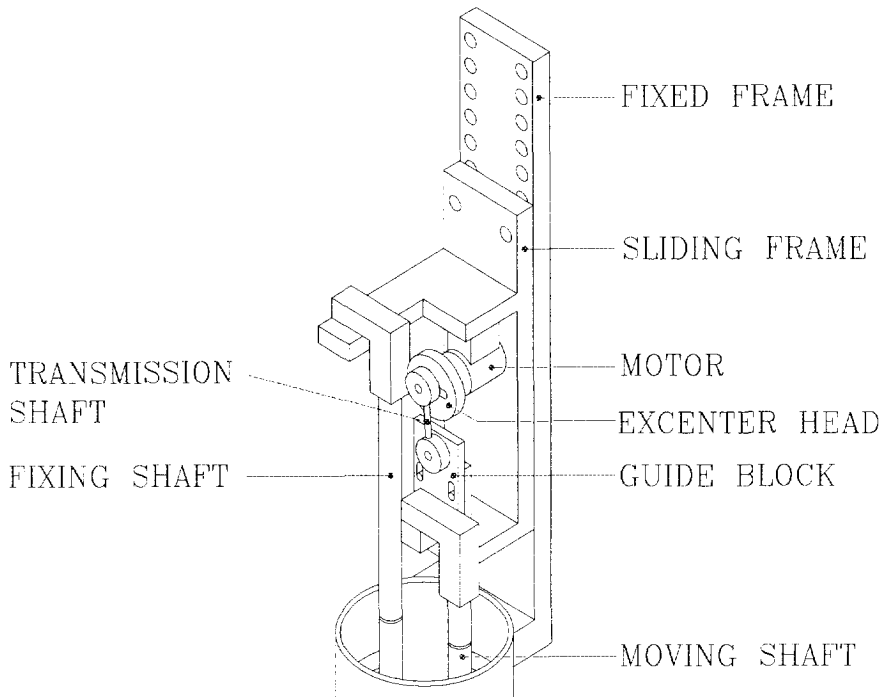


Figure V.2: Sketch of the driver mechanism.

For two of the disturbers the vertical movement of the long shaft is converted to a horizontal one. This is accomplished as shown in Figure V.3. At the bottom of a lever the piece of cadmium or the vacuum box is fixed. At the top there are two turning-points. One of these is connected to the long moving shaft from the 'driver' part, the other is fixed to a frame. By moving the short arm of the lever up and down, the long end will move along a small part of the arc of a circle. Since the ratio of the small arm and the long arm is 1:12 and the maximum displacement of the long shafts is 1 mm the maximum amplitude of the vibration of both horizontal disturbers is about 12 mm.

As for the disturber which moves vertically no extra mechanism is needed, since the movement of the long shaft is already up and down. However, the maximum amplitude is only 1 mm. Since this is too small another mechanism is required. This mechanism is already

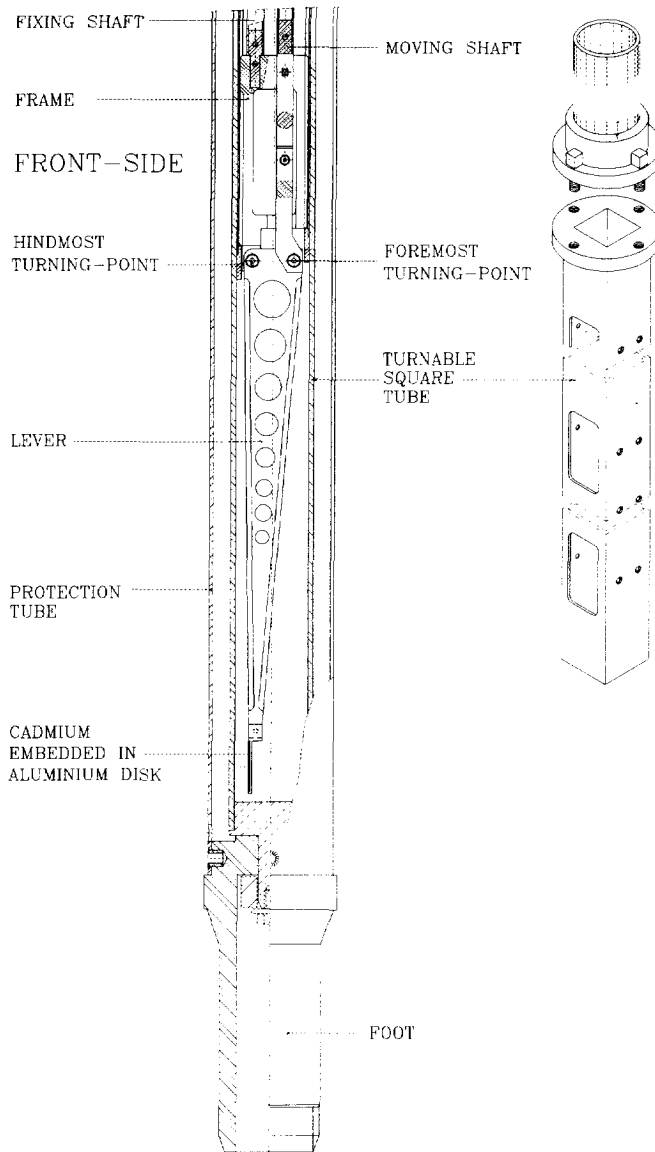


Figure V.3: Sketch of the lever that changes the vertical movement of the shaft attached to the driver mechanism to the horizontal movement for the vacuum box and one of the cadmium disturbers

mounted in the 'driver' part and enlarges the displacement of the long shaft by a factor of 12. This means that the long shaft of the vertically moving disturber already has a maximal amplitude of 12 mm.

The stepping motor type Phytron ZSS 52-200-2.5 is connected to an electric supply type Phytron ASM-02A and a steering unit type Phytron PLS-02A. The unit is used to start the motor, change the direction of the movement and change the speed of rotation. The unit is driven by a PC via the standard RS-232 serial port. The mechanical construction of the total facility is designed to be able to move the disturbers with a maximum speed of about 10 rotations per second. A disk with a small groove was fixed at the axis of the motor. Since this disk passed through an optocoupler, one electric pulse was available for every rotation of the motor axis. This pulse could, for example, be used as a trigger.

#### **V.2.4 The 'disturber' part of DISTY**

Besides the disturbers, this part consists of a square tube of 50 mm by 50 mm and a length of 1.25 metre. Two rails are mounted on the inside walls of this tube. The rails are needed to guide three frames. In this way the frames can be slid up and down. Since one end of the lever of the horizontally moving disturbers is fixed to the frame, as described in the previous section, the disturbers can be put at different heights with respect to the core. Due to a clicking mechanism, which is situated above the water level, there are 12 possible positions in height ranging from 0 cm to 55 cm in steps of 5 cm.

The square tube is mounted in a foot, which fits into the grid plate of the reactor. But it is not fixed to the foot and can be rotated. In this way the disturbers can be put at different orientations with respect to the core. There are 12 possible orientations from  $0^{\circ}$  to  $360^{\circ}$  in steps of  $30^{\circ}$ . Large holes in two side walls of the square tube allow the water to flow into the tube. This means that all disturbers and the screen are surrounded by water.

A large round protection tube of 9 metres in length and a diameter of 7 cm protects all the parts described above. It is also used to prevent

parts of the equipment getting into the basin if something breaks. A number of small holes in the wall of this tube are needed to allow water to flow inside.

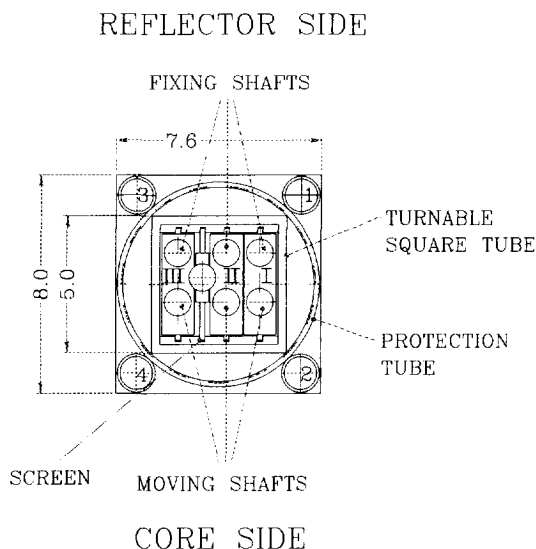


Figure V.4: Horizontal cross section of DISTY at the axial position of the disturbers. In the corners the tubes from the self-powered neutron detectors are indicated by the numbers 1 to 4. The orientation of DISTY in this figure is  $0^\circ$ .

In Figure V.4 a horizontal cross section of the 'disturber' part has been drawn. It shows the protection tube and the square turnable tube with the three disturbers. The figure also shows the positions of the local detectors, which will be described in more detail in the next section, and a screen between disturbers II and III. This screen is a piece of hafnium embedded in aluminium in the same way as the pieces of cadmium of the disturbers are embedded in alu-

minium. The dimensions of this sheet of hafnium are 50 mm x 30 mm x 0.5 mm. The idea of this screen is to put it in between a moving disturber and one of the local detectors, thereby stopping the local component whereas the global component will still be sensed by this detector.

### **V.2.5 The detectors**

Since the round protection tube will be put into the rectangular grid plate of the reactor (76 mm by 80 mm) some space is left at the corners (see Figure V.4). This space is occupied by smaller tubes with a diameter of 12 mm, which contain small self-powered neutron detectors and are numbered 1 to 4. At positions 1, 3 and 4 strings of two axially displaced detectors are available. The fixed axial distance of the detectors in strings 1 and 4 is 10 cm and in string 3 it is 14 cm. In the following the upper detector will be denoted by 'A' and the lower one by 'B'. So the upper detector at position A will be described as '1A' and so on. The detectors all have a cadmium-magnesium emitter of 3 mm diameter and of 20 mm length. At position 2 only one self-powered neutron detector with a cobalt emitter of 2 mm diameter and of 210 mm length is available. In contrast with the square tube with the disturbers, the detectors have fixed positions in the horizontal plane. This means that detectors 2 and 4 are always closest to the core. However, in vertical direction the detectors can be slid continuously. Therefore the detectors can be put at various positions axially and the distances between the detectors and the disturbers can be varied continuously from as small as 3 cm to more than 1 metre. For this purpose a scale was drawn on the shafts of the detectors. However, this scale was a relative scale with respect to the lowest position the detectors could be pushed into the detector tubes. The actual position of the effective materials in the detectors with respect to the bottom of the detector was only known approximately.

### **V.2.6 The electrical equipment**

The current of the self-powered neutron detectors is led to a home-made high-quality differential amplifier. To suppress part of the background noise, generated by gamma interaction and other electric sources, we use a compensation wire as the second input of the differential amplifier. In case of the self-powered neutron detectors in one string the same compensation is used for both detectors.



The signals of the two ionization chambers of the standard reactor equipment are connected to the amplifiers of the reactor instrumentation, which have different characteristics. Unfortunately the cut-off frequency of these amplifiers is 4 Hz.

The signal of all detectors after the first amplification is led to a second home-made high-quality differential amplifier. In most cases the AC-coupling of the amplifiers is used, which has a lower cut-off frequency of 0.04 Hz.

After this second amplification a SCADAS II SC 212-1 filter system is used to low-pass filter the signal. Normally the adjustable cut-off frequency of this filter is set to 15 Hz. If necessary the signal is amplified once more after filtering. The filtered signals are sampled and stored on digital disks. In some cases the analogue signals are also recorded on magnetic tape, for which we use a Honeywell Model 101 Portable Magnetic Tape Recorder/Reproducer with Ampex 797 wideband tapes.

### **V.3 The reactor and the position of DISTY**

The reactor in Delft, the 'Hoger Onderwijs Reactor', is a small swimming pool type reactor with a core dimension of approximately 60 cm x 60 cm x 60 cm. The nominal power is 2 MW. Figure V.5 shows a schematic view of a horizontal cross section of the core and the labelling of the grid positions. The core is set-up on a 6x7 positions grid plate with a pitch of 77 mm x 81 mm. Another grid plate is attached to this grid plate, into which experimental devices like DISTY can be placed. A gap of 17 mm separates the two grid plates.

The core itself consists of 26 standard fuel elements and 4 control elements (indicated by Fu and CR, respectively). The fuel is a compound of aluminum and uranium. The uranium is enriched in  $^{235}\text{U}$  to about 93% for fresh fuel assemblies (Siemens AG-KWU, 1993). Water is used both as moderator and coolant. To conserve the highest possible quantity of neutrons in the core, Beryllium reflector elements are placed almost all around the core (indicated by Be). A

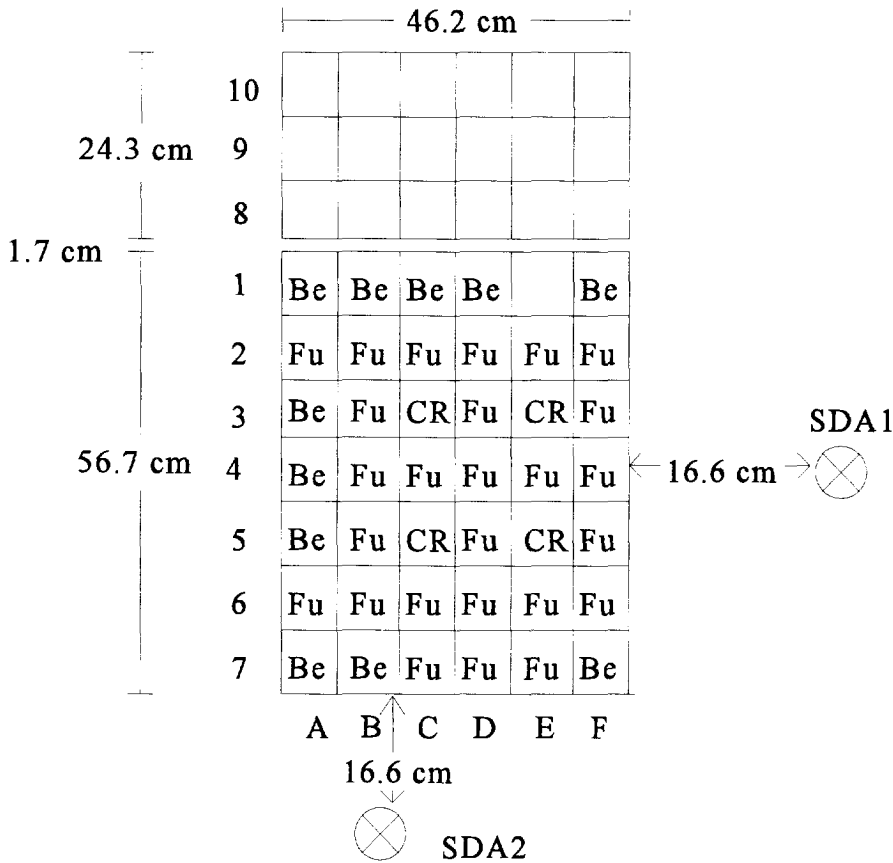


Figure V.5: Horizontal cross section of the core of the “Hoger Onderwijs” reactor in Delft. ‘Fu’ and ‘CR’ indicate fuel elements and control rod position respectively. ‘Be’ indicates the position of Beryllium elements. All other position are filled with water. On the bottom and at the left side the numbering of the grid position is shown. The positions of the two safety channels used in the experiments has also been indicated.

circulating pump allows the water to flow from the top of the core downwards into a funnel.

Ionization chambers serve as safety channels. They are placed at the right side (SDA1) and the front end of the core (SDA2). The axial position varies but is normally about 50 cm above the top of the core.

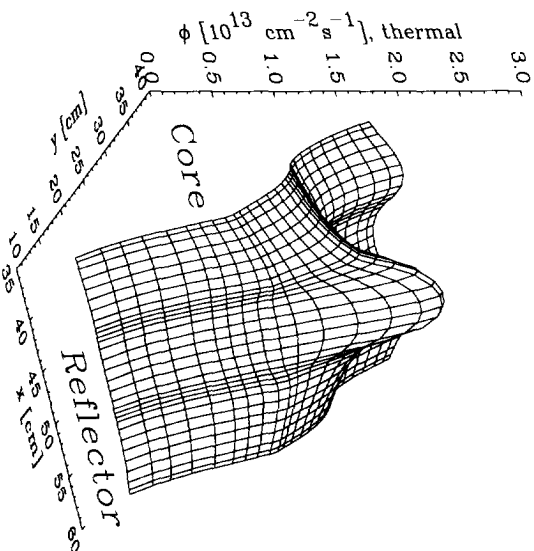


Figure V.6: Three-dimensional impression of the unperturbed thermal flux at position D1 from a five-energy group calculation performed with Bold Venture (Vondy *et al.*, 1981).

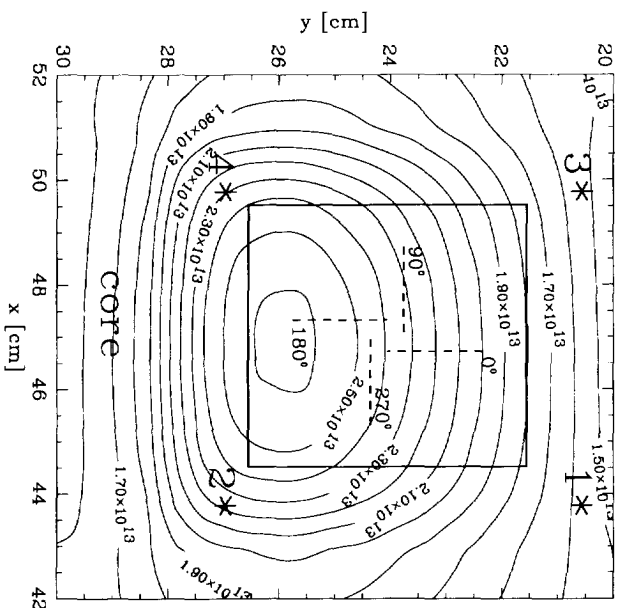


Figure V.7: Contour plot of the thermal flux at position D1. The square indicates the contour of the square tube of the disturber part of DISTY and the asterisks in the corners of position D1 show the positions of the detectors. The dashed lines show the lines along which disturber II (Cd-H) moves in the different orientations.

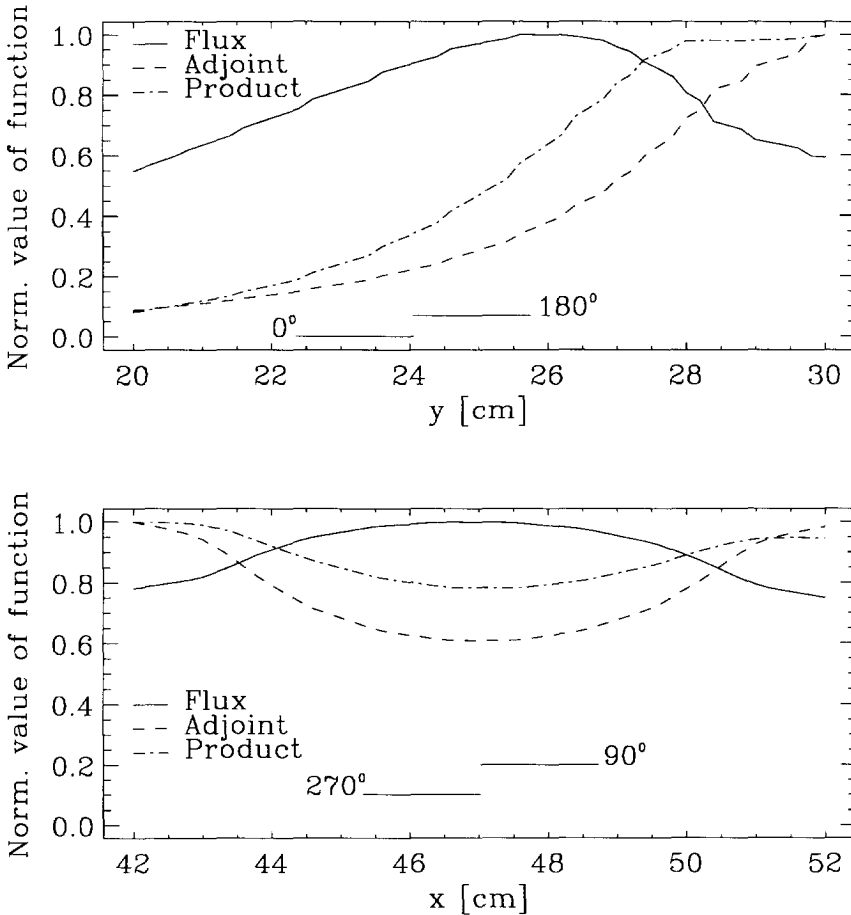


Figure V.8: Thermal flux, (thermal) adjoint function and the product of both at position D1. The upper plot is a cross section in the y-direction through the middle of D1, the lower one is a cross section in the x-direction through the middle of D1. The functions are normalized to their maximum.

This means that the minimum distance between the position of the disturbers in DISTY and the safety channels is at least 60 cm.

As can be seen, during normal operation position E1 is not occupied by either a fuel element or a beryllium element. This position can be used for experiments which need to be placed close to the core. If

necessary beryllium elements at the other positions in row 1 can be moved to E1. The empty position can then be used for experiments. Due to regulations it is prohibited to put experiments between the fuel elements at rows 2 to 7. Since DISTY was too wide to fit into positions at columns A and F, the positions available for our facility were B1 to E1 and B8 to E8.

To get an impression of the unperturbed flux at position D1, when the beryllium of D1 is moved to position E1 and thus position D1 only contains water, we have done calculations with the static diffusion computer code Bold Venture (Vondy *et al*, 1981). In Figures V.6 and V.7 the thermal flux as a result of a five-energy group calculation are shown. The contour plot of Figure V.7 also shows the lines along which the horizontally oscillating cadmium moves in the orientations  $0^0$ ,  $90^0$ ,  $180^0$  and  $270^0$ . The thermal flux in both figures clearly shows the reflector peak due to the thermalization of the higher energy neutrons in the water. To get a more qualitative view in Figure V.8 cross sections through the middle of position D1 in y- direction and x- direction have been plotted for the thermal flux, the (thermal) adjoint function and their product. This product, usually called the worth function, is exactly the function, which must be used to get the reactivity effect of the purely absorbing thermal disturber (see Eq. IV.26).

## V.4 Testing the facility

Before the facility is placed in the basin of the reactor some tests are carried out to see whether the facility worked as planned. Since all parts of the 'disturber' section of DISTY are made of aluminium and water is supposed to lubricate, the facility is tested in a tube filled with water. The tube has a diameter of about 15 cm and a height of about 6 metres. The lower part of about 1 metre of the tube is transparent. In this way we can observe the movement of the disturbers as they will behave in the reactor.

To investigate whether the movement of the disturbers is smooth, a video-camera is used. By playing back this tape at a low speed, we can

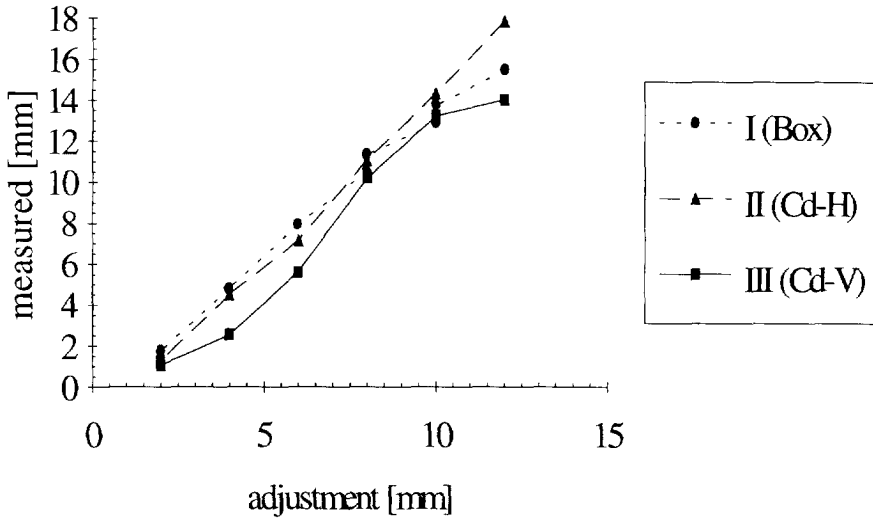


Figure V.9: The measured displacements by the photographic method as a function of the adjustment indication of DISTY.

see that the movement is very close to sinusoidal. However, due to the fact that it is only a visual inspection, it is not possible to say whether the movement is exactly sinusoidal. It can not be excluded that there are higher harmonics in the movement, but if they exist they have to be small.

Besides the shape of the movement, another important issue during the tests is its amplitude. To investigate this we take photographs of the moving disturbers with a shutter time of at least 10 seconds. In this way the maximum displacement of the disturbers can be measured. In Figure V.9 the displacement of the disturbers as a function of the adjustment of DISTY is plotted for a frequency of 2 Hz. As we can see the displacement is higher than the values of the adjustments. And in contrast with the linear relation for the two other disturbers, for the piece of cadmium that moves up and down (Cd-V) the relation is not linear. The reason for this non-linearity lies in the construction in the 'driver' part, which magnifies the amplitude of the guide block about 12 times. The construction is not capable of doing this in a fully

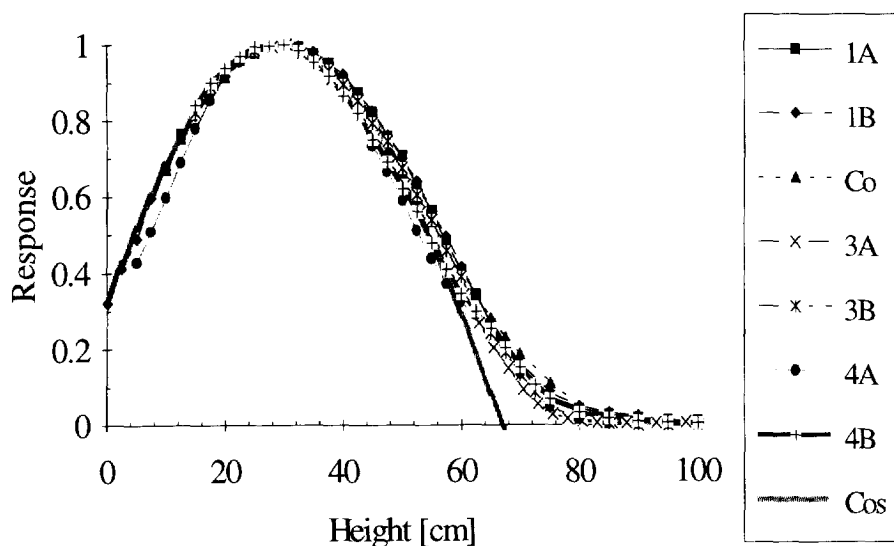


Figure V.10: Detector responses (DC-values) of all local self-powered neutron detectors versus their axial height during normal reactor operation

proportional way for the different adjustments. For frequencies up to 5 Hz we get the same results. However, for frequencies that are higher than 5 Hz the motor is not always able to drive the disturbers, especially for the vertically moving piece of cadmium and for larger values of adjustments of the amplitude.

## V.5 Testing the detectors

### V.5.1 The axial position and the axial flux distribution

As mentioned in section V.2.5, the exact axial position of the effective volume of the self-powered neutron detectors with respect to the core is only known approximately. Therefore in Figure V.10 results of measurements of the response of the detectors as a function of their height are shown. During the measurements the reactor is at its nominal power of 2 MW. The legend indicates the different detectors

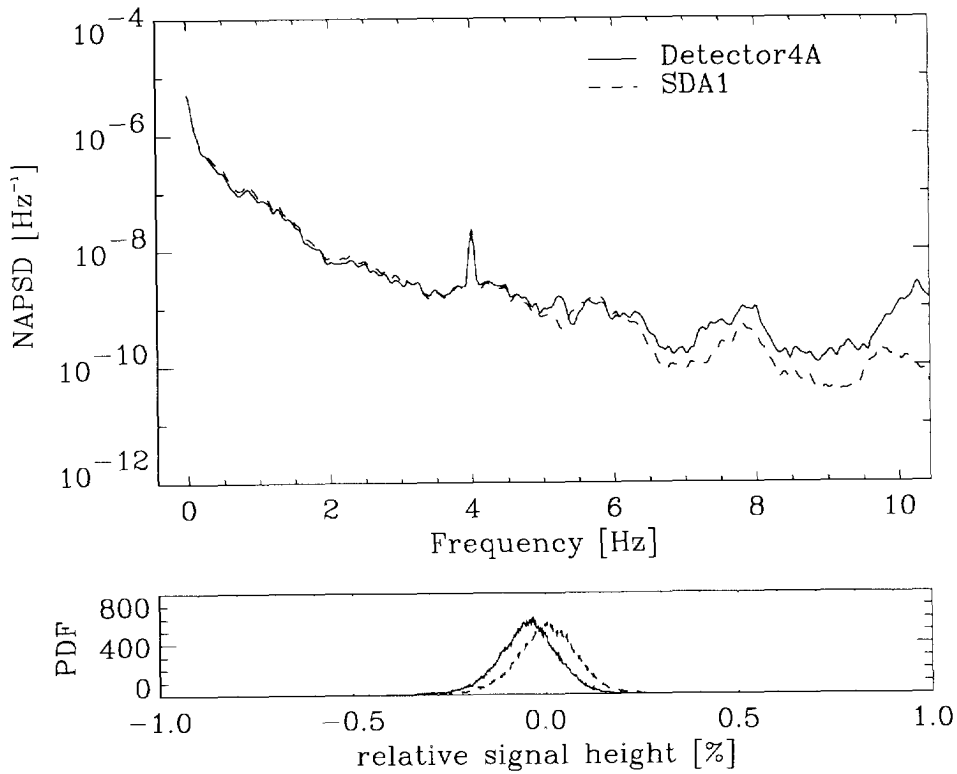


Figure V.11: Normalized auto power spectrum and probability density function during normal reactor operation of detector 4A and the safety channel SDA1. The motor was rotating at a speed of 4 Hz, whereas no disturber was coupled to it.

and the adjustment of the axial position with respect to the scale. The solid line with the open circles is a cosine fit to the points up to 60 cm. This fit can be used in calculations for the axial flux distribution of the reactor during nominal power operation. The effective height of the core is 75 cm, which is about 15 cm longer than the actual height of the core. Due to the reflection property of the water above the core we can observe a deviation from the cosine shaped curve for axial positions higher than 60 cm.



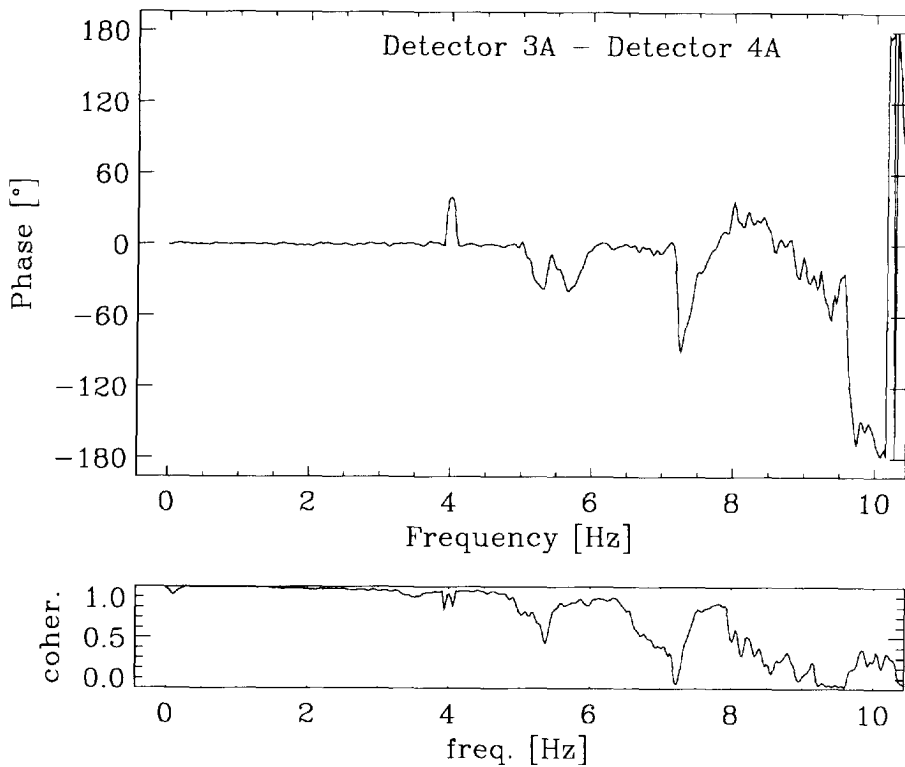


Figure V.12: Phase and coherence between detectors 3A and 4A during normal reactor operation. The motor was rotating at a speed of 4 Hz, whereas no disturber was coupled to it.

### V.5.2 Frequency spectrum of detector signals during normal operation

To have a good reference for the experiments described in Chapter VI the frequency spectrum with and without the motor rotating but with no disturber coupled is measured several times during normal operation. In Figure V.11 typical spectra of detector 4A and the safety channel SDA1 with the motor rotating at a speed of 4 Hz are shown.

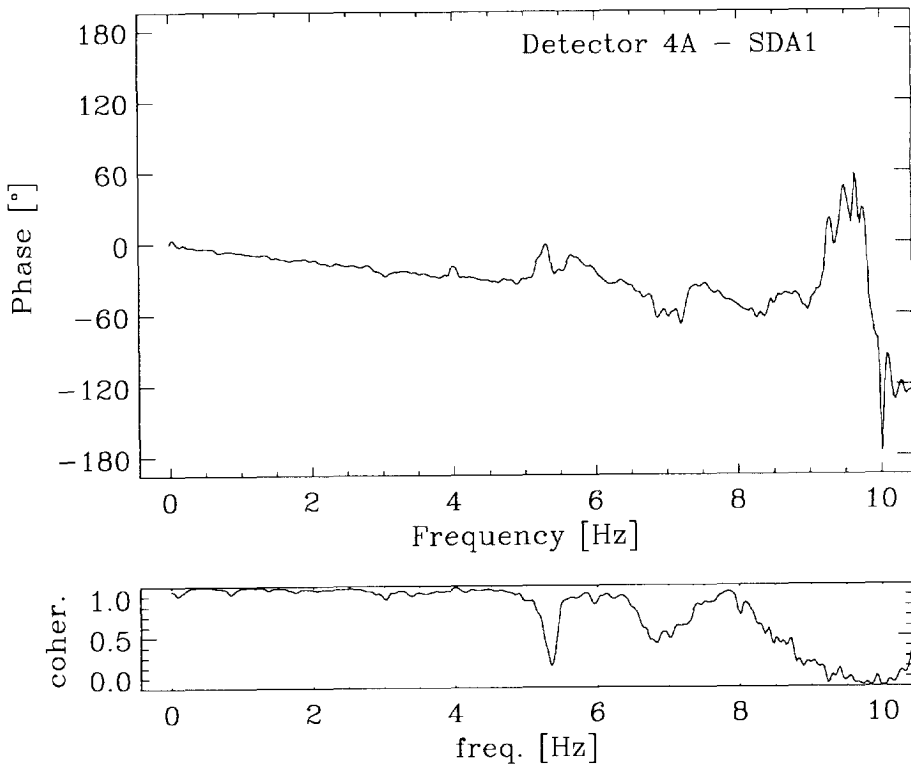


Figure V.13: Phase and coherence between detector 4A and the safety channel SDA1 during normal reactor operation. The motor was rotating at a speed of 4 Hz, whereas no disturber was coupled to it.

The spectra are the results of measurement with 100 records of 2048 samples with a sampling time of 10 ms. The sampled signals are first properly normalized using the DC-value of the detectors. After that they are Fourier transformed using a Hanning window. The frequency spacing after transformation is 0.0244 Hz. As we can see the spectrum for both detectors show some structure around 1 Hz and 2 Hz. At frequencies higher than about 4 Hz the influence of the cut-off frequency of 4 Hz of the amplifiers of the reactor instrumentation can clearly be noticed in the spectrum of the safety channel. Very remarkable is the narrow peak at 4 Hz, the frequency of the motor.

This comes from the vibration of the total facility inducing some reactivity effect. The probability density functions of both detectors are characteristic for the reactor noise in the Delft reactor.

Since we are interested in the phase changes that might occur in the results of the experiments, it is necessary to know the phase shifts between the detectors in the normal situation. In Figure V.12 the phase shift and the coherence of the detector 3A with respect to the detector 4A are plotted. The phase shift up to about 5 Hz is approximately zero and the coherence is high. Above that frequency the coherence becomes lower and the phase begins to deviate from zero. At a frequency of 4 Hz a phase change between the detectors can be observed.

Since the amplifiers of the safety channel and the amplifier of the self-powered neutron detector differ, it is possible that this has an effect on the phase shifts between the detectors. In Figure V.13 we can indeed see that there is a linear phase change. This indicates a time shift between the signals of detector 1A and the safety channels. The time delay  $\Delta t$  can be calculated from the linear phase shift and is 20.8 ms in this case. In the following this value has been used to correct for the delay in the signals of both safety channels.

## **V.6 Methods of analysis of perturbation experiments**

### **V.6.1 Frequency-averaged spectra**

Figure V.14 shows a typical example of the spectrum of one of the perturbation experiments. In this experiment the horizontally moving piece of cadmium is used as the disturber. The frequency of the movement is 1.0 Hz. Although we will go into detail on the physical aspects of the experiments in chapter VI, in this chapter some comments on the signal processing and methods of analysis of such spectra will be made.

The normalized auto power spectrum from Figure V.14 is generated by Fourier transforming, using a Hanning window, 100 records of 2048 samples with a sampling time of 10 ms one by one. The 100

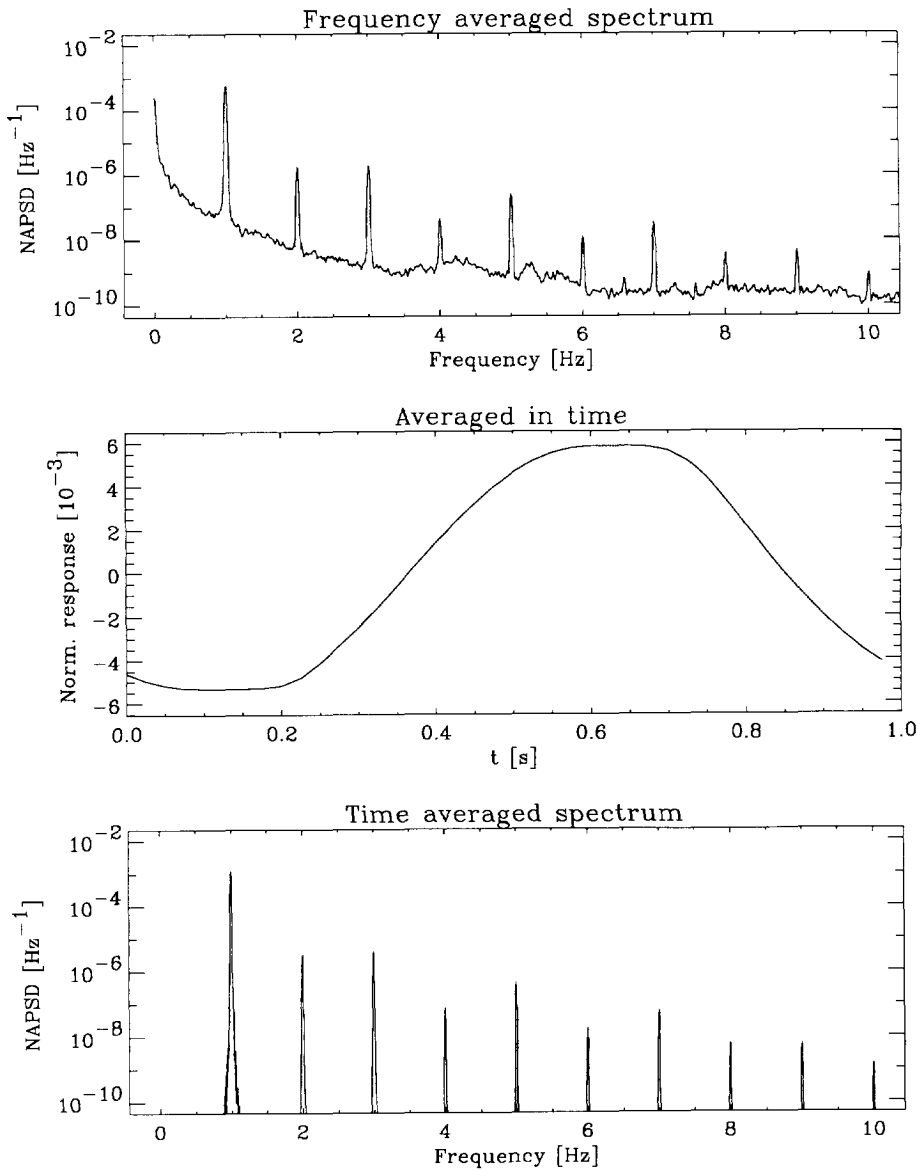


Figure V.14: A typical response of a self-powered neutron detector during the measurements. The upper plot shows the frequency-averaged normalized auto power spectrum and the lower one the time-averaged normalized auto power spectrum. The middle part shows the time averaged normalized response. In this measurement disturber II was rotated at a speed of 1 Hz.

spectra are then averaged resulting in the figure shown. This way of averaging we will call frequency-averaging. This is the standard procedure used in neutron reactor noise applications. In the spectrum a clear peak can be seen at 1.0 Hz. Besides this peak at the basic frequency, peaks at higher harmonics also appear in the spectrum. Between the peaks a spectrum similar to the normal spectrum of Figure V.11 can be seen, which is understandable since the experiments take place close to the core.

### **V.6.2 Time-averaged spectra**

We can also use another way of averaging. Remember that a pulse is available every cycle of the motor axis. This pulse can be used to trigger the averaging of the signals in time. The resulting time-average signal is also shown in Figure V.14. The oscillation of 1 Hz is apparent, but the curve is not completely sinusoidal. In order to make a spectrum of this time signal, we extend it. This extended curve is Fourier transformed using a Hanning window. In Figure V.14 the resulting spectrum is shown. The peaks at the basic frequency of 1.0 Hz and the higher harmonics are still visible. But in contrast with the frequency averaged spectrum of Figure V.14 between the peaks the power spectrum is zero. We will call this spectrum the time-averaged spectrum.

### **V.6.3 Peak contents**

In order to investigate the results of the measurements, information can be obtained from global inspection of the (averaged) time signals, the global shape of the amplitude and phase of the spectrum or the probability density function. Although this information is valuable, we also need quantitative information. Especially the values around the basic frequency and the higher harmonics of the disturber will contain useful information. However, due to the nature of the discrete Fourier transform information is only available at the discrete frequencies of the spectrum. Therefore instead of taking the local maximum at the

peaks in the normalized auto power spectrum  $C_{xx}(f)$  it is better to take an integral value as a measure of the amplitude. This value  $C_{\text{peak}}$ , which will be called the peak content, is taken as the integral over a small region  $[f-\delta f, f+\delta f]$  around the frequency  $f$  in focus:

$$C_{\text{peak}} = \int_{f-\delta f}^{f+\delta f} C_{xx}(f) df \quad (\text{V.1})$$

For the time-averaged spectra the width of the region is not very critical, since the spectrum between the peaks is very small and will not influence the integral value at all. In the frequency-averaged spectrum more care must be taken in the choice of the frequency band. However, in most cases  $C_{xx}(f)$  is orders of magnitude smaller between the peaks and therefore will only have a small influence on the integral value of the peak content.

#### V.6.4 Factorization into a set of sine waves

Instead of looking at the spectrum, either frequency-averaged or time-averaged, there is another possible method of studying the detector responses. In that approach the signals are fitted to a function which is the sum of several sine waves with predefined frequencies:

$$p(t) = \sum_i a_i \sin(2\pi f_i t + \phi_i) \quad (\text{V.2})$$

where  $f_i$  are the predefined frequencies,  $\phi_i$  and  $a_i$  the variables representing the phase and the amplitude respectively and  $p(t)$  is the total function to fit. The choice of which frequencies are taken into account has to be made on physical grounds. In our case for example the basic frequency of the disturber and its higher harmonics are a

good choice. The number of higher harmonics to take must be such that the variances in the estimators are as small as possible.

### **V.6.5 Discussion on the different methods**

To compare the methods discussed in this chapter, we apply all methods to the example in section V.6.1. As expected the fitting method and the time-averaged spectral method give practically the same results for all peaks, since they use the same information and only differ in the mathematical formulation. The result of the frequency-averaged spectrum for the basic frequency of oscillation falls within the standard deviation of the other two methods. For increasingly higher harmonic frequencies the frequency-averaged spectral method shows increasingly higher values than both other methods. The reason lies in the fact that in the frequency-averaged method the background is present, whereas for both other methods this background has been averaged out. Since the values for the higher harmonic frequencies are smaller the influence of the background is larger then for the peak at the basic frequency.

### **V.6.6 Variances**

An estimation of the variance of different spectral estimators can be given as follows (Jenkins & Watts, 1968):

$$\text{Var}[C_{xx}] \approx C_{xx}^2 \cdot \frac{W_b}{N} \quad (\text{V.3})$$

$$\text{Var}[A_{12}] \approx A_{12}^2 \cdot \left(1 + \frac{1}{\gamma_{12}^2}\right) \cdot \frac{W_b}{2N} \quad (\text{V.4})$$

$$\text{Var}[\gamma_{12}] \approx (1 - \gamma_{12}^2)^2 \cdot \frac{W_b}{2N} \quad (\text{V.5})$$

$$\text{Var}[\phi_{12}] = \left( \frac{1}{\gamma_{12}^2} - 1 \right) \cdot \frac{W_b}{2N} \quad (\text{V.6})$$

where  $C_{xx}$  is the auto power spectral density,  $A_{12}$  is the cross power spectral density,  $\gamma_{12}$  is the coherence,  $\phi_{12}$  is the phase,  $W_b$  is the windowing factor and  $N$  is the number of records used for averaging. The windowing factor is dependent on the type of windowing used for the Fourier transform. For a boxcar window it is 2, for a Hanning window it is 0.75.

The variance in the estimators of the procedure, in which a sum of sines is fitted to the time-averaged signals, is calculated following the least-square method with weighted error bands. The variance in the normalized detector response  $h^n(t)$  is calculated from the normalized response of the different records  $h_i^n(t)$  as follows:

$$\text{Var}[h^n(t)] = \frac{1}{N-1} \sum_{i=1}^N (h_i^n(t) - \bar{h}^n(t))^2 \quad (\text{V.7})$$

where the bar denotes the average of the normalized detector response.





# **Chapter VI**

## **Experiments with DISTY**

### **VI.1 Introduction**

In this chapter results of measurements with DISTY are described. First we show measurements in which the horizontally moving piece of cadmium (disturber II) is used. Since some aspects occur in all experiments the measurements with disturber II in an orientation of  $0^0$  and  $90^0$  are described in more detail. After that measurements with DISTY at all possible orientations are shown. In that section the detector responses as calculated in numerical simulations for all possible orientations are compared with the experimental results. In the next section the vertically moving piece of cadmium (disturber III) is coupled to the driver mechanism. The series of measurements with this disturber is meant to investigate the influence of the axial position of the self-powered neutron detector on the response. Finally, we look at the influence of changing the frequency of movement of the disturber.

### **VI.2 Measurements with disturber II with DISTY at an orientation of $0^0$**

#### **VI.2.1 Description of the normalized time response**

In the experiments described in this section the piece of cadmium that moves in the horizontal plane (II, in Figure V.4) is used. The axial position of the middle of the cadmium disturber is 34 cm. The frequency of the movement is 1 Hz. The AC-signals of all detectors ( $f_{ac} = 0.05$  Hz) are amplified and filtered by a filter with a cut-off frequency of 15 Hz and sampled with a sample time of 10 ms. For all

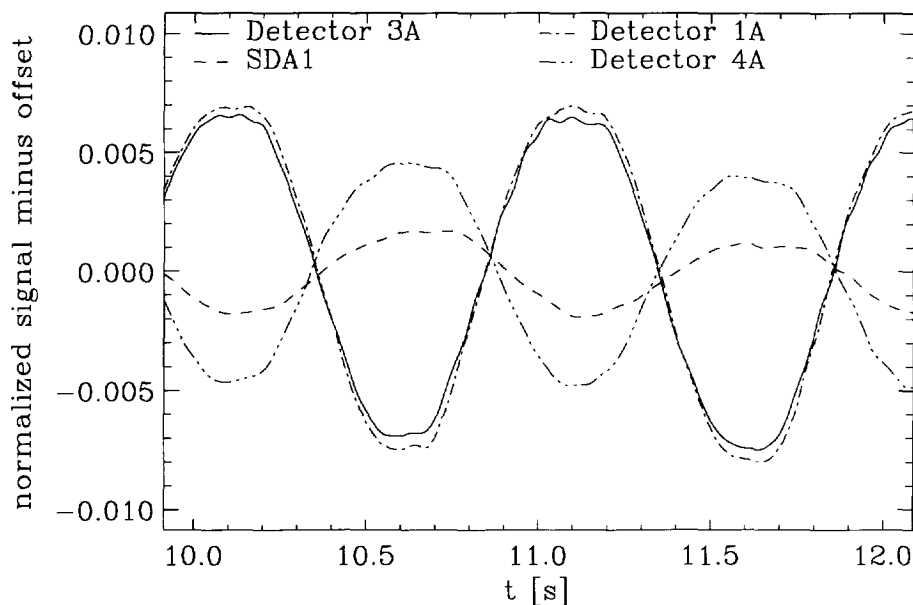


Figure VI.1: Normalized response in time-domain of detectors 1A, 3A, 4A and SDA1 due to the 1 Hz movement of disturber II. The orientation of DISTY was  $0^\circ$ .

measurements 100 records of 2048 samples are taken. These sampled responses are divided by the properly scaled DC-values of the detector signals as a normalization. The signals are Fourier transformed using a Hanning window giving a frequency spacing of 0.0244 Hz.

The axial position of the middle of detectors 1A and 3A is 36 cm from the bottom. For detector 4A it is 31 cm and for the middle of the cadmium disturber it is 34 cm. In the first measurement the orientation of the turnable tube with the disturber is as shown in Figure V.4. The normalized response during 2 seconds of the detectors 1A, 3A, 4A and the safety channel SDA1 are shown in Figure VI.1. We can clearly observe a periodic response with a frequency of 1 Hz and a normalized amplitude of approximately 0.75% for detector 1A, 0.7% for detector 3A, 0.45% for detector 4A and 0.2% for SDA1.

For detectors 1A, 3A and 4A the response can be explained looking at that detector as an almost purely local detector. If the piece of cadmium is close to the detector, the flux in the vicinity of the detector is depressed. This means that the response of the detector is small. If the piece of cadmium then moves away from the detector, the flux around the detector increases, resulting in an increasing detector response. Once the cadmium is farthest from the detector the response is maximal.

For the response of detector SDA1 this local concept cannot be used since the distance between the cadmium and the detector is more than 60 cm, which means several times the diffusion length in the surrounding water. However, this detector senses the reactivity effect induced by the moving cadmium. As explained in section V.3 to calculate the reactivity effect one can use first-order perturbation theory. In one-energy group approximation the reactivity value due to a point absorber will be negative proportional to worth function. Since, apart from the reflector peak, the worth function at the boundary of the core is higher than the worth function at a certain distance of the boundary, the reactivity effect of a point absorber close to the core is more negative than when the absorber is farther away. The global response of detector in the reactor is proportional to the reactivity and therefore the detector signal increases, i.e. becomes less negative, when the absorber moves away from the core. So, if we set the zero-offset at the average of the detector response, the positive values correspond to positions of the cadmium far from the core, whereas negative values are coupled to positions close to the core.

In Figure V.4 we can see that when the piece of cadmium moves away from the core and detector 4A, it moves towards detectors 1 and 3. This means that when the response of detectors 1A and 3A decreases due to the increasing flux depression, the signal of detector 4A increases due to the decreasing flux depression and the signal of the global detector SDA1 increases due to the decreasing reactivity. This explains the opposite phase of the signals in Figure VI.1.

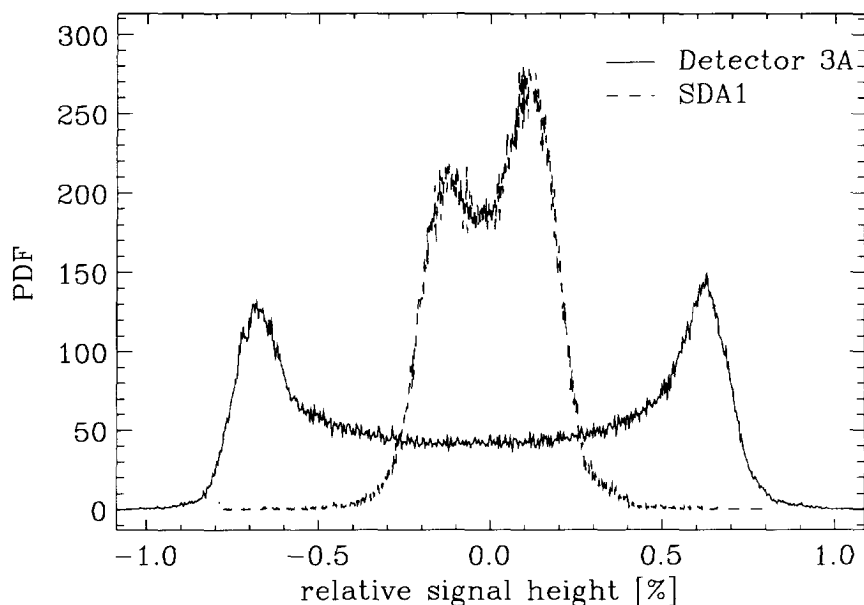


Figure VI.2: Probability density function of detectors 3A and SDA1. Disturber II was moved with a frequency of 1 Hz. The orientation of DISTY was  $0^\circ$ .

### VI.2.2 Discussion on the probability density function

In Figure VI.2 the corresponding probability density functions of detector 3A and the safety channel SDA1 are shown. Both functions show a clear bimodal behaviour, which is characteristic for a sinusoidal response, since if the response is exactly sinusoidal:  $x(t) = a_0 \sin(\omega t)$  the (normalized) probability density function is:

$$\text{PDF}(u) = \frac{1}{\pi \sqrt{a_0^2 - u^2}} \quad (\text{VI.1})$$

which is a symmetrical function around  $u = 0$  with the maximum at the value  $u = a_0$  and  $u = -a_0$  and a value of  $1/(\pi a_0)$  at  $u = 0$ . The response of the detector 3A meets this characteristic the best. The maxima lie at  $-0.65\%$  and  $+0.65\%$ , which means that the value of the probability density function at  $0\%$  must be 49. The actual value is a little lower, about 45, which comes from the fact that the values are smeared out due to the noise in the system.

The shape of the probability density function of the safety channel SDA1, however, is not symmetrical at all. As we can see the peak at positive values is higher than the peak at negative values. As mentioned above the positive values correspond to positions of the cadmium far from the core. Apparently the sinusoidal move of the piece of cadmium leads to a detector response that is more flat for positive values, i.e. for positions of the cadmium far from core.

The explanation for this more flat detector response can be given from the curve of the worth function in Figure V.8. Since the shape of the worth function is not flat, the relationship between the position of the disturber and the detector response is not linear. Therefore the response is not a pure sine if the movement of the absorber is sinusoidal. The gradient of the worth function is smaller for positions of the piece of cadmium far from the core and thus the response is more flat for these positions of the cadmium. In the probability density function this is reflected in a higher value for the positive values.

Looking more carefully at the response of detector 3A, we can see that even for this detector the height of the maxima in the probability density function is not identical either. The peak at positive values is a little higher. This shape of the probability density function can partly be explained by the same mechanism as the safety channel, since detector 3A senses both a local and a global effect. But even if the detector is a pure local detector a nonsymmetrical shape can appear. As shown in chapter IV, the relation between the position of the disturber and the detector response can be described by an exponential function of the distance between the disturber and the detector divided by the distance. Since the gradient of that function is smaller for larger distances, the relation between the position of the disturber and the

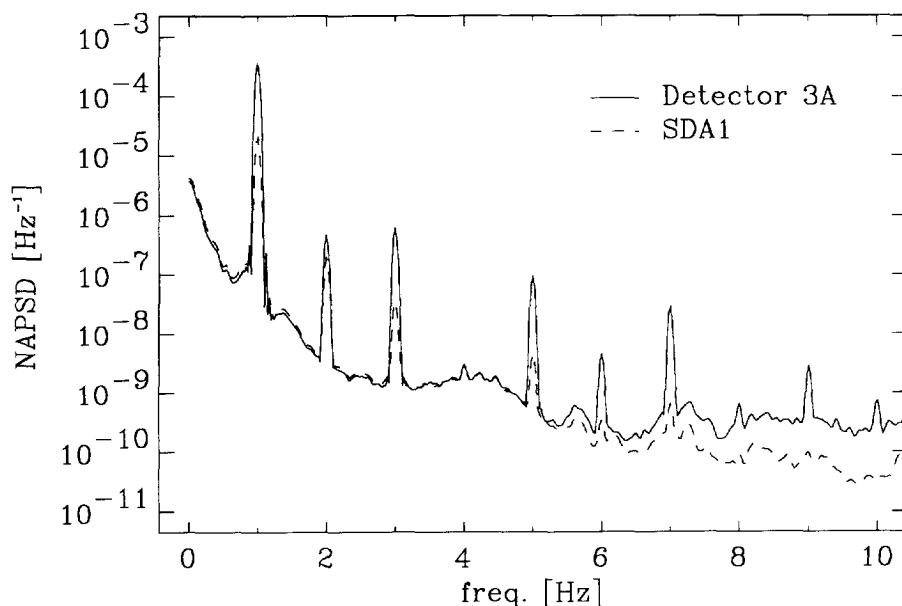


Figure VI.3: Normalized auto power spectra of detector 3A and the safety channel SDA1 in orientation  $0^\circ$  of disturber II. The frequency of movement is 1 Hz. The cut-off frequency of the amplifier of the safety channel is 4 Hz.

detector is nonlinear, resulting in a flat shape for positive values of the response.

### VI.2.3 Discussion on the normalized auto power spectrum

The normalized auto power spectra of detector 3A and the safety channel SDA1 in Figure VI.3 show a similar picture as the normal spectrum of Figure V.11, apart from the peaks at 1 Hz and the higher harmonics of this frequency. The reason for the existence of the peak at 1 Hz is given above describing the normalized time response. A quantitative discussion on the height of the peak at the base frequency is left to section VI.4, in which the results of the moving disturber II in all possible orientations are discussed.

The reason for the existence of the higher harmonics in the spectra is a combination of two effects. The first one is the nonlinear relationship between the position of the disturber and the detector response. For the local effect this nonlinearity arises mainly from the exponential function in Eq. IV.35. The curvature in the worth function of Figure V.8, is the nonlinearity of the global effect. The second possible effect is that the higher harmonics already appear in the source term, i.e. the movement of the disturber is not purely sinusoidal. To distinguish between the two effects it is mandatory to show the results at different orientations as is done in section VI.4.

In the spectrum of the safety channels SDA1 similar characteristics as those of detector 3A can be seen. However, the influence of the lower cut-off frequency of the reactor instrumentation amplifiers at 4 Hz can be noticed for both the background spectrum and the peaks at the higher harmonics above that frequency.

#### VI.2.4 Discussion on the phase

In the upper plot of Figure VI.4 we can see that the phase change between detector 3A and the safety channel SDA1 is about  $0^\circ$  for all frequencies in between the basic and harmonic frequencies up to about 7 Hz. This phase behaviour can be ascribed to the effect of the global reactor noise, which affects both the safety channel and the self-powered neutron detectors in the facility in the same way. It is basically identical to the phase diagram of Figure V.12 except for the correction of the delay time in the safety channel.

We can see that for the basic frequency of 1 Hz the phase difference between the detector signal 3A and the safety channel SDA1 the phase is  $172^\circ$ . The reason for this almost opposite phase is already explained above. The  $-8^\circ$  difference between the exact opposite phase and the response of detector 3A can be attributed to the phase change of the reactivity. From the reactivity transfer function as mentioned in chapter IV we can learn that for this reactor and for this frequency of 1 Hz the phase shift of the reactivity will be about  $-4^\circ$ . Together with the  $180^\circ$



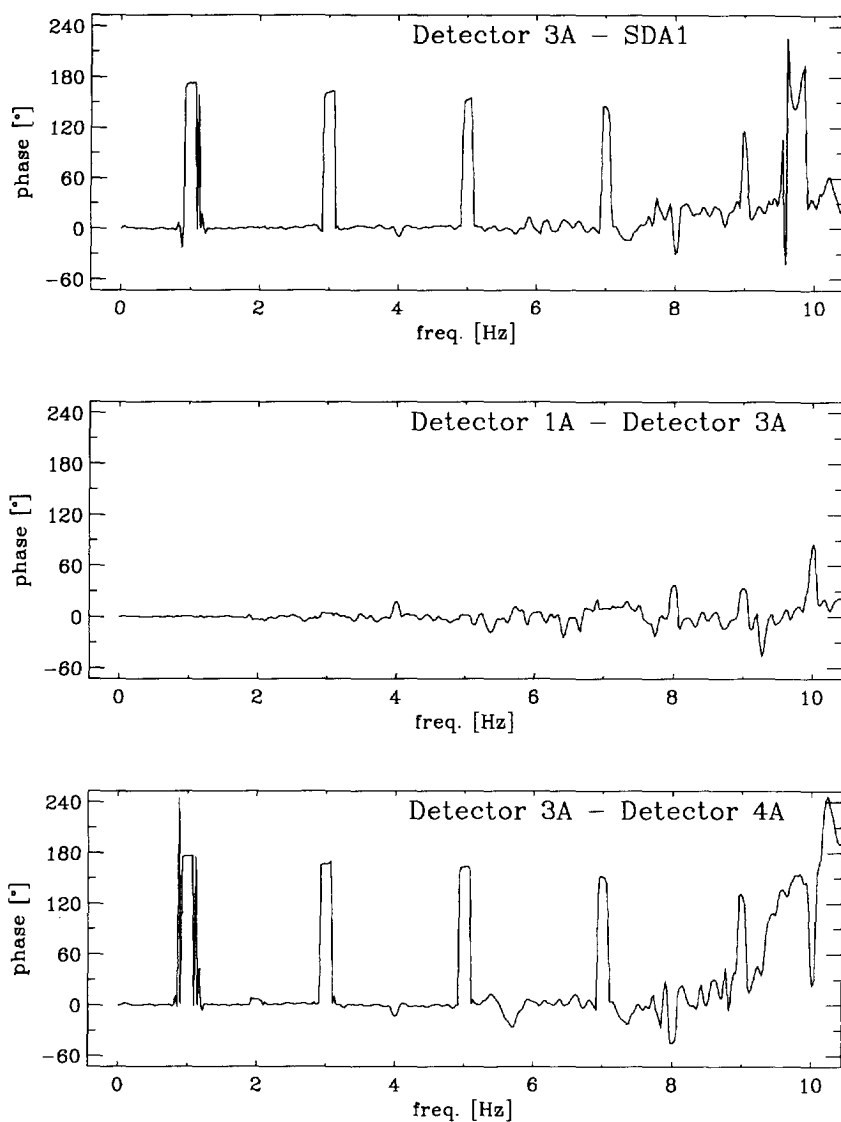


Figure VI.4: Phase difference between detector 3A and the safety channel SDA1 (upper), detector 3A and detector 1A (middle) and detector 3A and detector 4A (lower). Disturber II is moving at 1 Hz at an orientation of  $0^\circ$ .

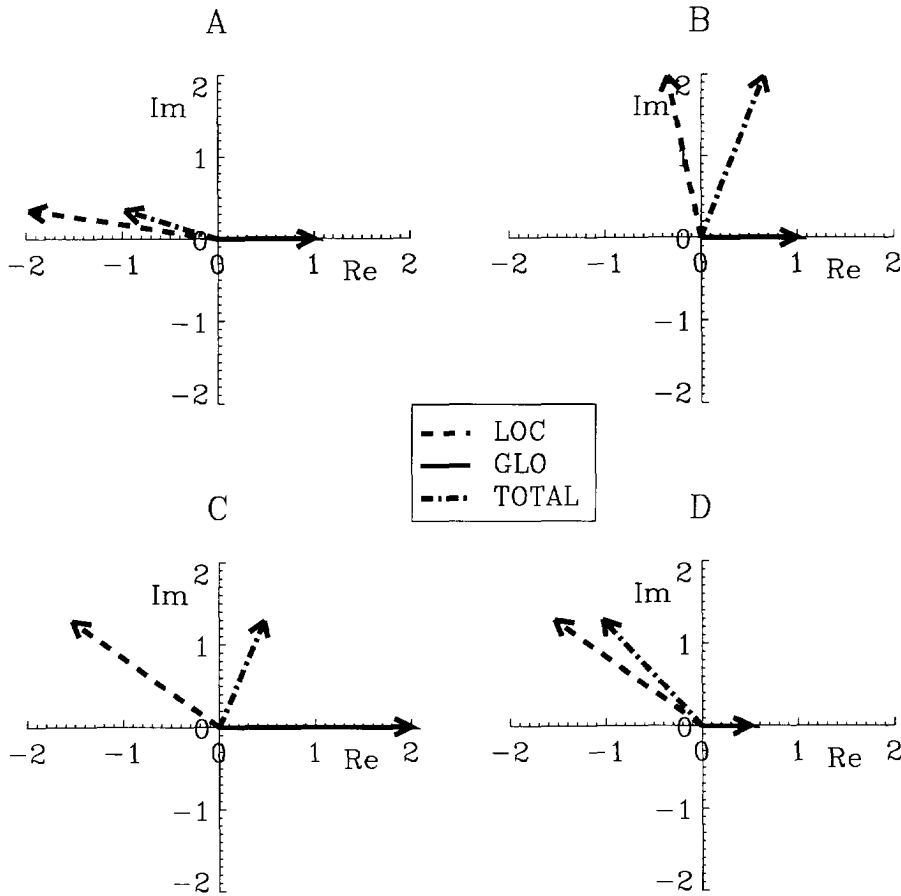


Figure VI.5: Explanation of phase shifts of the total detector response of detectors with a combined local and global component. Diagram A is used to explain the phase shift between detector 3A and the safety channel SDA1. Diagrams B, C and D show the effect on the phase shift of the total response if the phase (C) or the amplitude (C and D) of the local component changes.

phase shift, mentioned above, this results in a phase shift between a purely local and a global detector of  $176^{\circ}$ . However, the measured difference is smaller. This can be explained in the context of the

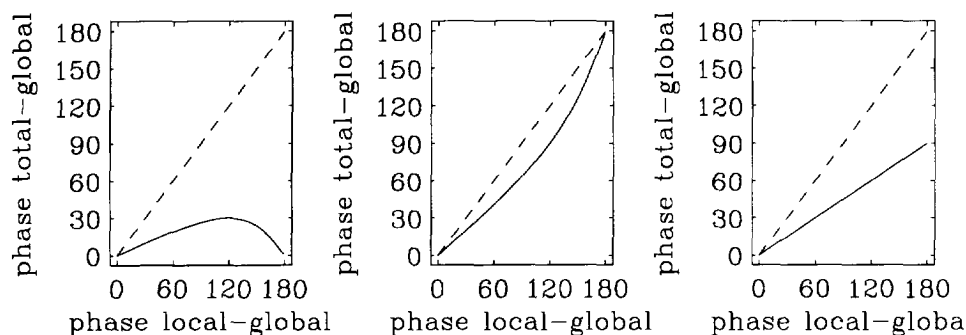


Figure VI.6: Phase between the total response and the global component for different values of the phase between the local and the global component. Three different situations are sketched: global part dominant (left), local part dominant (middle) and equal size of the components (right)

so-called 'kinematical method' as described by Wach and Kosály (1974) and which is based on the fact that a detector response can be built up of a local and a global component.

Suppose the phase of the global part is  $0^\circ$ , the phase of the local part is  $170^\circ$  and the amplitude of the local part is 2 times the amplitude of the global part. Then the phase of the vectorial sum of both components becomes  $160^\circ$  (see Figure VI.5). Since the vectorial sum denotes the total response of the detector, the phase difference between a global effect (for example safety channel SDA1) and the response of the detector is  $160^\circ$ , which is about  $10^\circ$  smaller than the phase difference between a global detector and a purely local detector. In general the angle between the total vector and the global component is always equal to or smaller than the angle between the local component and the global component as shown in Figure VI.6. Since angles in the imaginary plane express phase shifts between detector signals in practice, the vector diagram explains the measured value of  $172^\circ$  instead of  $176^\circ$  for the phase shift between detector 3A and the safety channel SDA1. The other diagrams of Figure VI.5 show the results of the total response if either the phase of the local component changes

(diagram A) or the amplitude of the local component with respect to the global component changes (diagrams C and D).

In the upper plot of Figure VI.4 we can also observe that the phase shifts for the odd higher harmonics is approximately  $0^\circ$ , whereas for the even ones they tend to an opposite phase behaviour. However, the phase shifts for the even higher harmonics are not exactly  $180^\circ$  but a little lower:  $161^\circ$ ,  $152^\circ$ ,  $146^\circ$  and  $116^\circ$  for the second, fourth, sixth and eighth harmonic respectively. The explanation of this difference with respect to the  $180^\circ$  phase partly comes from the fact that the phase of the reactivity transfer function becomes gradually more negative:  $-8^\circ$ ,  $-13^\circ$ ,  $-18^\circ$  and  $-22^\circ$  for the respective harmonics. The extra phase shift comes again from the fact that detector 3A is not a purely local detector. In the same way for the basic frequency the vectorial sum of the local and the global component results in a smaller phase shift. As can be seen in Figure VI.6, depending on the phase shift between the local and global component and the relative size of the components the phase shift becomes increasingly different from  $180^\circ$ .

The phase changes between the detectors 1A and 3A show a more quiet picture. For almost all frequencies the value is about zero, except for the higher frequencies. The phase for the basic frequency has a value of  $0.5^\circ$ . The reason for this in-phase behaviour has already been given above.

The signals of detectors 3A and 4A show a clear  $180^\circ$  phase change at the basic frequency. This is again in accordance with the out-of-phase behaviour mentioned above. The odd higher harmonics all have approximately a phase shift of  $0^\circ$ , whereas the phase for the even higher harmonics gradually decreases from  $167^\circ$  for the second harmonic to  $131^\circ$  for the eighth one. The reason of this gradual decrease is similar to reason of the decrease of the phase between detector 3A and the safety channel SDA1. However, in this case both detector responses consist of a local and a global component. This means that the total response of both detector are influenced by the change in phase of the global component and the change in the relative amplitude of the global and local component.

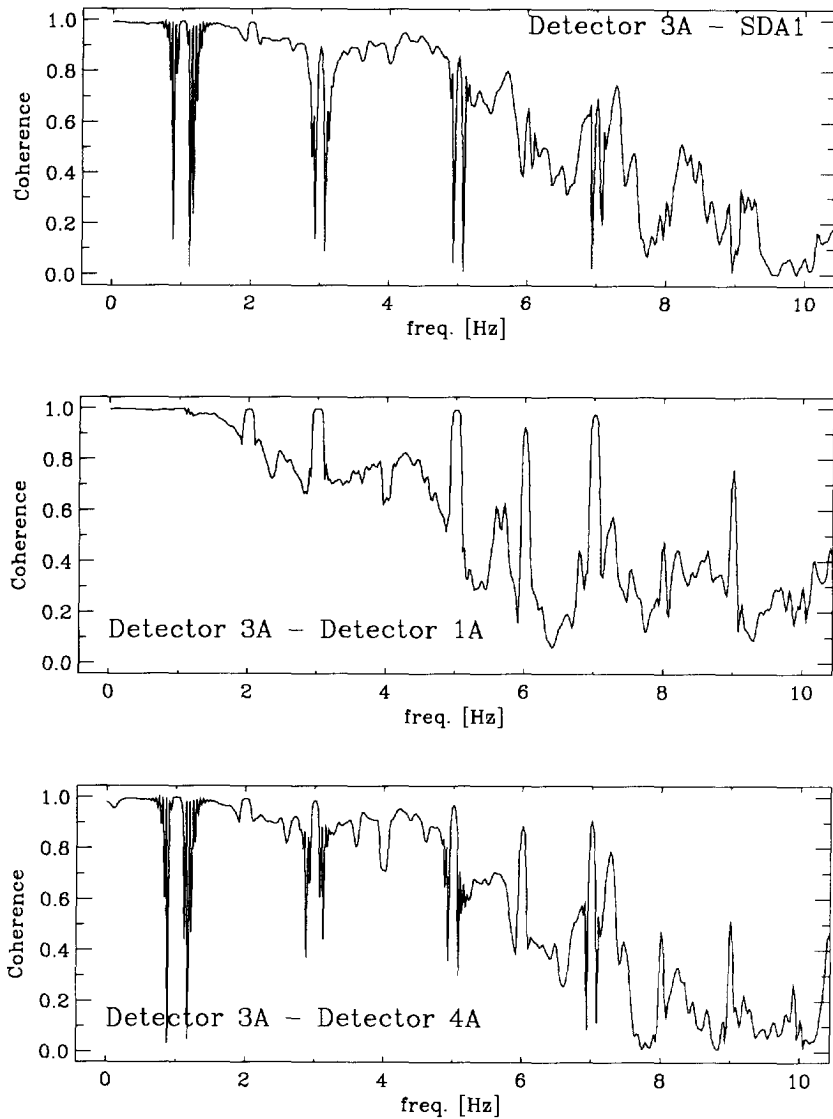


Figure VI.7: The coherence between detector 3A and the safety channel SDA1 (upper), detector 3A and detector 1A (middle) and detector 3A and detector 4A (lower). Disturber II is moving at 1 Hz at an orientation of  $0^\circ$ .

### VI.2.5 Discussion on the coherence

In Figure VI.7 a particular behaviour can be seen for the coherence between detector 3A and the safety channel SDA1. The coherence is high for almost all frequencies up to at least 8 Hz except for some small regions around the basic frequency and its harmonics. To explain this phenomenon some numerical experiments are performed in which the responses of two detectors are modelled. One of them is assumed to respond only to global variations in the reactor and is called the global detector. The other one, the local detector, will measure both global variations and a local sinusoidal variation. Formally the response of the global detector  $x(t)$  can then be written as follows:

$$x(t) = \sin(\omega_0 t) + R\epsilon(t) \quad (\text{VI.2})$$

and the response of the local detector  $y(t)$  as follows:

$$y(t) = \sin(\omega_0 t) + R\epsilon(t) + r\sin(\omega_0 t + \phi) \quad (\text{VI.3})$$

In these expressions  $\epsilon(t)$  is a global white noise,  $R$  and  $r$  are the amplitudes of the global white noise and the local sinusoidal variations relative to the amplitude of the global sinusoidal variations,  $\omega_0$  is the angular frequency of the global and local variations and  $\phi$  is the phase shift between the local variation and the global variation. The coherence between these two detectors for an infinite number of records can be calculated, resulting in:

$$\gamma = \begin{cases} \frac{[1 + re^{j\phi} + R^2]^2}{[1 + R^2][1 + r(e^{j\phi} + e^{-j\phi}) + r^2 + R^2]} & \text{for } \omega = \omega_0 \\ 1 & \text{for } \omega \neq \omega_0 \end{cases} \quad (\text{VI.4})$$

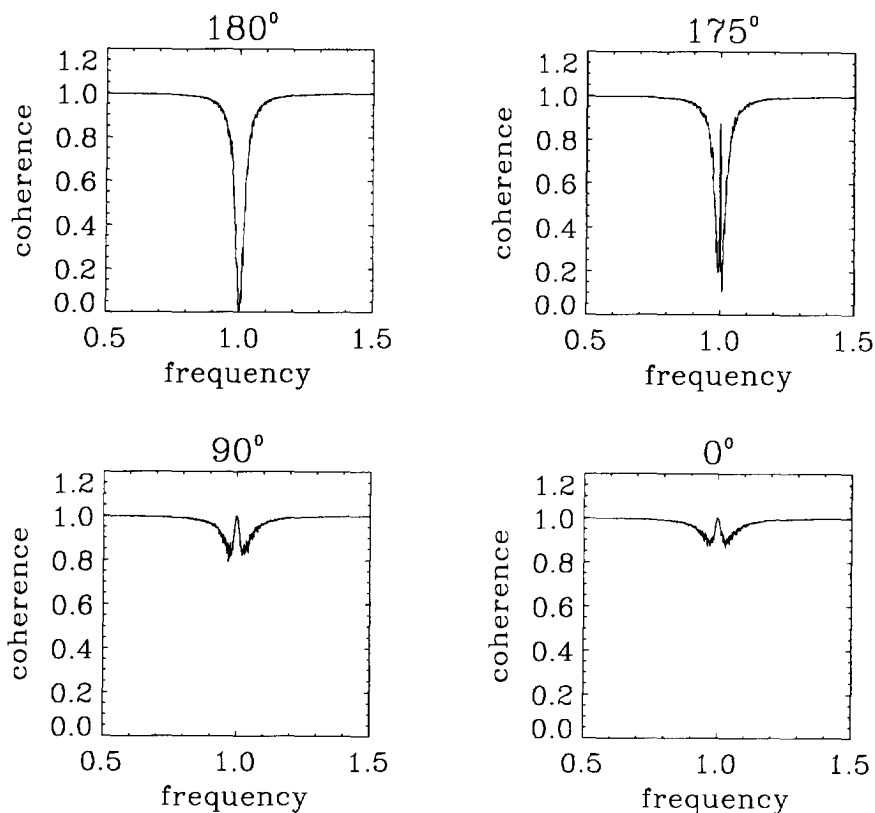


Figure VI.8: Simulated coherence between a global and a local detector around the frequency of the sinusoidal perturbation. The parameter varied is the phase shift  $\phi$ .

We see, then, that the coherence is 1 for all angular frequencies not equal to  $\omega_0$ . For an angular frequency of  $\omega_0$  the coherence will depend on the values of  $r$ ,  $R$  and  $\phi$ . Suppose the global noise is small compared to global sinusoidal fluctuation ( $R \ll 1$ ). Then the coherence at  $\omega = \omega_0$  is:

$$\gamma = \frac{[1 + re^{j\phi}]^2}{[1 + r(e^{j\phi} + e^{-j\phi}) + r^2]} \quad (\text{VI.5})$$

For  $\phi = 0$ , so if the local and the global sinusoidal variations are in phase the coherence is 1. If  $\phi = \pi$  and  $r = 1$ , for example,  $\gamma = 0$ .

However, above presented analytical results only are true, if the averaging is with an infinite number of records. In practice that is not possible. Therefore the coherence is simulated for a finite number of records, varying  $R$ ,  $r$  and  $\phi$ . The simulated responses are Fourier transformed using a Hanning window and from the spectra coherences are calculated. In Figure VI.8 the results varying  $\phi$  with  $R = 1$ ,  $r = 1$  for frequencies around  $\omega_0$  are shown. Since the absolute value of this frequency is not important, the values of the x-axis are frequencies relative to  $\omega_0$ . As we can see the simulated results for a phase shift of  $175^\circ$  resemble the measured results well in a qualitative manner. The coherence at the basic frequency and at frequencies relatively far from this basic frequency is approximately one. Only at frequencies closely around the basic frequency the coherence is lower. We also can see that the shape of the coherence heavily depends on the phase  $\phi$ . If this phase is exactly  $180^\circ$  the coherence for the basic frequency  $\omega_0$  is zero, whereas for frequencies closer to zero, the coherence at  $\omega_0$  is one.

This means that the peculiar shape of the coherence around the basic frequency and its harmonics is merely a signal processing effect than a real physical effect. However, since in practice we always have to deal with a finite number of records, a coherence that has this typical shape can indicate the existence of a sinusoidal perturbation in the vicinity of a detector. This can be valuable information in practical situations.

### VI.3 Measurements with disturber II and DISTY at an orientation of $90^\circ$

The pictures change drastically if we turn around DISTY by  $90^\circ$ . In that case the movement of the cadmium is along the side of the reactor. This means that the cadmium piece moves between the side of the detectors 3A and 4A and the side of detectors 1A and 2. In contrast with the  $0^\circ$  orientation situation above, it will move in a much milder flux gradient (Figures V.7 and V.8).



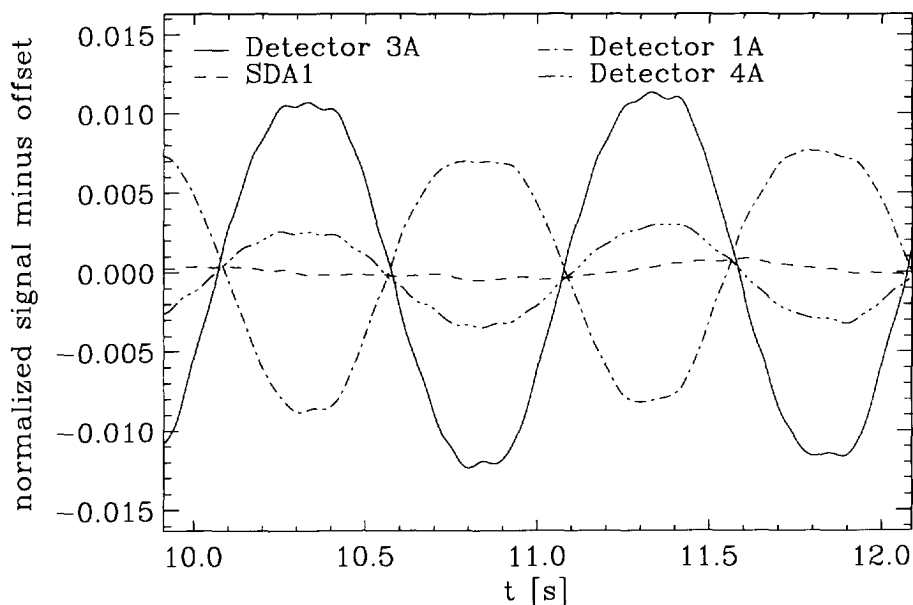


Figure VI.9: Normalized time response of detectors 1A, 3A, 4A and SDA1 due to the 1 Hz movement of disturber II. The orientation of DISTY was  $90^\circ$ .

The differences in the normalized time responses of Figure VI.9 with regard to Figure VI.1 are apparent. The responses of both detectors 1A and 3A are larger: about 0.9% and 1.2% instead of 0.75% and 0.7%, respectively. However, the response of detector 4A is smaller: 0.25% instead of 0.45% in case of  $0^\circ$  orientation. But the most radical change is in the response of the safety channel SDA1. In this orientation it is hardly possible to see a periodicity of 1 Hz. This comes from the fact that the gradient in the worth function is very small. Since the detector response of the safety channel comes from the changing reactivity, the response will approximately be zero if the movement does not generate a reactivity effect. As mentioned above the reactivity is in first-order proportional to the worth function (Figure V.8). Since the change in the product along the line of

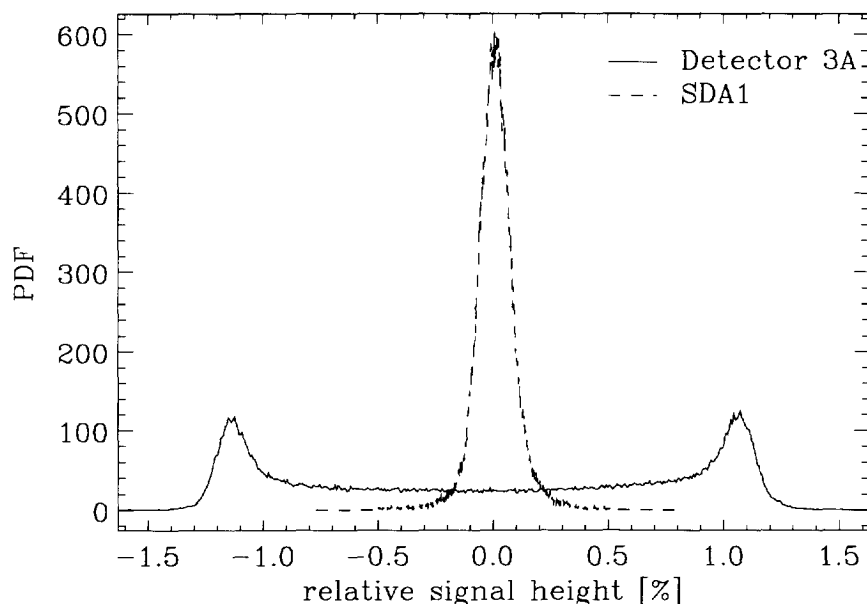


Figure VI.10: Probability density function of detectors 3A and SDA1. Disturber II was moved with a frequency of 1 Hz. The orientation of DISTY was  $90^\circ$ .

movement of the cadmium in an orientation of  $90^\circ$  is only 4%, whereas in the  $0^\circ$  orientation the change in the product is 18%, the worth function is practically flat for the  $90^\circ$  orientation and thus the reactivity effect will be about zero. Therefore the safety channel will give practically no response.

This zero reactivity effect also explains the reason of the change in the amplitude for the self-powered neutron detectors. The response of these detectors is a summation of a local effect and a global, reactivity effect. Since in the zero orientation case the local effect for detector 4A and the global effect are in phase the local response of detector 4A are enlarged in the zero orientation case. In the case of detector 1A and 3A the local and global effect are out-of-phase. This means that the local response is reduced for these detectors in zero orientation. In the  $90^\circ$  orientation the global effect almost totally disappears. This means that

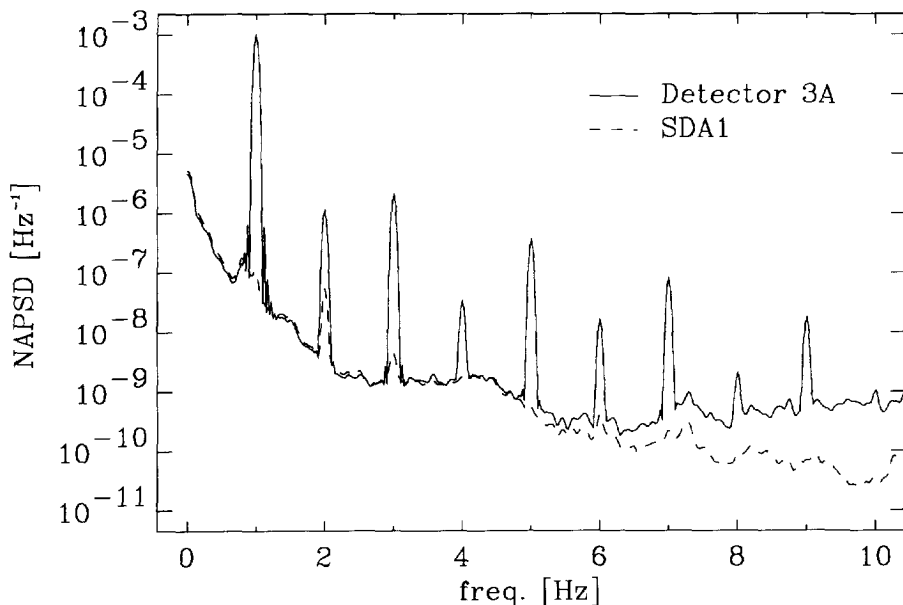


Figure VI.11: Normalized auto power spectra of detector 3A and the safety channel SDA1 in orientation  $90^\circ$  of disturber II. The frequency of movement is 1 Hz. The cut-off frequency of the amplifier of the safety channel is 4 Hz.

the total response of detector 4A becomes smaller and the total response of detectors 1A and 3A becomes larger.

Another important observation is the change of the phases relative to the phase of detector 3A, for example. Now the signals of detector 3A and 4A are in-phase, whereas the signals of 3A and 1A are out-of-phase. As mentioned above the cadmium now moves from the side of detector 3A and 4A to the side of detector 1A. This means that if the cadmium moves towards detector 1A the signal of detector 1A becomes small due to the increasing flux depression, but the signals of detectors 1A and 3A increase due the decreasing flux depression.

In the figure of the probability density function (Figure VI.10) we again notice the bimodal shape of the response of detector 3A. The shape of the signal of the safety channel SDA1, however, is not

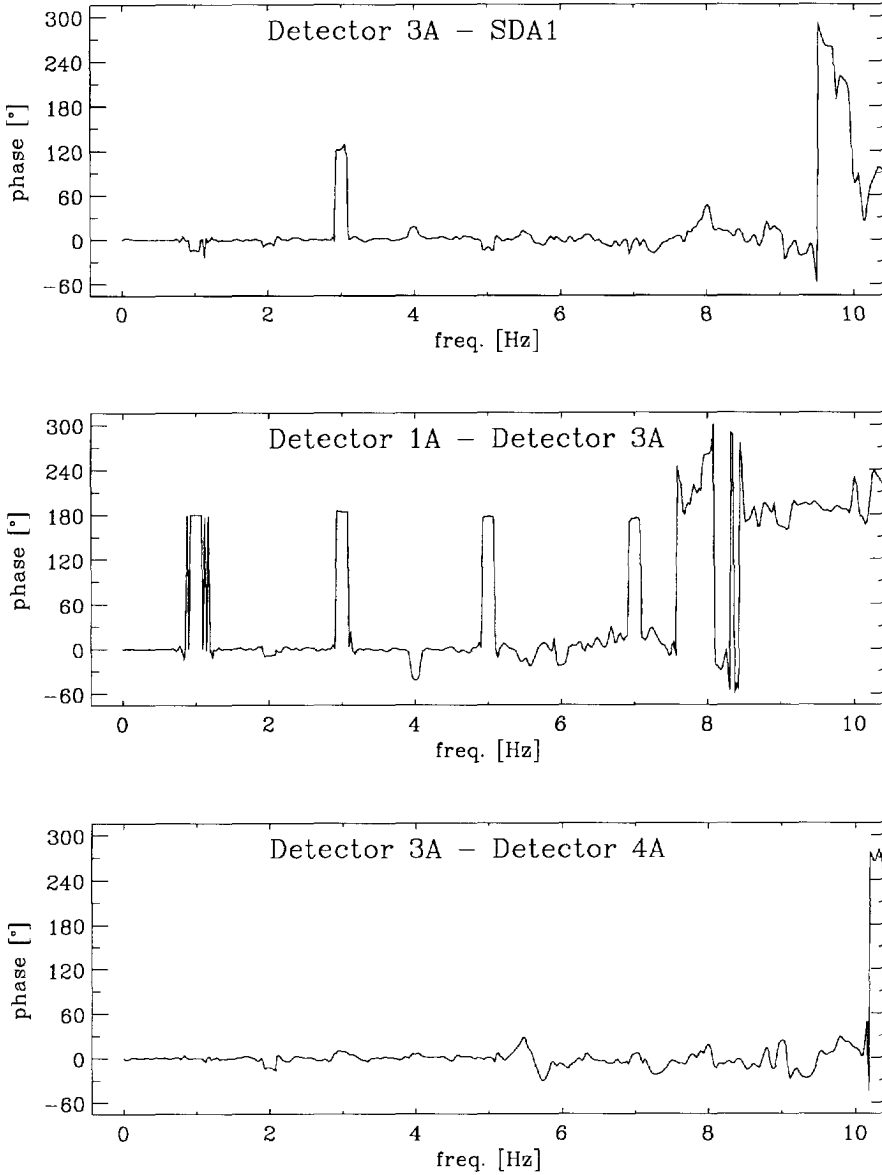


Figure VI.12: Phase difference between detector 3A and the safety channel SDA1 (upper), detector 3A and detector 1A (middle) and detector 3A and detector 4A (lower). Disturber II is moving at 1 Hz at an orientation of  $90^\circ$ .

bimodal anymore. It is more like the probability density function of the normal full-power reactor background (Figure V.11).

The normalized auto power spectrum of detector 3A in  $90^\circ$  orientation (Figure VI.11) is similar to the normalized auto power spectrum of the same detector in  $0^\circ$  orientation (Figure VI.3). But apart from the larger amplitude of all existing peaks with respect to earlier spectrum, the main differences are the peaks at 4 Hz and 8 Hz, which can hardly be found in the spectrum of Figure VI.3. As expected from the time response of the safety channel SDA1 the amplitude at 1 Hz in the normalized auto power spectrum is much smaller. A peak at 2 Hz, though a little smaller, still remains and even a peak at 3 Hz is still there. We come back on the subject of the higher harmonics in the next section.

In Figure VI.12 the phase change between detector 3A and the safety channel SDA1 is shown for this orientation. In contrast with Figure VI.4 now the phase difference is  $-11^\circ$ . This is again a little larger than expected from the reactivity transfer function, due to the vectorial summation of the local and the global component of this detector.

The phase differences for the basic frequency of movement of 1 Hz between the detectors 1A and 3A and between the detectors 3A and 4A fit perfectly in an almost purely local concept. An exact out-of-phase relation between detector 1A and 3A exists, which is in accordance with their position relative to the moving disturber. The same can be said of the in-phase behaviour of detectors 3A and 4A.

The coherences between the detectors in Figure VI.13 are mainly given for completeness. They show the same peculiar behaviour around the basic frequency and its harmonics as we discussed already above.

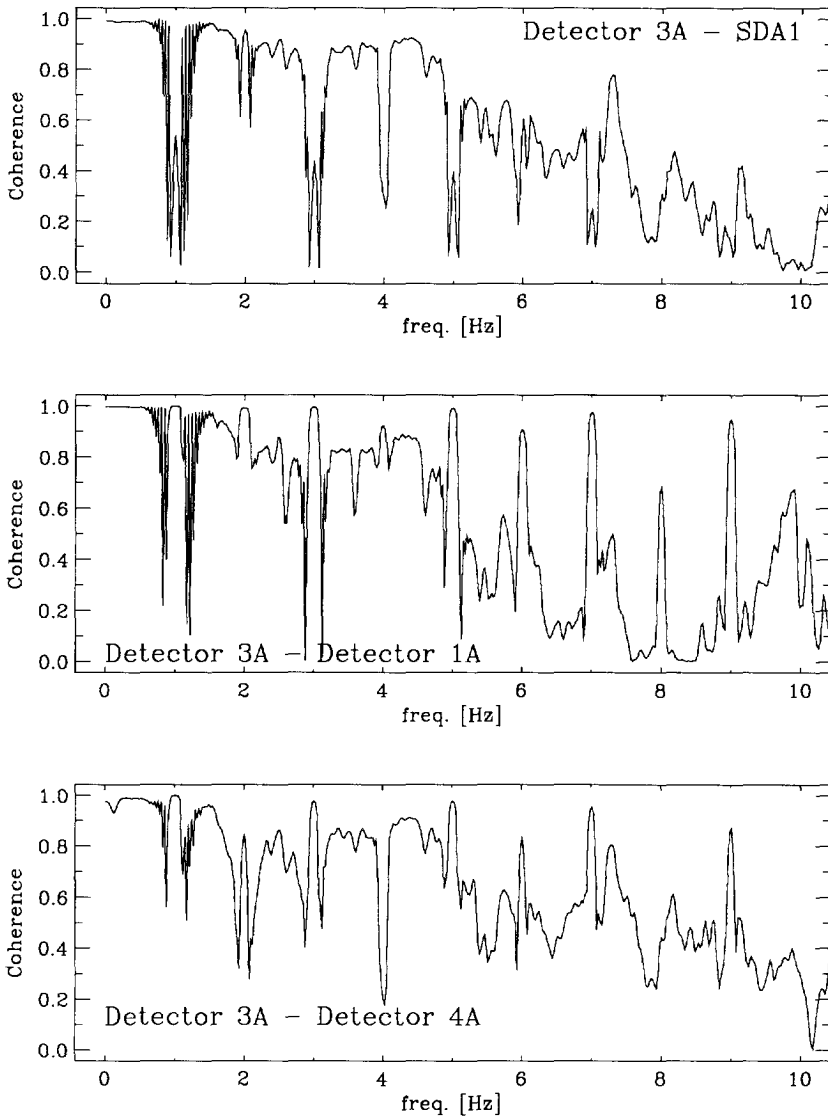


Figure VI.13: The coherence between detector 3A and the safety channel SDA1 (upper), detector 3A and detector 1A (middle) and detector 3A and detector 4A (lower). Disturber II is moving at 1 Hz at an orientation of  $90^\circ$ .

## **VI.4 Measurements with disturber II in all possible orientations**

The measurements described above are two of a series, in which DISTY is put at all possible orientations. In Figure VI.14 the results of the whole series are shown for the safety channel SDA1 and the self-powered neutron detectors 1A, 3A and 4A by the asterisks. The meaning of the solid lines is explained later.

As we can see the detector response of the safety channel SDA1 varies significantly with the orientation of DISTY. As expected and already described in the previous section the response has a (local) maximum for orientations around  $0^\circ$  and a minimum around  $90^\circ$ . However, for the orientations around  $180^\circ$  the maximum is much larger. This can be explained from Figure V.8. The worth function at position D1 shows a negative curvature in the  $y$ -direction. This means that the total change in reactivity is larger if the cadmium moves close to the core boundary. From the contour plot of Figure V.7 we can learn that the cadmium is closer to the core in the orientation of  $180^\circ$ .

The response of detectors 1A and 3A for the different orientations has a completely different shape. The amplitude of detector 1A, for example, has its maximum in an orientation of  $300^\circ$ . This can be understood as follows. From Eq. IV.35 we can say that the response of a purely local detector is roughly proportional to the difference in the maximum and minimum distance between the absorber and the detector. In case of an orientation of  $300^\circ$  the detector lies almost exactly in the line of the movement of the disturber. This means that the difference between the maximum and minimum distance of the disturber to the detector is about the total length of the movement. If the orientation is  $30^\circ$ , however, the line from the middle of the movement of the disturber to the detector is almost perpendicular to the line of movement. In that case the difference between maximum and the minimum distance is very small, resulting in a small detector response.

The solid curves in the figure give a stronger evidence of this reasoning. The curves, namely, show results of numerical experiments

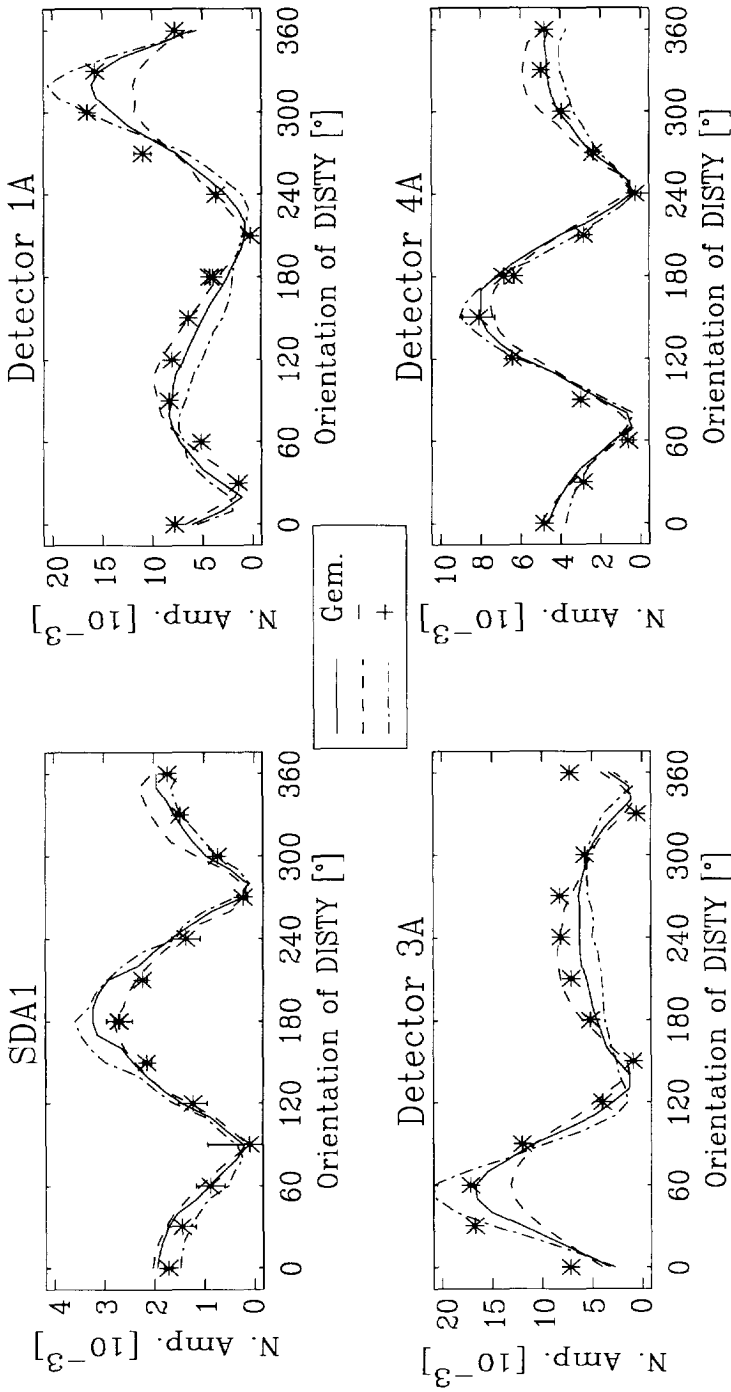


Figure VI.14: Measured (asterisks) and calculated amplitude (solid lines) of the response of the safety channel SDA1 (upper left), detector 1A (upper right), detector 3A (lower left) and detector 4A (lower right) versus the orientation of DISTY. The frequency of movement of disturber II is 1 Hz.



to simulate the amplitude of the response of the detectors. In the calculations we use the combination of the global and local theory with appropriate parameters as presented in chapter IV in Eqs. IV.34 and IV.35. For the calculation of the global effect we use the flux and the adjoint function of the thermal group as calculated by Bold Venture, which is already referred to above. The thermal flux of this Bold Venture calculation is also used to estimate the local effect. For the absorption cross section, the volume and the self-shielding factor of the cadmium the following values are taken:  $\Sigma_a^{Cd} = 114 \text{ cm}^{-1}$ , being the 2200 m/s cross section for cadmium (ANL-5800, 1963),  $V^{Cd} = 0.08 \text{ m}^3$  and  $\alpha^{Cd} = 0.107$ . The self-shielding factor is calculated using  $\alpha^{Cd} = 1/(2d\Sigma_a)$  (Beckurtz & Wirtz, 1964), with  $d$  being the thickness of the cadmium foil which is 0.4 mm. The effective fraction of precursors  $\beta$  is 0.75% (Siemens, 1993). The movement of the disturber in the orientation of  $0^\circ$  is between  $x = 22.35 \text{ cm}$  and  $x = 24.05 \text{ cm}$  at  $y = 47.0 \text{ cm}$ . For the other orientations this line is rotated around the middle of position D1 (24.05 cm, 47.0 cm).

To simulate the amplitude of the response of the safety channel SDA1 only the global effect is used. As we can see that simulation is quite good although for values around  $180^\circ$  it is little too high. For the detectors 1A, 3A and 4A we use a summation of the global and the local effect to predict to response. As we can see this prediction is very good for detector 4A. The curve lies within the error bounds of  $2\sigma$  for practically every point. For both other detectors the curves are less accurate. However, the qualitative shape is estimated well.

The reason of the deviations between the numerical results and the experiments lies in the fact that the simulations are very sensitive to the exact position of the disturber during its movement. Although the position of the cadmium is known within a few millimetres, changing the position of the disturber in the simulation along that distance has a large effect on the result. This is shown by the two dashed lines in the figures. The lines show the theoretical responses shifting the line of movement by 1 mm.

In Figure VI.15 the measured phase of the detector response relative to the trigger is plotted versus the orientation. A clear jump in phase of

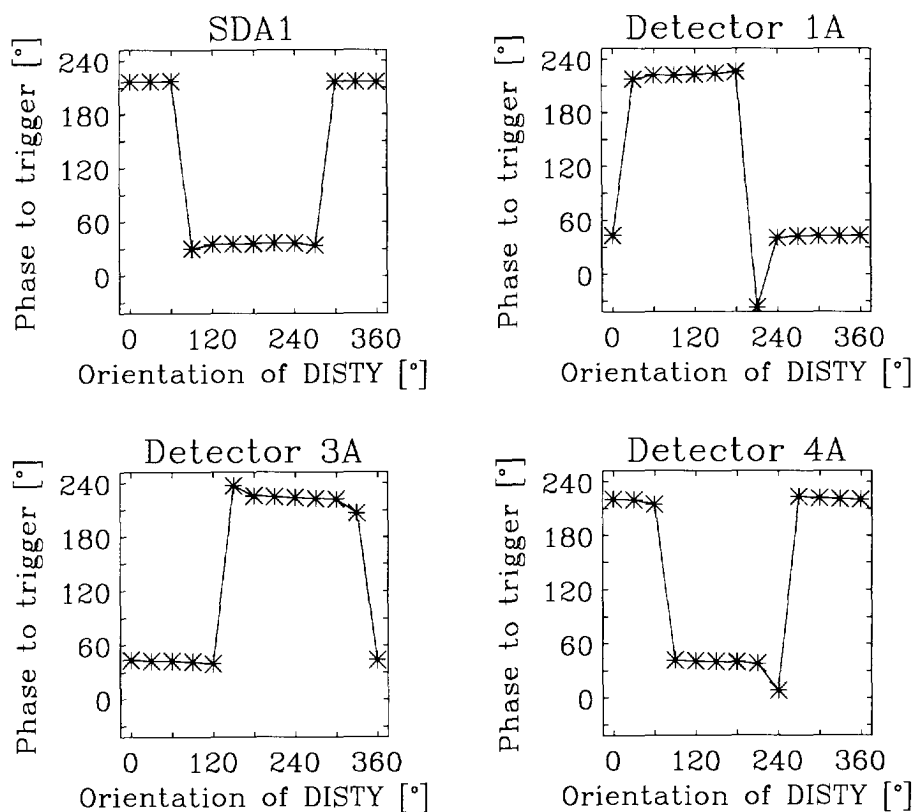


Figure VI.15: Phase relative to the trigger of the response of the safety channel SDA1 (upper left), detector 1A (upper right), detector 3A (lower left) and detector 4A (lower right) versus the orientation of DISTY. The frequency of movement of disturber II is 1 Hz.

approximately  $180^\circ$  can be seen in all the curves. But the place of this jump depends on the position of the detector. For the safety channel the jump occurs between  $60^\circ$  and  $90^\circ$  and between  $270^\circ$  and  $300^\circ$ . This means that the phase shift around  $0^\circ$  orientation has an opposite phase to the orientation around  $180^\circ$ . This is understandable since if the movement in the orientation  $0^\circ$  is toward the core, in  $180^\circ$  orientation the movement is away from the core. This results in an opposite phase in the reactivity for these orientations and thus an opposite phase in the detector response of the safety channel.

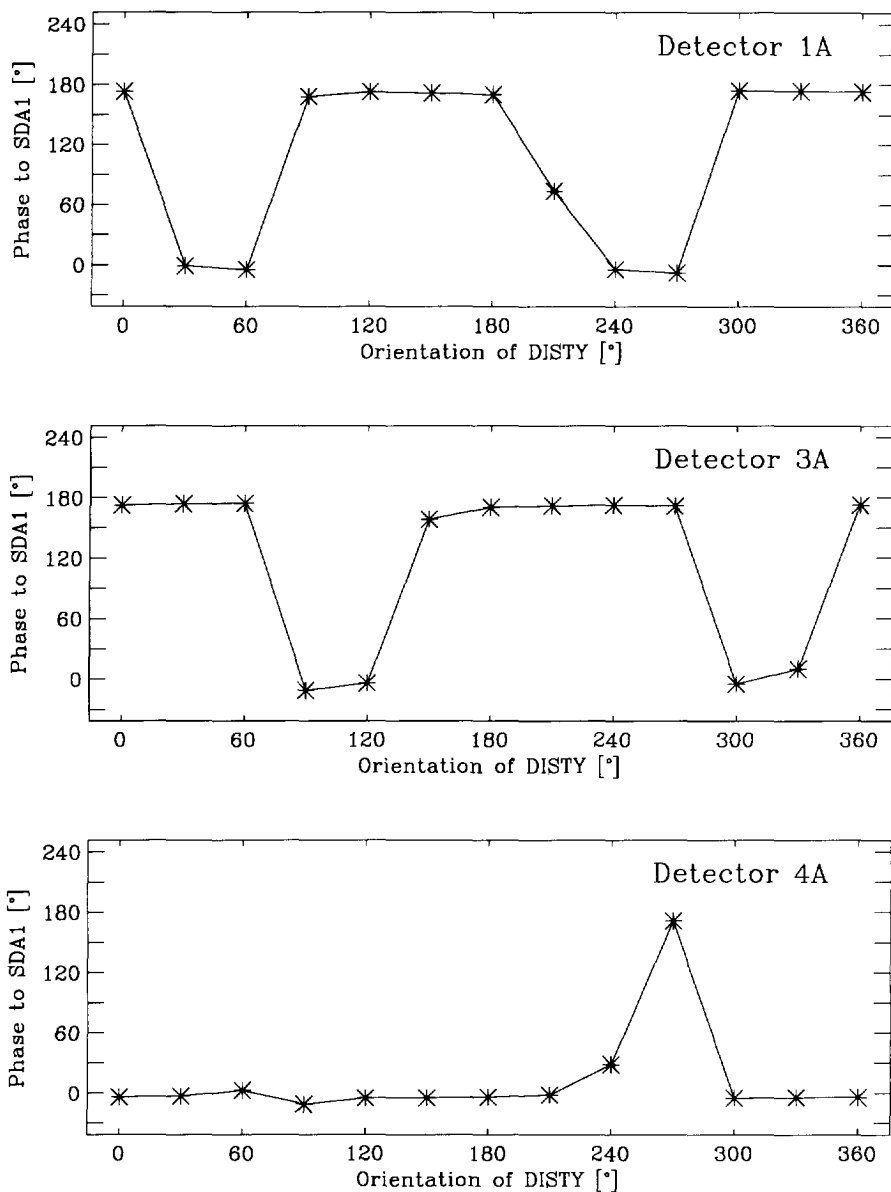


Figure VI.16: Phase change between the safety channel SDA1 and the three self-powered neutron detectors 1A, 3A and 4A versus the orientation of DISTY. The frequency of movement of disturber II is 1 Hz.

The general phase behaviour of the other three detectors can be understood in a purely local context. If the disturber moves toward detector 1A at an orientation of  $90^0$ , the movement is in the opposite direction in the orientation of  $270^0$ . This results in a  $180^0$  phase shift between the detector response around the orientation of  $90^0$  and  $270^0$ . For the other two detectors a same explanation can be found for their opposite phase behaviour although at different absolute orientations.

If we plot the phase differences between the self-powered neutron detectors 1A, 3A and 4A and the safety channel SDA1 as in Figure VI.16, the behaviour of the phase of the detectors can be understood better. For example, the phase shift of detector 4A to SDA1 is a few degrees negative for orientations, which show a relatively large amplitude for detector 4A and the safety channel SDA1, i.e. all orientations except  $60^0$ ,  $90^0$ ,  $240^0$  and  $270^0$ . We can even see a gradual increase going from an orientation of, for example,  $120^0$  to  $210^0$  from a phase difference of  $-5.1^0$  to  $-1.6^0$ . The  $-5.1^0$  phase shift can be explained as coming from the phase of the reactivity transfer function for a frequency of 1 Hz for this reactor. The gradual increase to about  $0^0$  phase difference between the phase of detector 4A and the safety channel SDA1 shows the growing influence of the global component on the total response of detector 4A. For both detectors 1A and 3A a similar behaviour can be seen except for the fact that there exists a  $180^0$  phase shift due to the position of the detectors far from the core.

The last subject we discuss on this series of measurements with varying orientation is the amplitude of the first harmonic. As said before the existence of the higher harmonics can either be due to their existence already in the source, so the movement of the disturber or due to nonlinearities in the response. If the harmonics already exist in the source their amplitude relative to the amplitude at the basic frequency do not depend on the orientation. But in Figure VI.17 we can see that for detectors 1A and 3A the changes in amplitude of different orientations are significant. As we can see the largest amplitude arises at an orientation of about  $180^0$ . For the safety channel SDA1 and detector 4A the relative amplitude of the first harmonic does not

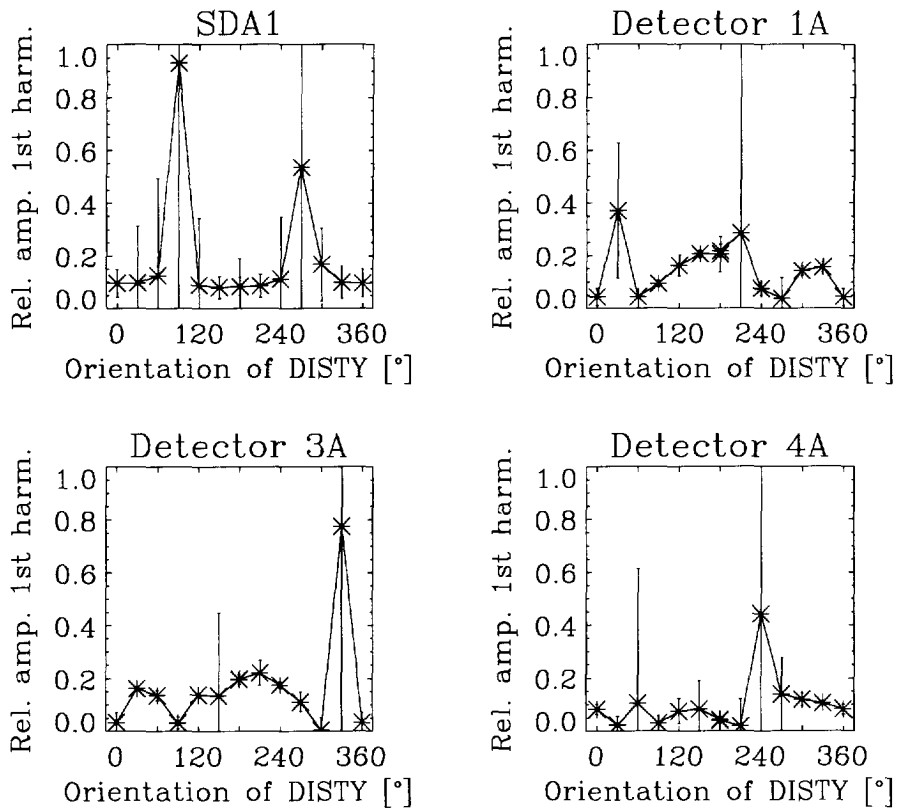


Figure VI.17: Amplitude of the first harmonic relative to the amplitude at the basic frequency of 1 Hz of the response of the safety channel SDA1 (upper left), detector 1A (upper right), detector 3A (lower left) and detector 4A (lower right) versus the orientation of DISTY due to the movement of disturber II.

change significantly with the orientation of DISTY. It is therefore impossible to say whether or not the higher harmonics in these spectra come from the source or from a nonlinear relationship between the disturber position and the detector response.

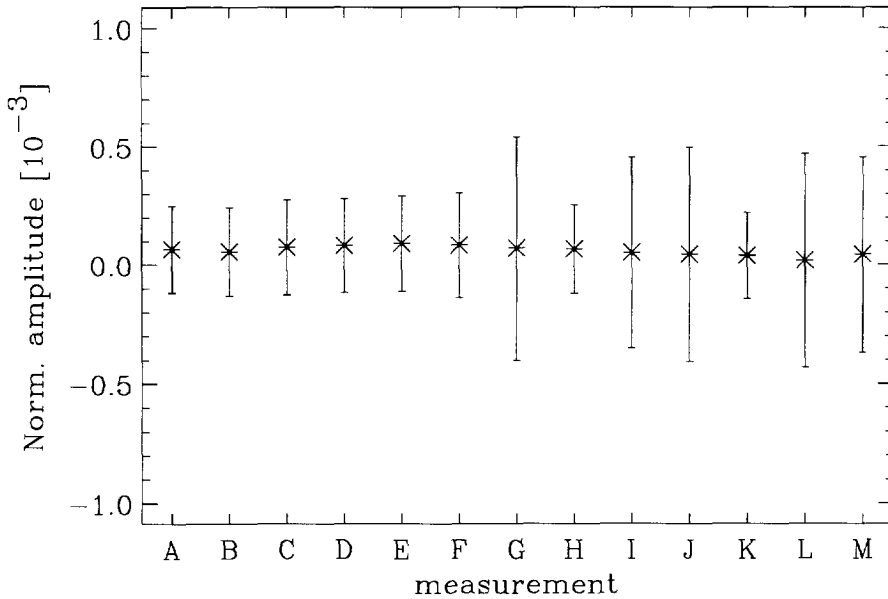


Figure VI.18: Response of the safety channel SDA1 to the disturber III, which moves vertically. The frequency is 1 Hz. The position of the self-powered neutron detectors was varied over the series of measurements.

### VI.5 Experiments with disturber III and detectors at varying axial positions.

In this section results of a series of experiments done with disturber III are discussed. This disturber is the one with a piece of cadmium that moves vertically. During the measurement it oscillates with an peak-to-peak amplitude of 12 mm around an axial position of 34 cm. During the experiment the axial position of the self-powered neutron detectors is varied from their lowest possible axial position to about 40 cm higher. Since for all measurements the position the safety channels do not change, the response of the safety channels does not vary. This is confirmed in Figure VI.18. As can be seen during the 13

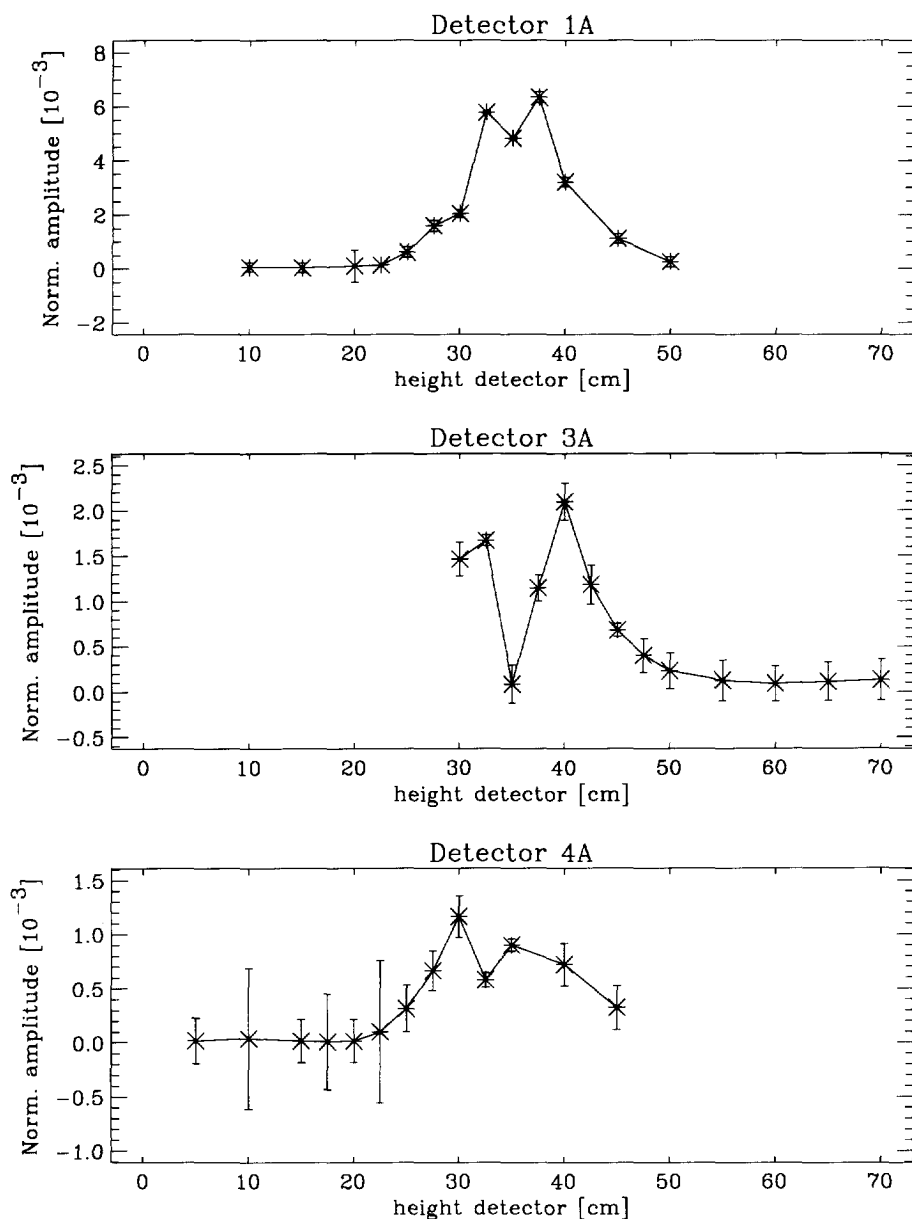


Figure VI.19: Measured amplitude of the response of detector 1A upper, detector 3A (middle) and detector 4A (lower) versus their axial position. Disturber III, the vertical moving cadmium, has a frequency of 1 Hz.

measurements the amplitude of the safety channel does not change significantly. We can even see that the absolute value is very small. This comes from the fact that if the cadmium is at a axial position of 34 cm it moves in a region of relatively flat flux. Therefore the reactivity effect is small and so the response of the distant detector SDA1.

Figure VI.19 shows that the response of the self-powered neutron detectors is not small. When moving them in the axial direction we can see that between a height of about 20 cm and 50 cm the amplitude is significant. We can also see that for all three detectors two peaks can be seen with a local minimum at about 34 cm. The increase in amplitude between 20 and 50 cm comes from the fact that at these position the cadmium is relatively close to the detectors. If the cadmium moves towards the detector the flux in the vicinity of the detector is depressed. This results in a decreasing detector response as already explained in the previous sections. If the piece of cadmium then moves away the flux depression is less and therefore the detector response increases. Since the amplitude of the detector response for the basic frequency can be seen as the maximum difference in detector response the amplitude is not dependent on the absolute value of the flux depression. It rather depends on the maximum variation. This is important to realize, since it explains the local minimum around the axial position of 34 cm. At that point the detectors are closest to the disturber and thus the flux depression due to the piece of cadmium is maximal. However, moving the cadmium foil has practically no effect on the detector response. If the cadmium is at one side of the detector or at the other one the flux depression remains approximately constant. Therefore the amplitude of the detector response is almost zero. But if we move the detector a little higher, such that the highest axial position of the disturber is at the same height as the detector, then the detector response is maximal. If the disturber is at its highest position the flux depression at the detector position is largest. If the cadmium foil then moves away the flux at the detector position increases relatively rapidly, due to the exponential term in Eq. IV.35.



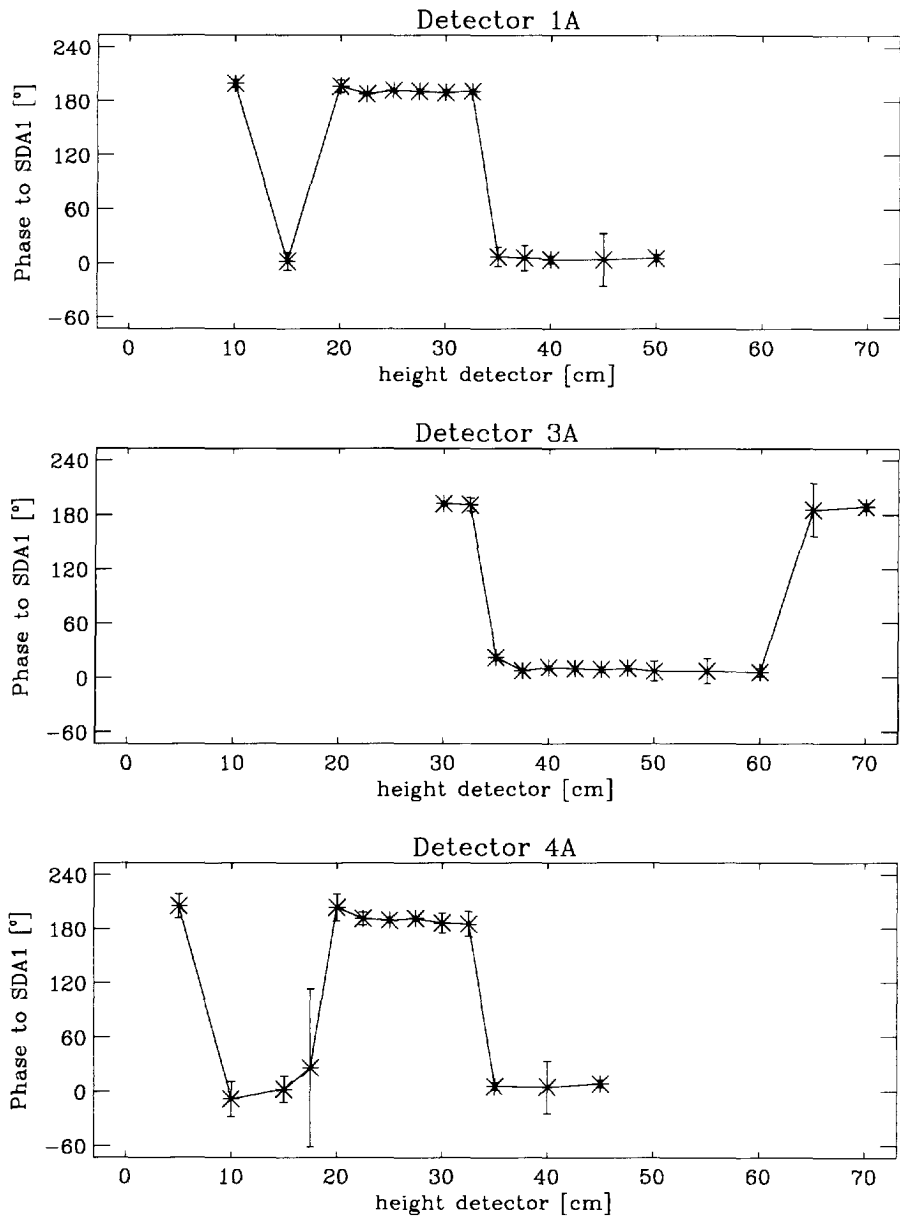


Figure VI.20: Phase difference between the safety channel and four self-powered neutron detectors. The titles on top of each plot show which detector is used in the measurements.

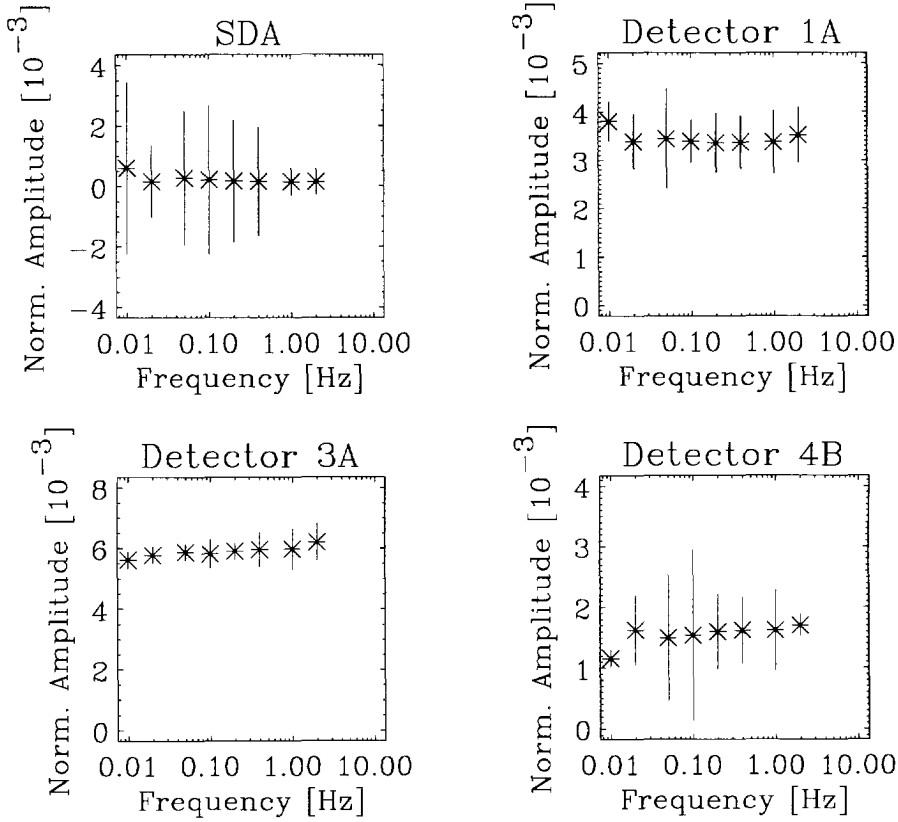


Figure VI.21: Amplitude of the detector response versus the frequency of movement of disturber II (horizontally moving cadmium foil at orientation  $300^\circ$ ). The titles on top of each plot show which detector is used in the measurements.

Looking at the phase of the response of the detectors (Figure VI.20) we can see the jump of  $180^\circ$  going from one side of the disturber to the other as expected from the numerical experiment in chapter IV. The reason for the phase shifts at the very low and very high heights of the detectors remains an open question.

## **VI.6 Experiment varying the frequency of movement of disturber II**

The last series of measurements that are discussed are the ones in which the frequency of the movement of the disturber is varied. From a theoretical point of view the range of interest lies at frequencies higher than about 15 Hz and lower than about 0.01 Hz, since that are frequency ranges that do not lie in the plateau region for this reactor. However, in practice it is very difficult to do experiments in that range of frequencies. As told in chapter V the maximum frequency that can be realized with the facility is about 5 Hz. But due to a problem with the trigger signal we can show only results up to 2 Hz. For the range of very low frequencies we have other problems. The first one is that it takes a very long time to perform the measurements with acceptable statistical accuracy. Besides that the measurement becomes more and more sensitive to long term reactivity effect as, for example, the poisoning of the fuel. Altogether we can only show results of measurements in the range of 0.01 Hz to 2 Hz, which is within the plateau region of this reactor. This means that both the amplitude and the phase of the detector responses at the basic frequency of the movement of the disturber are expected not to change significantly with frequency. This is indeed confirmed in Figure VI.21 and Figure VI.22. The only exception is the phase behaviour of the safety channel SDA1. The reason for that behaviour, however, is not clear.

Since in all measurements higher harmonics up to the ninth can be seen, in the case of the movement of the disturber at a frequency of 2 Hz some of the higher harmonics reach the boundary of the plateau region. However, from these single measurements no conclusions can be made so far.

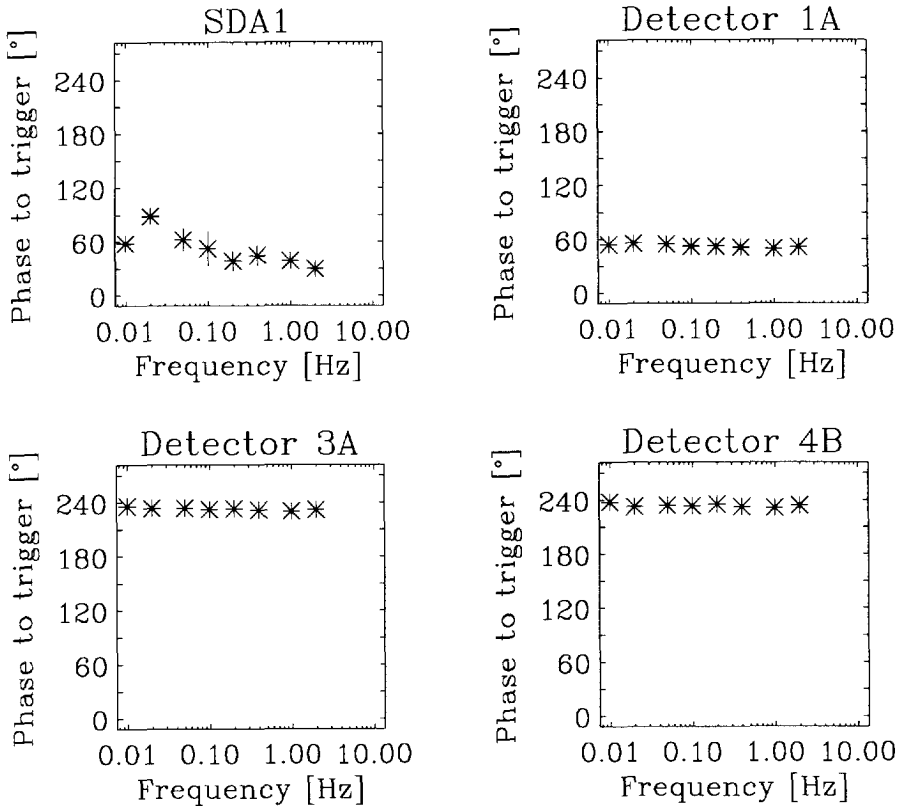


Figure VI.22: Phase differences between the trigger and four detectors versus the frequency of movement of disturber II (horizontally moving cadmium foil at orientation  $300^\circ$ ). The titles on top of each plot show which detector is used in the measurements

## VI.7 Discussion and conclusion

We have shown that with the DISTY-facility high quality measurements of the disturber effects on the responses of neutron detectors are possible. Almost all features that can be seen in the figures for the basic frequency, can well be described in a qualitative global/local concept. The quantitative example of Figure VI.14 shows a high amount of agreement. Discrepancies in the absolute value can be

ascribed to uncertainties in the exact position of the detectors and the disturber. We have to keep in mind that the calculations are not straightforward, since the flux and the adjoint function must be calculated with a static diffusion computer code. This calculation, which must be performed on the total reactor, has to be very accurate in order to give a flux as good as possible at the small area, where DISTY is placed.

In the calculations the unperturbed flux from Figure V.6 is used. However, putting the facility with the cadmium disturbers in the reflector perturbs the flux. Especially at the side of the cadmium facing away from the core a severe screening effect arises. However, the piece of cadmium is small so only a small region is influenced. The influence of this screening effect can be measured using the hafnium screen, which until now has not been used. Another possibility is to perform the measurements with the vacuum box, since that disturber does not have a screening effect. However, in preliminary experiments with the vacuum box it has become clear that such measurements need long measuring time to get significant results, since the effect on the detector responses is very small.

As shown, in the experiments with the cadmium disturbers higher harmonics at least up to the ninth can be observed. In principle it is possible to calculate the amplitudes of the higher harmonic frequencies. Knowing the flux and the adjoint function, the exact position of disturber and using Eqs. IV.34 and IV.35 the time response of the detectors can be found. In the theoretical results of Figure VI.14 these time response are used to estimate the amplitude at the basic frequency, but it is possible to separate the calculated function in harmonics. However, since the amplitude of higher harmonics is at least one order of magnitude smaller than the peak at the basic frequency, the input for the calculations must be very accurate. Another problem is that the existence of the higher harmonics already in the source can not be excluded, which gives another uncertainty. From the responses of detectors 1A and 3A in Figure VI.17 we can nevertheless say that part of the appearance higher harmonics comes from the nonlinear relation between the detector response and the

position of the disturber. More detailed investigation on the behaviour of the higher harmonic frequencies is therefore desirable.

As a general conclusion we can say that the separation of the detector responses in a component that comes from the changing reactivity and a part that describes the local effect is a effective and intuitive one. Although some aspects need more research, no evidence has been found that the results can not be explained by separate local and global theory.



# References

- ANL-5800, *Reactor Physics Constants*, United States Atomic Energy Commission (1963)
- B. Baggoura, T. Hamidouche and A. Bousbia-Salah, "RETRAC: A program for the analysis of materials test reactors", *Nucl. Sci. & Eng.*, **118**, 65 (1994)
- R. Beauwens, J. Devooght, E. Mund, R. Rydin and M. R. Wagner, "A 3D multi group transport kinetics code in hexagonal geometry for fast reactor transients analysis", *SFEN*, 75, *International Conference on the Physics of Reactors: Operation, Design and Computation. Volume 2*, Marseille, France (1990)
- K. H. Beckurts and K. Wirtz, *Neutron Physics*, Springer-Verlag, Berlin (1964)
- K. Behringer, G. Kosály and Lj. Kostić, "Theoretical investigation of the local and global components of the neutron-noise field in a BWR", *Ann. Nucl. Energy*, **63**, 306 (1977)
- K. Behringer, G. Kosály and I. Pázsit, "Linear response of the neutron-field to a propagating perturbation of the moderator density (two group theory of BWR noise)", *Nucl. Sci. & Eng.*, **72**, 304 (1979)
- G. I. Bell and S. Glasstone, *Nuclear reactor theory*, Van Nostrand Reinhold Company, New York, USA (1970)
- G-S. Chen, J. M. Christenson and D-Y. Yang, "Stability improvement of the alternating direction implicit method for two-dimensional space-time reactor kinetics applications", *Nucl. Sci. Eng.*, **111**, 279 (1992)
- Gy. Csom and F. Lévai, *The nuclear training reactor of the Budapest technical university*, (1983)



- H. van Dam, "Neutron noise in boiling water reactors", *Atomkernenergie*, **27**, no. 1, 8 (1976)
- H. van Dam, "On the adjoint-space in reactor noise theory", *Ann. Nucl. Energy*, **4**, 185 (1977)
- H. L. Dodds Jr., "Accuracy of the quasi static method for two-dimensional thermal reactor transients with feedback", *Nucl. Sci. Eng.*, **59**, 271 (1975)
- J. J. Duderstadt and L. J. Hamilton, *Nuclear reactor analysis*, John Wiley & Sons, New York, USA (1976)
- J. R. Fisher, R. L. Grow, D. Hodges, J. S. Rapp and K. M. Smolinske, *Evaluation of Discrepancies in Assembly Cross-Section Generator Codes, Volumes 1 & 2*, **NP-6147**, Electric Power Research Institute, Palo Alto, California, USA (1989)
- T. B. Fowler, D. R. Vondy and G. W. Cunningham, *Nuclear Reactor Core Analysis Code: CITATION, Revision 2*, **ORNL-TM-2496, Rev. 2**, Oak Ridge National Laboratory, Oak Ridge, Tennessee, USA (1971)
- R. Fuge, J. Valkó, T. Czibók, D. Kätzmer and M. Vasilescu, "Measurements of the local and global effect of bubbles in a water-moderated reactor", *Ann. Nucl. Energy*, **4**, 161 (1977)
- E. Greenspan, "On the adjoint-space in reactor-theory", *Ann. Nucl. Eng.*, **3**, 323 (1976)
- T. H. J. J. van der Hagen, J. E. Hoogenboom and H. van Dam, "A multidimensional multi group diffusion model for the determination of the frequency-dependent field of view of a neutron detector", *Nucl. Sci. Eng.*, **110**, 237 (1992)
- T. van der Hagen, "Proof of principle of a nuclear turbine flowmeter", *Nucl. Techn.*, **102**, 167 (1993)
- P. T. Hansson and L. R. Foulke, "Investigations in spatial kinetics", *Nucl. Sci. Eng.*, **17**, 528 (1963)
- A. F. Henry, *Nuclear-Reactor Analysis*, The MIT Press, Cambridge, Massachusetts, USA (1975)
- A. F. Henry and N. J. Curlee, "Verification of a method for treating neutron space-time problems", *Nucl. Sci. Eng.*, **4**, 727 (1958)

- D. L. Hetrick, *Dynamics of nuclear reactors*, The University of Chicago Press, Chicago, USA (1971)
- G. M. Jenkins and D. G. Watts, *Spectral analysis and its application*, Holden-Day, San Francisco (1968)
- S. Kaplan, O. J. Marlowe and J. Bewick, "Application of synthesis techniques to problems involving time dependence", *Nucl. Sci. Eng.*, **18**, 163 (1964)
- J. Keijzer, *Detector response theory and its applications*, **IRI-131-92-019**, Interfaculty Reactor Institute, Delft, The Netherlands (1992)
- E. Kleiss and H. van Dam, "Analysis of neutron detector response to bubbles in a water moderated reactor", *Ann. Nucl. Energy*, **6**, 385 (1979)
- G. Kosály, L. Maróti and L. Meskó, "A simple space dependent theory of the neutron noise in a boiling water reactor", *Ann. Nucl. Energy*, **2**, 315 (1975)
- G. Kosály, L. Meskó and I. Pázsit, "Investigation of the possibility of using static calculations (adiabatic-approximation) in the theory of neutron-noise", *Ann. Nucl. Energy*, **4**, 79 (1977)
- G. Kosály, "Noise investigations in boiling-water and pressurized-water reactors", *Prog. Nucl. Energy*, **5**, 145 (1980)
- J. March-Leuba and E. D. Blakeman, "A Mechanism for Out-of Phase Power Instabilities in Boiling Water Reactor", *Nucl. Sci. Eng.*, **107**, 173 (1991)
- E. Laggiard, J. Runkel and D. Stegemann, "One-dimensional bimodal model of vibration and impacting of instrument tubes in a boiling water reactor", *Nucl. Sci. & Eng.*, **115**, 62 (1993)
- J. Lewins, *Importance, The Adjoint Function*, Pergamon Press, New York (1965)
- J. Lewins, *Nuclear Reactor Kinetics and Control*, Pergamon Press, Oxford (1977)
- OECD/NEA Data Bank, *JEF2-2 Nuclear Data Library*, (1995)
- K. O. Ott and D. A. Meneley, "Accuracy of the quasi static treatment of spatial reactor kinetics", *Nucl. Sci. Eng.*, **36**, 402 (1969)
- K. O. Ott and R. J. Neuhold, *Introductory nuclear reactor dynamics*, American Nuclear Society, La Grange Park, Illinois, USA (1985)

- I. Pázsit, "Investigation of the space-dependent noise induced by a vibrating absorber", *Atomkernenergie*, **30**, 29 (1977)
- I. Pázsit, "Two-group theory of noise in reflected reactors with application to vibrating absorbers, *Ann. Nucl. Energy*, **5**, 185 (1978)
- J. Pohlus and J. Scholz, "Space-dependent investigations in zero power reactors", *Kernenergie*, **24**, 425 (1981)
- W. Seifritz and F. Cioli, "On-load Monitoring of Local Steam Velocity in BWR Cores by Neutron Noise Analysis", *Trans. Am. Nucl. Soc.*, **17**, 451 (1973)
- Siemens AG · Power Generation Group (KWU), *Contributions to the safety analysis report of HOR Interfacultair Reactor Instituut TU Delft*, **IRI/HOR-130-93-04** (1993)
- R. A. Shober, T. A. Daly and D. R. Ferguson, *FX2-TH: A two-dimensional nuclear reactor kinetics code with thermal-hydraulic feedback*, **ANL-78-97**, Argonne National Laboratory, Argonne, Illinois, USA (1978)
- A. J. C. Stekelenburg, "Two-phase flow monitoring by analysis of in-core neutron detector noise signals - a literature survey", *Ann. Nucl. Energy*, **20**, 611 (1993)
- D. R. Vondy, T. B. Fowler and G. W. Cunningham, *The Bold Venture Computation System for Nuclear Reactor Core Analysis*, **ORNL-5711**, Oak Ridge National Laboratory, Oak Ridge, Tennessee, USA (1981)
- J. W. de Vries, *Tweegroepsberekeningen voor de Hoger Onderwijs Reactor*, **IRI-Int-74-RBG/01**, Interfaculty Reactor Institute, Delft, The Netherlands (1974) (in Dutch)
- D. Wach and G. Kosály, "Investigation of the joint effect of local and global driving sources in in-core neutron noise measurements", *Atomkernenergie*, **23**, no. 4, 244 (1974)
- E. L. Wachpress, R. D. Burgess and S. Baron, "Multichannel flux synthesis", *Nucl. Sci. Eng.*, **12**, 381 (1962)
- A. M. Weinberg and H. C. Schweinler, "Theory of oscillating absorber in a chain reactor", *Phys. Res.*, **74**, 851 (1948)

- M. M. R. Williams, "Investigation of the joint random vibration of control rods and fuel elements", *Nucl. Sci. Eng.*, **39**, 144 (1974)
- J. B. Yasinsky and A. F. Henry, "Some numerical experiments concerning space-time reactor kinetics behaviour", *Nucl. Sci. Eng.*, **22**, 171 (1965)



# Nomenclature

## Greek symbols

$\alpha^{\text{Cd}}$	self-shielding factor
$\beta$	total fraction of delayed neutrons
$\beta^{\text{eff}}$	effective total fraction of delayed neutrons
$\beta_i$	fraction of delayed neutrons from precursor group i
$\beta_i^{\text{eff}}$	effective fraction of delayed neutrons from precursor group i
$\gamma$	coherence between a local and a global detector
$\gamma_{12}$	coherence between signal 1 and signal 2
$\epsilon$	normalized global white noise
$\Theta$	ratio of the size of a reactor to its migration length
$\Lambda$	neutron generation time [s]
$\lambda_i$	decay constant of precursor group i [ $\text{s}^{-1}$ ]
$\nu$	averaged number of neutrons per fission
$\rho$	dynamic reactivity
$\rho_{\text{as}}$	asymptotic reactivity
$\delta\rho$	variation in the dynamic reactivity
$\delta\tilde{\rho}$	Laplace transform of $\delta\rho$
$\kappa$	inverse diffusion length [ $\text{cm}^{-1}$ ]
$\Sigma_a$	absorption cross section [ $\text{cm}^{-1}$ ]
$\Sigma_a^{\text{Cd}}$	absorption cross section of cadmium [ $\text{cm}^{-1}$ ]
$\delta\Sigma_a$	variation in the absorption cross section [ $\text{cm}^{-1}$ ]
$\Sigma_d$	macroscopic detector cross section [ $\text{cm}^{-1}$ ]
$\Sigma_f$	fission cross section [ $\text{cm}^{-1}$ ]
$\Sigma_{f,0}$	fission cross section in the stationary system [ $\text{cm}^{-1}$ ]
$\delta\Sigma_f$	variation in the fission cross section [ $\text{cm}^{-1}$ ]
$\delta\tilde{\Sigma}_f$	Laplace transform of $\delta\Sigma_f$ [ $\text{cm}^{-1}$ ]
$\Sigma_s$	scattering cross section [ $\text{cm}^{-1}$ ]
$\Sigma_{s,0}$	scattering cross section in the stationary system [ $\text{cm}^{-1}$ ]

$\delta\Sigma_s$	variation in the scattering cross section [ $\text{cm}^{-1}$ ]
$\delta\tilde{\Sigma}_s$	Laplace transform of $\delta\Sigma_s$ [ $\text{cm}^{-1}$ ]
$\Sigma_t$	removal cross section [ $\text{cm}^{-1}$ ]
$\Sigma_{t,0}$	removal cross section in the stationary system [ $\text{cm}^{-1}$ ]
$\delta\Sigma_t$	variation in the removal cross section [ $\text{cm}^{-1}$ ]
$\delta\tilde{\Sigma}_t$	Laplace transform of $\delta\Sigma_t$ [ $\text{cm}^{-1}$ ]
$\phi$	phase shift between local and global sinusoidal variations
$\phi_i$	phase of sine wave $i$
$\phi_{12}$	phase between signal 1 and signal 2
$\varphi$	flux density [ $\text{cm}^{-2}\text{s}^{-1}$ ]
$\varphi_0$	flux density in the stationary system [ $\text{cm}^{-2}\text{s}^{-1}$ ]
$\delta\varphi$	variation in the flux density [ $\text{cm}^{-2}\text{s}^{-1}$ ]
$\delta\tilde{\varphi}$	Laplace transform of $\delta\varphi$ [ $\text{cm}^{-2}\text{s}^{-1}$ ]
$\psi$	time dependent shape function [ $\text{cm}^{-2}\text{s}^{-1}$ ]
$\psi_0$	shape function of the stationary system [ $\text{cm}^{-2}\text{s}^{-1}$ ]
$\psi^\dagger$	adjoint function of the initial steady state of the system
$\chi_p$	prompt neutron spectrum
$\chi_i$	delayed neutron spectrum from precursor group $i$
$\chi_t$	combined prompt and delayed neutron spectrum
$\omega$	angular frequency [ $\text{s}^{-1}$ ]
$\omega_0$	angular frequency of the modulation or oscillation of a disturber [ $\text{s}^{-1}$ ]

## Arabic symbols

1D	one-dimensional
1G	one-energy group
2D	two-dimensional
2G	two-energy group
3D	three-dimensional
AC	alternating current
DC	direct current
$A_{12}$	cross power spectral density
$a$	one-dimensional size of a reactor [ $\text{cm}$ ]
$a_0$	normalised amplitude of a sine wave

$C_i$	concentration of precursor group $i$ [ $\text{cm}^{-3}$ ]
$C_{i,0}$	concentration of precursor group $i$ in the stationary system [ $\text{cm}^{-3}$ ]
$C_{\text{peak}}$	peak content
$\delta C_i$	variation in the concentration of precursor group $i$ [ $\text{cm}^{-3}$ ]
$\tilde{\delta C}_i$	Laplace transform of $\delta C_i$ [ $\text{cm}^{-3}$ ]
$C_{xx}$	normalized auto power spectral density [ $\text{Hz}^{-1}$ ]
$C_{xx}^{\text{sine}}$	normalized auto power spectral density of a sine wave [ $\text{Hz}^{-1}$ ]
$c_i$	effective concentration of precursor group $i$
$d$	thickness of the cadmium foil [mm]
$D$	diffusion coefficient [cm]
$D_0$	diffusion coefficient in stationary system [cm]
$\delta D$	variation in the diffusion coefficient [cm]
$\tilde{\delta D}$	Laplace transform $\delta D$ [cm]
$E$	energy
$E_{\text{fast}}$	energy of the fast group
$E_{\text{th}}$	energy of the thermal group
$f$	frequency [Hz]
$f_{\text{ac}}$	cut-off frequency of the AC-filter of the differential amplifiers [Hz]
$f_i$	frequency of sine wave $i$ [Hz]
$g$	adjoint detector response function
$G$	sub-critical zero-power reactivity transfer function
$h_i$	response of detector $i$
$h_i^N$	normalized response of detector $i$
$j$	$\sqrt{-1}$
$k$	propagation number [ $\text{cm}^{-1}$ ]
$\langle l^2 \rangle$	mean square length of the fission chain [ $\text{cm}^2$ ]
$L$	diffusion length [cm]
$L_\omega$	"complex" diffusion length [cm]
$m$	number of precursor groups
$M$	migration length [cm]
$N$	number of records used for averaging frequency spectra
$n$	amplitude function



$n_0$	amplitude function of the stationary system
$\delta n$	variation in the amplitude function
$\delta \tilde{n}$	Laplace transform of $\delta n$
$p$	sum of sine waves with predefined frequencies
PDF	probability density function
$Q$	ratio of square root of $\langle l^2 \rangle$ to the migration length
$Q_0$	strength of a point source [ $s^{-1}$ ]
$\delta Q$	variation in the strength of a point source [ $s^{-1}$ ]
$r$	amplitude of the local sinusoidal variations relative to the amplitude of the global sinusoidal variations
$\mathbf{r}$	space coordinate
$\mathbf{r}_{Cd}$	position of the cadmium piece
$\mathbf{r}_1, \mathbf{r}_2$	position of the endpoints of the oscillating disturber
$R$	amplitude of the global white noise relative to the amplitude of the global sinusoidal variations
$R(t)$	detector response [ $s^{-1}$ ]
$R(\omega)$	frequency-dependent detector response [ $s^{-1}$ ]
$R_0$	detector response without disturber
$s$	Laplace parameter
SDA	shut down amplifier, used to indicate the signal of the safety channels
$t$	time [s]
$u$	normalized amplitude coordinate
$v$	velocity [ $cm\ s^{-1}$ ]
$V^{cd}$	volume of the cadmium piece [ $cm^3$ ]
$V_i$	effective volume of detector $i$ [ $cm^3$ ]
$V_{det}$	volume of a detector [ $cm^3$ ]
$W_b$	windowing factor
$x$	position coordinate in a one-dimensional model
$x_{det}$	position coordinate of the detector in a one-dimensional model
$x(t)$	time signal of a global detector
$y(t)$	time signal of a local detector

# Summary

Investigations of the spatial effects in nuclear reactor kinetics are described in this thesis. First the influence of shape changes of the neutron flux on the behaviour of a reactor is investigated theoretically. This is done by proposing a quantitative characterization method of the expected behaviour of the shape during a transient in terms of the size of the system and the strength of the perturbation. It is based on the fact that the spatial coupling in the reactor varies with the ratio between the physical size of the reactor and the migration area of the prompt fission chains. The proposed characterization method can, for example, be helpful in the choice of the numerical method for a detailed calculation of the kinetics of the system.

A more detailed characterization is proposed in another parameter: the space-time dependent reciprocal period. This parameter can be used to distinguish regions in a reactor that contribute more or less to the kinetic behaviour at a certain time after the start of the transient.

Numerical experiments are used to verify the two methods and also to underline the important role of the shape changes of the precursor concentration in the kinetic behaviour of reactors, which is underexposed in the existing literature. It is shown that the influence of the retardation effect of the precursors on the change of the shape of the flux and on the total power largely depends on the size of the system compared to the neutron migration length in the system.

Verification of the theory is one of the reasons to perform transient experiments in the research reactor of the Technical University of Budapest. Since this reactor is relatively small the theory indicates that no large shape changes should occur, which indeed is confirmed. The experiments, however, are also meant to get experience with the techniques to measure dynamic processes in nuclear reactors and to show that it is possible to measure the changes in the flux in a low power reactor with small self-powered neutron detectors.

For the behaviour of a reactor under small periodic disturbances other aspects play a more important role and therefore other theoretical methods can be used. In the thesis two methods, the field-of-view theory and a combination of local and global theory, are compared. Although both concepts are described in the literature earlier, in this work they are worked out in numerical experiments for some specific problems.

In one of the numerical experiments the response of three detectors to a modulating absorber at a specific position in a one-dimensional one-energy group model of a light water reactor is calculated. The results of the two methods show a close similarity. In another calculation a more realistic disturber is modelled: the vibrating absorber. The modelling is done by treating the vibrating absorber as two modulating absorbers, which oscillate at the basic frequency of the vibration with mutual phase shifts according to their position. Results of the calculations with this model of a moving absorber show the disappearance of a reactivity effect of such disturber when it acts in a region of flat neutron flux.

To verify the theory a new experimental facility, called DISTY, has been built. This facility is able to measure responses of different detectors due to well-known perturbations in detail. The facility consists of three disturbers, which move sinusoidally with a fixed frequency in all experiments. The facility is designed to put self-powered neutron detector as close as about 3 cm to the disturbers. The responses of these detectors and of detectors much farther away from the facility are described in the thesis.

In the spectra of detector responses peaks at the basic frequency of the moving disturber and the higher harmonics of this frequency can be seen. The height of the peaks is largely dependent on the specific set-up. The measurements of the amplitude of the detector response due to the movement of one of the disturbers show close similarity with theoretical predictions. The deviations between the theory and the experiment can be ascribed to the uncertainties in the position of the cadmium and the uncertainty of the shape of the flux as calculated by the static diffusion code used in the theory. The dependence of phase

shifts between the response of different detectors and the orientation of the cadmium disturber can also be explained.

In the range between 0.01 Hz and 2 Hz no dependence of the amplitude of the response at the frequency of the movement of the piece of cadmium can be seen. This is in agreement with the theory. For the frequencies above 10 Hz the theory predicts a dependence of the response with the frequency. However, it unfortunately appears to be impossible to move the piece of cadmium at a higher frequency than 5 Hz.

The existence of the higher harmonics in the spectra can be due to two phenomena. They can either be evoked by the not purely sinusoidal movement of the disturber or they come from a nonlinear function between the position of the disturber and the detector response. It is shown that in some cases the first higher harmonic in the response must come at least partly from the nonlinearity of the transfer function.

The experiments show that with DISTY high-quality measurements can be made. It is shown that the features in the measurements related to the basic frequency of the disturber can be explained heuristically. Especially the existence of local and global effects can be shown not only in a qualitative manner but also quantitatively. More research, however, must be done to resolve the features that appeared in the higher harmonics.

We conclude that in small research reactors spatial effects in the kinetics do not play a role for relatively large transients. However, for small periodic disturbances spatial effects appear and can be modelled using separate local and global theory. Experiments in larger reactors are desirable to investigate the spatial decoupling of large cores.



# Samenvatting

In dit proefschrift is onderzoek beschreven naar de spatiële effecten in de nucleaire reactor kinetica. Ten eerste is de invloed van vormveranderingen van de neutronenflux op het gedrag van de reactor theoretisch onderzocht. Dit is gedaan door een kwantitatieve karakteriseringsmethode te poneren, die het verwachte gedrag van de fluxvorm gedurende een transiënt beschrijft door de grootte van het systeem te relateren aan de sterkte van de verstoring. Deze methode is gebaseerd op het feit dat de spatiële koppeling in de reactor varieert met de verhouding van de fysieke grootte van de reactor en het migratiegebied van de snelle splijtingsketens. De voorgestelde karakteriseringsmethode kan bijvoorbeeld helpen bij het maken van een keuze voor een bepaalde numerieke methode ter berekening van de kinetica van het systeem.

Voor een meer gedetailleerde karakterisering is een andere parameter geïntroduceerd: de ruimte-tijd afhankelijke reciproke periode. Deze parameter kan gebruikt worden om gebieden in de reactor te onderscheiden die meer of minder bijdragen aan het kinetisch gedrag van de reactor op een bepaalde tijd na het starten van de transiënt.

Er zijn numerieke experimenten uitgevoerd om de twee methoden te verifiëren én om de belangrijke rol van de vormveranderingen van de concentratie van moederkernen in het kinetisch gedrag van reaktoren te onderstrepen. Dit laatste aspect is onderbelicht in de bestaande literatuur. De invloed van het vertragende effect van de nakomende neutronen emitters op de verandering van de vorm van de flux en het totale vermogen blijkt vooral afhankelijk te zijn van de afmeting van het systeem ten opzichte van de neutronen migratielengte in het systeem.

Verificatie van deze theorie is één van de redenen om transiënt-experimenten uit te voeren in de onderzoeksreaktor van de Technische

Universiteit in Boedapest. Omdat deze reaktor relatief klein is voorspelt de theorie dat er geen grote vormveranderingen zullen optreden, hetgeen inderdaad bevestigd wordt. De experimenten waren echter ook bedoeld om ervaring op te doen met technieken om dynamische processen in nucleaire reactoren te meten en om aan te tonen dat het mogelijk is om fluxveranderingen in een laag vermogensreactor te meten met kleine 'self-powered' neutronen detectoren.

Bij het kinetisch gedrag van een reaktor ten gevolge van kleine periodieke verstoringen spelen andere aspecten een belangrijkere rol. Er kunnen dan andere theoretische methoden worden gebruikt. In dit proefschrift zijn twee methoden met elkaar vergeleken: de 'field-of-view' theorie en een combinatie van een lokale en globale theorie. Hoewel beide concepten al eerder in de literatuur zijn beschreven, worden ze in dit werk voor een aantal specifieke problemen uitgewerkt met behulp van numerieke experimenten.

In één van de numerieke experimenten wordt de respons van drie detectoren op een modulerende absorber op één specifieke positie berekend in een één-dimensionaal één-energiegroepsmodel van een lichte waterreactor. De resultaten van de twee methoden vertonen een sterke mate van gelijkheid. Voor een andere berekening is een meer realistische verstoorder beschouwd: de vibrerende absorber. Dit type verstoorder is gemodelleerd door twee afzonderlijk modulerende absorbers, die beiden oscilleren met een frequentie evengroot als de basisfrequentie van de vibratie en met een fasedraaiing, die afhankelijk is van hun respectievelijke positie. De berekeningen met dit model laten het verdwijnen van het reaktiviteitseffect zien, wanneer de vibrerende absorber in een gebied met een vlakke neutronenflux wordt geplaatst.

Om de theorie te verifiëren is een nieuwe experimentele opstelling gebouwd, genaamd DISTY. Deze opstelling is in staat de respons van verschillende detectoren op bekende verstoringen in detail te meten. De opstelling bestaat uit drie verstoorders, die in alle experimenten sinusoidaal met een vaste frequentie bewegen. De opstelling is zo ontworpen dat de 'self-powered' neutronendetectors tot op slechts drie

centimeter van de verstoorders geplaatst kunnen worden. De respons van deze detectoren en van de detectoren die verder van de opstelling afliggen worden in dit proefschrift beschreven.

In de spectra van de detectorresponses zijn pieken te zien op de basisfrequentie van de bewegende verstoorder en de hogere harmonischen van deze frequentie. De hoogte van de pieken is vooral afhankelijk van de specifieke experimentele opzet. De metingen van de amplitude van de reaktorrespons, veroorzaakt door de beweging van één van de verstoorders, laten een grote overeenkomst zien met theoretische voorspellingen. De geconstateerde afwijkingen ten opzichte van de theorie kunnen worden toegeschreven aan de onzekerheden in de positie van het cadmium en de onzekerheid in de vorm van de flux zoals berekend door de statische diffusie code die in de theorie is gebruikt. De afhankelijkheid van fasedraaiingen tussen de respons van verschillende detectoren en de oriëntatie van de cadmium verstoorder kunnen ook worden verklaard.

Tussen 0.01 Hz en 2 Hz is geen afhankelijkheid van de amplitude van de respons op de frequentie van de beweging van het stukje cadmium gemeten, zoals de theorie voorspelt. Voor de frequenties boven de 10 Hz voorspelt de theorie wel een afhankelijkheid tussen de respons en de frequentie. Het blijkt helaas echter onmogelijk om met deze opstelling het stukje cadmium op een hogere frequentie dan 5 Hz te bewegen.

Het bestaan van hogere harmonischen in de spectra kan twee oorzaken hebben. De hogere harmonischen kunnen ofwel veroorzaakt worden door een niet zuiver sinusoidale beweging van de verstoorder of zij zijn toe te schrijven aan een niet-lineaire functie tussen de positie van de verstoorder en de detector respons. In een aantal gevallen blijkt de eerste hogere harmonische in de respons in ieder geval gedeeltelijk toegeschreven te kunnen worden aan de niet-lineariteit van de overdrachtsfunctie.

De experimenten laten zien dat met DISTY kwalitatief goede metingen gedaan kunnen worden. Er is aangetoond dat de kenmerken in de metingen die gerelateerd zijn aan de basisfrequentie van de verstoorder heuristisch verklaard kunnen worden. Met name het



bestaan van lokale en globale effecten kan niet alleen op een kwalitatieve maar ook op een kwantitatieve manier worden aangetoond. Er dient echter meer onderzoek gedaan te worden naar de karakteristieken van de hogere harmonischen.

We kunnen concluderen dat in kleine onderzoeksreactoren spatiële effecten in de kinetica geen rol spelen voor relatief grote transiënten. Voor kleine periodieke verstoringen kunnen wel spatiële effecten worden gemeten, die met behulp van gescheiden lokale en globale theorie goed kunnen worden gemodelleerd. Experimenten in grotere reactoren zijn wenselijk om de spatiële ontkoppeling van grote kernen te onderzoeken.

# Curriculum Vitae

De schrijver van dit proefschrift werd op 14 april 1967 in Amsterdam geboren. Na het behalen van zijn VWO-diploma op het Stedelijk Gymnasium te Leiden in 1985, heeft hij Natuurkunde gestudeerd aan de Universiteit van Leiden. Zijn doctoraalonderzoek heeft hij verricht in het Academisch Ziekenhuis Leiden op de afdeling Keel-, Neus- en Oorheelkunde. In mei 1990 slaagde hij voor zijn doctoraalexamen Experimentele Natuurkunde. Vervolgens is hij gedurende een halfjaar in dienst geweest bij de Nederlandse organisatie voor Wetenschappelijk Onderzoek (NWO). Hij werkte hier aan een onderzoek naar cues die een rol spelen bij het dieptezien bij de vakgroep Medische en Fysiologische Fysica aan de Rijksuniversiteit te Utrecht. In juni 1991 is hij vervolgens in het kader van het in dit proefschrift beschreven onderzoek in dienst getreden bij de Technische Universiteit Delft op het Interfacultair Reaktor Instituut. Sinds december 1995 is hij werkzaam als systeemontwikkelaar bij Origin in Utrecht.